School of Medicine

Oregon Health & Science University

CERTIFICATE OF APPROVAL

This is to certify that the PhD dissertation of

Amy Bittel

has been approved

Summer Gibbs, Ph.D.
Associate Professor, Advisor

Sandra Rugonyi, Ph.D.
Professor

Xiaolin Nan, Ph.D.
Assistant Professor

Bill Rooney, Ph.D.
Associate Professor

Rob Strongin, Ph.D.
Professor

SYNTHESIS AND CHARACTERIZATION OF BODIPY-BASED FLUOROPHORES FOR MULTICOLOR MICROSCOPY

By

Amy Marie Bittel

A DISSERTATION

Presented to the Department of Biomedical Engineering
of the Oregon Health & Science University
School of Medicine
In partial fulfillment of the requirements for the degree of

Doctor of Philosophy
In Biomedical Engineering

July 2017

Table of Contents

List of Figures

List of Tables

List of Abbreviations

3CP: 3-(carboxy)-2,2,5,5-tetramethyl-1-pyrrolidinyloxy

AA: ascorbic acid

ACN: acetonitrile

βME: 2-mercaptoehtanol

BODIPY: boron-dipyrromethene

COT: cyclooctatetraene

CTC-PS: 2-chlorotrityl chloride polystyrene

CV: coefficient of variance

DAPI: 2-(4-amidinophenyl)-1H -indole-6-carboxamidine

DCM: dichloromethane

DFT: density functional theory

DIEA: diisopropylethylamine

DMF: dimethyl formamide

DMSO: dimethylsulfoxide

ESI: electrospray ionization

FPLC: fast protein liquid chromatography

FTIR: Fourier transform infrared spectroscopy

FWHM: full-width-at-half-maximum

HATU: 1-[Bis(dimethylamino)methylene]-1*H*-1,2,3-triazolo[4,5-*b*]pyridinium 3-oxid hexafluorophosphate

HOMO: highest occupied molecular orbital

HPLC: high performance liquid chromatography

HRMS: high resolution mass spectrometry

LC/MS: tandem liquid chromatography, mass spectroscopy

LSM: laser scanning microscopy

LUMO: lowest unoccupied molecular orbital

MEA: 2-mercaptoethylamine

MV: methyl viologen

NA: numerical aperture

NHS: N-hydroxysuccinimide

NIR: near-infrared

NMR: nuclear magnetic resonance

PALM: photoactivated localization microscopy

PBS: phosphate-buffered saline

PVA: polyvinyl alcohol

SBR: signal-to-background ratio

SMLM: single-molecule localization microscopy

SNR: signal-to-noise ratio

SRM: superresolution microscopy

STORM: stochastic optical reconstruction microscopy

TCEP: tris(2-carboxyethyl)phosphine

TFA: trifluoroacetic acid

TN: tris-buffered saline

UV: ultraviolet

Acknowledgements

First, I'd like to thank my advisor, Dr. Summer Gibbs. I am forever grateful for her guidance and motivation throughout graduate school.

Special thanks also goes to the rest of my dissertation committee - Sandra Rugonyi, Xiaolin Nan, Bill Rooney, and Rob Strongin - for their thoughtful input and advice in developing my research projects.

Lastly, I'd like to thank my family for all their love and encouragement. In particular, I'd like to extend my appreciation to my husband, Brad, for his endless support.

Abstract

Synthesis and Characterization of BODIPY-Based Fluorophores for Multicolor Microscopy

Amy Marie Bittel

Department of Biomedical Engineering
School of Medicine
Oregon Health & Science University

July 2017

Dissertation Advisor: Summer Gibbs, PhD

Multicolor microscopy tools necessary to localize and visualize the complexity of subcellular systems are limited by current fluorophore technology. While commercial fluorophores cover spectral space from the ultraviolet to the near infrared region and are optimized for conventional bandpass based fluorescence microscopy, they are not ideal for multicolor microscopy as they tend to have short Stokes shifts, restricting the number of fluorophores that can be detected in a single sample to four or five. Herein, we synthesized a library of 95 novel BODIPY (boron-dipyrromethene)-based fluorophores and screened their photophysical properties for conventional and superresolution multicolor microscopy applications. A subset of our BODIPY-based fluorophores with varied length Stokes shifts were utilized with confocal laser scanning microscopy and linear unmixing to create a five color image using a single excitation laser line for the first time. Using these novel fluorophores in combination with commercial fluorophores would enable a nine to ten color image using linear unmixing. We also demonstrated the applicability of our novel BODIPY-based fluorophores for single-molecule localization superresolution microscopy (SMLM). Using our developed screening methodology for efficient characterization of fluorophore photoswitching properties, we identified high-quality photoswitchable BODIPY-based fluorophores from our library that fill voids in commercially available fluorophore spectral space, facilitating multicolor superresolution microscopy (SRM) using conventional SMLM instrumentation. Overall, the fluorophores generated from our BODIPY-based library will enable both conventional and SRM multicolor imaging applications alone or in conjunction with commercially available fluorophores, increasing the available color palette for imaging.

CHAPTER 1: Introduction

1.1 Project Rationale

Multicolor microscopy is a powerful tool to detect and visualize multiple subcellular entities in a single sample. Whether using conventional or superresolution microscopy (SRM) for imaging, the number of colors that can be resolved depend on a combination of the methodologies used for spectral separation and the availability of fluorophores with varied spectral properties. Bandpass filters can typically resolve four to five colors when the fluorophore emissions are spread throughout spectral space, resulting in one color being resolved per excitation color. Commercially available fluorophores are readily compatible with this configuration due to their characteristic short Stokes shifts and the routine availability of bandpass filtration microscopes.[1,2] However, to expand the number of resolvable colors using multicolor microscopy, multiple fluorophores must be excited and resolved per excitation color.[3,4] Whether spectral separation is completed with closely configured bandpass filters or with spectral imaging paired with linear unmixing, fluorophores are needed that when excited using a single color, have varied length Stokes shifts permitting spectral separation.

1.2 Dissertation Summary

Dissertation research focused on developing small molecule organic fluorophores for multicolor microscopy applications with the specific goal of creating fluorophores with varied length Stokes shifts that contained chemical moieties compatible with conjugation to affinity reagents. We synthesized and characterized a library of BODIPY-based (BAA) fluorophores that successfully ranged in Stokes shift lengths and contained carboxylic acid functionality for affinity reagent conjugation (Chapter 3). We demonstrated the utility of the BAA fluorophores for multicolor microscopy by creating a five-color image through tagged affinity reagent, which labeled five distinct subcellular structures and were imaged with confocal laser scanning microscopy using spectral imaging and linear unmixing. Unlike previous multicolor imaging applications,[4] our five-color image was attained on

spatially overlapping structures using a single laser for excitation, while emission spectra were distributed over just 60 nm of spectral space.

Furthermore, we wanted to apply the varied length Stokes shift BAA fluorophores to multicolor single-molecule localization microscopy (SMLM) as the BAA fluorophores provided advantageous spectral properties not available with commercial fluorophores. However, SMLM requires fluorophores to photoswitch in order to produce images with resolution of ~10-20 nm.[2,5] To facilitate screening of our 95 member BODIPY library, we developed a methodology to efficiently screen fluorophore photoswitching which entailed fixing single molecules in polyvinyl alcohol (PVA) enabling quantification of their photoswitching properties (Chapter 4).[6] We determined key photoswitching properties including total photons and duty cycle were significantly correlated to image quality, enabling identification of optimal photoswitchable fluorophores.

A key aspect of successful use of small molecule organic fluorophores as photoswitchable fluorophores for SMLM is having a suitable imaging buffer, as small molecule organic fluorophores do not innately photoswitch.[7,8] However, an optimal imaging buffer for BODIPY-based fluorophores was unknown, prohibiting routine application of BAA fluorophores to SMLM. Using our PVA screening methodology, we evaluated common imaging buffers and additives, resulting in a total of 35 tested conditions to identify optimal photoswitching conditions for the BODIPY fluorophore scaffold (Chapter 5). In the end, we found multiple buffer conditions that resulted in photoswitching of BODIPY FL. SMLM imaging of *in vitro* microtubules confirmed the imaging buffer conditions including 10 mM MEA and 100 mM MEA, both with oxygen scavenger, were optimal for BODIPY FL, through the production of high quality SMLM images.

Lastly, we selected BAA fluorophores with advantageous spectral properties for multicolor SMLM and evaluated their photoswitching capability utilizing PVA methodology and optimal imaging buffer conditions (Chapter 6). We found that the novel BAA fluorophores all photoswitched, where some BAA fluorophores had higher total photon output and

better localization precision than with the widely used fluorophore AlexaFluor568, predicting improved SMLM image quality over commercially available fluorophores. We further evaluated a long Stokes shift BAA fluorophore (**BAA-30a**) and a short Stokes shift BAA fluorophore (**BAA-5a**) for SMLM image quality using labeling of microtubules *in vitro*. Both BAA fluorophores demonstrated successful labeling of microtubules, confirming their utility as photoswitchable fluorophores while providing additional spectral options for multicolor SMLM. **BAA-30a** provides an option to create a two-color image using a single color excitation, 561 nm, when used with shorter Stokes shift fluorophores such as the conventional AF568 or the novel **BAA-5a**.

In summary, the BODIPY-based fluorophores developed in this work will extend the spectral resolution of multicolor images acquired with both conventional fluorescence microscopes equipped with spectra imaging and superresolution microscopes equipped with closely configured bandpass filters.

CHAPTER 2: Background

2.1 Small Molecule Fluorophores for Cellular Imaging

Small molecule fluorophores are powerful tools for detecting and visualizing subcellular components of intact live and fixed cells. Small molecule organic fluorophores consist of heterocyclic structures and are classified into base chemical structures including xanthene, rhodamine, BODIPY (boron-dipyrromethene), cyanine, and oxazine.[1,9] While these fluorophore classes emit throughout spectral space ranging in emission maximum from the ultraviolet (UV) to the near-infrared (NIR), they tend to have relatively short Stokes shifts, which is the difference between the maximum absorbance and emission wavelengths. For example, commercially available BODIPY based fluorophores are mostly limited to those with Stokes shifts of less than 15 nm.[1] AlexaFluor dyes, one of the most popular brands of fluorophores, are based on various fluorophore scaffolds and have a typical Stokes Shift of 20 nm or less.[1] While short Stokes shift fluorophores are ideal for multicolor imaging with conventional bandpass filter configurations, there is opportunity to develop complementary fluorophore options for multicolor microscopy equipped with spectral imaging and linear unmixing capabilities, particularly fluorophores with varied length Stokes shifts.

2.1.1 BODIPY-Based Fluorophores

BODIPY is an extensively utilized fluorophore scaffold due to its superior photophysical properties including its resistance to photobleaching, high quantum yield, and narrow emission spectrum.[10] The BODIPY scaffold is also particularly advantageous for novel fluorophore development since its chemistry can be customized using a variety of synthetic routes.[11,12] Libraries originating from various core BODIPY scaffolds have resulted in sensors for immunoglobin and glucagon, as well as BODIPY fluorophores that emit in various colors, although typically with short Stokes shifts.[13-16] Other BODIPY syntheses have successfully created long Stokes shift fluorophores for bioconjugation, but have been restricted to the NIR region.[17]

2.1.2 Labeling Methods

Some specific small molecule fluorophores are able to directly probe cells to detect certain chemistry or to localize to particular organelles.[18,19] However, such probes are limited to live cell analysis and must consist of small lipophilic fluorophores such as BODIPY to be cell permeable. Imaging with fluorophore tagged affinity reagents (antibodies, antibody fragments, nanobodies, affibodies, lectins, etc.) enables versatility in fluorophore choice based on photophysical properties rather than the direct staining pattern of the small molecule fluorophore.

Immunofluorescence is a widely used affinity tagging reagent strategy for precise cellular labeling as it enables fluorescence imaging of any antigen in which a corresponding specific antibody exists. Fluorophores with chemical moieties such as N-hydroxysuccinimide (NHS) esters or maleimides can be readily conjugated to the lysine and cysteine amino acids of antibodies, respectively. Labeling cells with primary antibodies directly conjugated to a fluorophore is known as direct immunofluorescence and is useful in preventing antibody crosstalk when labeling multiple antigens (Figure 2-1a). Indirect immunofluorescence involves first labeling cells with an unconjugated primary antibody before labeling with a compatible fluorophore-conjugated secondary antibody specific for the primary antibody. Indirect immunofluorescence is useful for increasing fluorescent signal through amplification, as multiple secondary antibodies can label each primary antibody (Figure 2-1b).

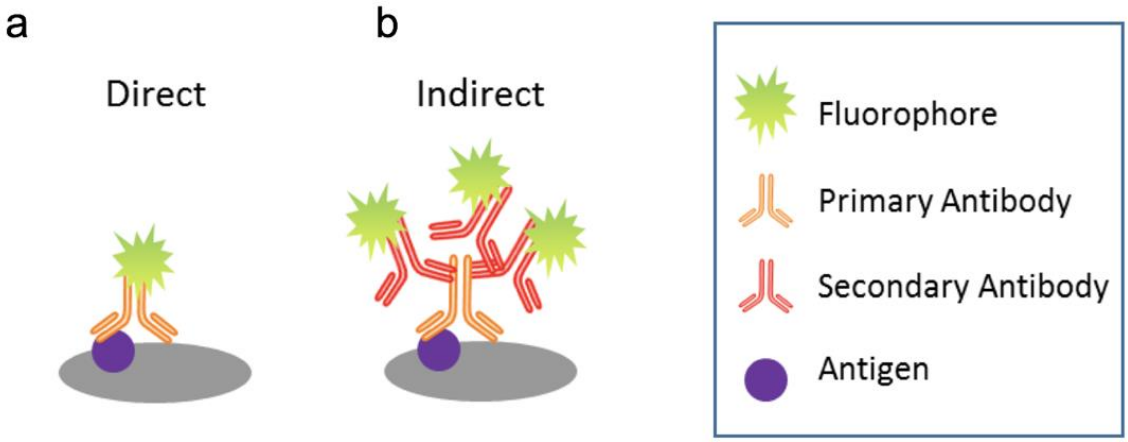

Figure 2-1 Schematic demonstrating immunofluorescence labeling with small molecule fluorophore via a) direct immunofluorescence and b) indirect immunofluorescence.

2.2 Multicolor Microscopy

Multicolor microscopy enables localization and visualization of complex subcellular structures in live and fixed cells. To prevent crosstalk between multiple fluorophores used to label a single sample, fluorophore selection must take into account the method used for spectral separation of fluorophore emission wavelengths for specific subcellular structure identification.

2.2.1 Bandpass Filters

Bandpass filters are commonly utilized on a variety of fluorescent microscopes including relatively simple epifluorescence and the more complex confocal instruments. Bandpass filters spectrally separate colors by transmitting a wavelength range corresponding to the selected fluorophore's emission spectra to the detector while blocking emitted light from the excitation source and fluorophores emitting at other wavelengths. To achieve accurate imaging of multicolor samples, consecutive images are taken with bandpass filter sets. Typical microscopes contain bandpass filter sets permitting excitation at slightly bluer wavelength and detection of only a single fluorophore corresponding to purple (UV), blue (Cy2), yellow/green (Cy3), and red visible spectral regions (Cy5), as well as the NIR (Cy7) on specialized instruments. This conventional configuration enables maximum color detection, with minimal spectral emission overlap between fluorophores using simplified equipment. However, this conventional microscope configuration limits detection to only four or five colors in a single sample. Additionally, for optimal spectral separation, the fluorophore used for each color region must exhibit a relatively short Stokes shift to accommodate the narrow region needed for ideal excitation and emission detection.

2.2.2 Spectral Imaging and Linear Unmixing

Microscopes equipped with spectral imaging and linear unmixing are not limited by bandpass configurations, but are able to simultaneously identify a number of fluorophores

based on signal intensity and the number of detector channels.[20,21] Five colors have been successfully separated on samples containing overlapping structures using two exciation lasers and five fluorophores that emit over 150 nm of the visible region.[4] Spectral imaging measures fluorophore emission in 2-10 nm wide detection channels and produces a stack of spectral images for each pixel. Linear unmixing algorithms subsequently assign colors to each pixel based on known spectral profiles, usually measured from single fluorophore stained samples using the same fluorophores imaged prior to the multicolor imaging study, resulting in a multicolor image. Confidence in separation of overlapping spectra is increased by using fluorophores with high contrast, making it strategic to choose labels with higher quantum yield and low background signal from untargeted molecules.[22] Spectral separation is also improved by using fluorophores without substantial overlap in their emission spectra, where fluorophores with relatively narrow and spectrally diverse emission maxima are desired. In contrast to short Stoke shift fluorophores required for bandpass spectral separation, fluorophores with varied length Stokes shifts are ideal for spectral imaging to maximize the number of separable fluorophores using a single excitation.

2.3 Superresolution Microscopy

Superresolution microscopy (SRM) has overcome the historic spatial resolution limit of light microscopy, enabling fluorescence visualization of subcellular structures and multi-protein complexes at the nanometer scale.[5,23,24] While there are several conventional light microscopy techniques that are capable of intracellular imaging, including wide-field and confocal microscopies, they cannot accurately localize cellular proteins to greater accuracy than ~250 nm, inhibiting the study of protein interactions, which control cellular function and play an integral role in diseases such as cancer. Furthermore, while electron microscopy can resolve features down to the nanometer scale, it is difficult to generate protein specific information as antibody labeling strategies remain challenging. SRM techniques that resolve antibody labeled subcellular structures and proteins with ~10-20 nm resolution generally fall into two main approaches, with one depending on optics and the other depending on fluorophores.

2.3.1 STED and SIM Depend on Instrumentation

One approach to SRM relies on spatially patterned excitation light, where the optics determine the achievable resolution. The most prominent of these include stimulated emission depletion (STED), where a donut shaped second excitation laser beam is used to suppress fluorescence emission of fluorophores located away from the center of excitation, and results in ~20 nm resolution of the detected fluorophores.[25,26] Structured illumination microscopy (SIM) uses a rotating grid pattern during image acquisition and specialized image reconstruction algorithms to achieve 100 nm resolution.[27]

2.3.2 SMLM Depends on Photoswitchable Fluorophores

Single-molecule localization microscopy (SMLM), another SRM approach, utilizes the conventional wide-field fluorescence microscope configuration but requires the use of photoswitchable fluorophores to achieve resolution of ~10-20 nm.[7] Subcellular features of interest must be densely labeled with photoswitchable fluorophores that have the ability to stochastically switch between the fluorescent “on” state where photons are emitted and the nonfluorescent “off“ state where the fluorophore appears dark.[28,29] Subdiffractive localization of individual fluorophores throughout a series of images via activation of a stochastic, small population of fluorophores in the on state facilitates reconstruction of a superresolution image (Figure 2-2).[30] SMLM techniques include photoactivated localization microscopy (PALM),[23,31] which require photoactivatable fluorescent proteins, and stochastic optical reconstruction microscopy (STORM),[5,32] which relies on photoswitchable small molecule organic fluorophores.

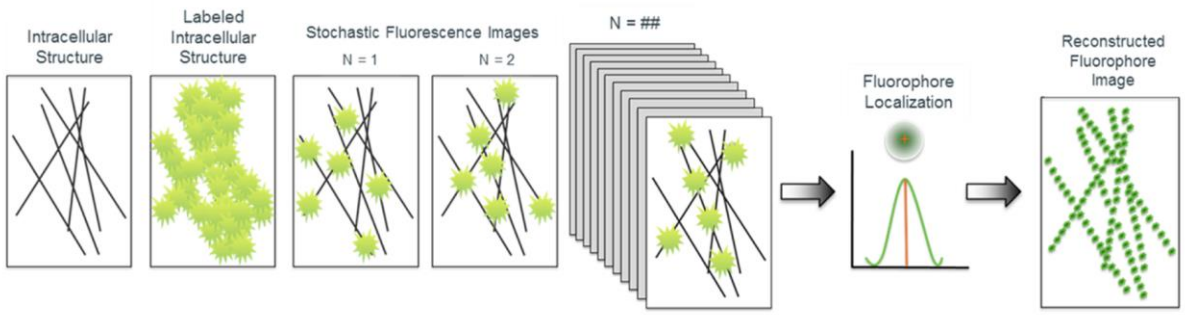

Figure 2-2 SMLM requires samples to be densely labeled with photoswitchable fluorophores. As fluorophores photoswitch during imaging, a small, stochastic population of fluorophores are “on” in each imaging frame enabling accurate localization of the center of each fluorophore’s point spread function. Fluorophores are localized in each frame and a final SMLM image is reconstructed.

2.4 Photoswitchable Fluorophores

Photoswitchable fluorophores enable subdiffractive fluorescence imaging with SMLM. Although a number of photoactivatable fluorescent proteins for PALM exist, some are more challenging to implement than others. The most conventionally used photoactivatable fluorescent proteins include photoactivatable green fluorescent protein (pa-GFP) and red fluorescent protein pa-mRFP1-1.[33] Coordinated low- and high-intensity excitation lasers are used to activate photoswitching of fluorescent proteins.

Small molecule organic fluorophores, used with STORM, are often preferred for SMLM as they are brighter than fluorescent proteins and offer more options in terms of spectral properties and chemical moieties for labeling cells.[34] Commercial fluorophores have been screened for their photoswitching ability with common choices including ATTO488 and AlexaFluor647.[2,35] Most SMLM-compatible fluorophores do not innately photoswitch, and must be driven by imaging conditions, particularly imaging buffer to generate the necessary switching for SMLM.

2.4.1 Photoswitching Photophysics

Fluorophore photoswitching involves a series of photophysical steps (Figure 2-3).[28,34] First fluorophores are excited from their ground state (S_0) to their singlet state (S_1) using laser excitation (k_{abs}) at the optimal excitation wavelengths for the selected probe. The excited fluorophore can either release its energy through fluorescence emission (k_{fl}) as it relaxes back to its ground state (S_0), creating fluorescence or an “on” event, or the fluorophore molecule experiences intersystem crossing (k_{isc}) to a triplet state (T_1), where the molecule is considered “off.” The molecule can be recovered from the triplet state back to the ground state directly with oxygen (k_T), or indirectly through redox reactions (k_{red}, k_{ox}, $k_{red'}$, $k_{ox'}$) with reductants or oxidants present in the imaging buffer that form radical cations ($F^{\bullet+}$) or radical anions ($F^{\bullet-}$).

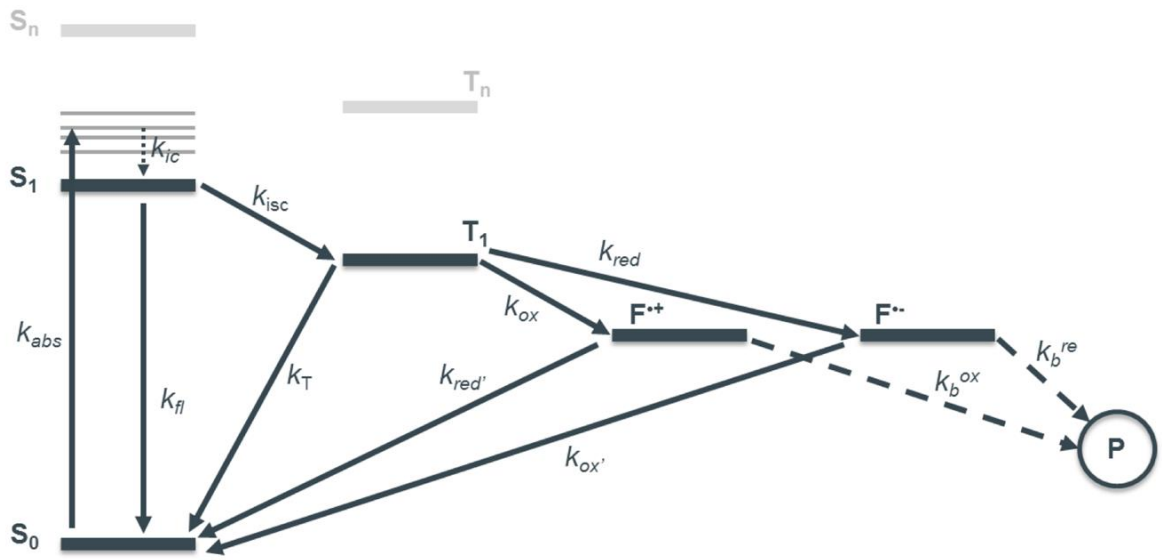

Figure 2-3 Jablonski diagram demonstrating the photophysical states related to fluorophore photoswitching, adapted from Ha *et al.*[28] Energy states are shown for ground state (S_0), first excited state (S_1), triplet state (T_1), radical cation ($F^{\bullet+}$), and radical anion ($F^{\bullet-}$). Rate constants, k, are shown for fluorophore excitation (k_{abs}), fluorescence (k_{fl}), intersystem crossing (k_{isc}), triplet state depopulation (k_T), and redox reactions leading to ion and ground states (k_{red}, k_{ox}, $k_{red'}$, $k_{ox'}$). Rate constants for redox reactions leading to photobleaching (P) are shown as well (k_b^{ox} and k_b^{re}).

Imaging buffers promote fluorophore photoswitching by creating an environment that is likely to sustain molecules in their “off” state.[28] Oxygen scavengers are used to reduce the probability of molecules transferring directly from their triplet state to the ground state, which often occurs when oxygen is present in the system resulting in photobleaching. Likewise, image buffers contain either a reducing agent, oxidizing agent, or a combination, to also prevent molecules from returning to the ground state directly from the triplet state by forming and stabilizing radical ions. It should be noted, however, that the concentration of oxygen scavenger and redox components should not retain the fluorophores in the triplet state permanently, which would prevent any “on” events from occurring.

2.4.2 Imaging Buffer Formulations

Imaging buffers are generally composed of three main components including the oxygen scavenger, redox reagent, and optional additives which can further enhance photoswitching. Different imaging buffer compositions are optimal for different fluorophore scaffolds, which is partially due to the differences in fluorophore redox potential.[2] The most popular oxygen scavenger is known as GLOX, and consists of glucose, catalase, and glucose oxidase. Common redox reagents include primary thiols such as 2-mercaptoethylamine (MEA) and 2-mercaptoethanol (βME), the reductant ascorbic acid (AA), and the oxidizer methyl viologen (MV).[36] Additives shown to improve photoswitching of certain fluorophore scaffolds include additional reductants such as tris(2-carboxyethyl)phosphine hydrochloride (TCEP)[37] with rhodamine, and additional oxidizers such as cyclooctatetraene (COT)[7] with cyanine, and brief treatments with sodium borohydride ($NaBH_4$)[38] with both cyanines and rhodamines.

CHAPTER 3: Varied Length Stokes Shift BODIPY-Based Fluorophores for Multicolor Microscopy[39]

[39]Bittel, A.M., Davis, A.M., Nederlof, M.A., Escobedo, J.O., Strongin, R.M., & Gibbs, S.L. *Varied Length Stokes Shift BODIPY-Based Fluorophores for Multicolor Microscopy*. Will submit for publication July 2017.

3.1 ABSTRACT

Multicolor microscopy tools necessary to localize and visualize the complexity of subcellular systems are limited by current fluorophore technology. While commercial fluorophores cover spectral space from the ultraviolet to the near infrared region and are optimized for conventional bandpass based fluorescence microscopy, they are not ideal for multicolor microscopy as they tend to have short Stokes shifts, restricting the number of fluorophores that can be detected in a single sample to four to five. Herein, we synthesized a library of 95 novel BODIPY (boron-dipyrromethene)-based fluorophores and screened their photophysical properties for conventional multicolor microscopy. A subset of our BODIPY-based fluorophores with varied length Stokes shifts were utilized with confocal laser scanning microscopy and linear unmixing to create a five-color image using a single excitation laser line for the first time. Using these novel fluorophores in combination with commercial fluorophores would enable a nine to ten color image using linear unmixing.

3.2 INTRODUCTION

Multicolor microscopy is an important tool to detect and visualize multiple subcellular entities in a single sample, which often relies on small molecule fluorophore tagged affinity reagents (antibodies, antibody fragments, nanobodies, affibodies, lectins, etc.) for specific biomolecule labeling. Conventional epifluorescence microscopes use bandpass

filters for multicolor detection, where the bandpass configuration is typically limited to four or five colors throughout ultraviolet to near-infrared spectral space. In contrast, microscopes equipped with spectral imaging and linear unmixing are able to simultaneously identify a number of overlapping fluorophore emission spectra, increasing multicolor imaging capability to around seven fluorophores spanning spectral space.[20,21] Previous linear unmixing studies have demonstrated five color images of overlapping subcellular entities labeled with five fluorophores using two excitation lasers and emission distributed over 150 nm of spectral space.[4]

Optimal fluorophores for multicolor epifluorescence microscopy have relatively short Stokes shifts and narrow emission spectral to minimize spectral emission overlap. Ideal fluorophores for linear unmixing based multicolor microscopy require high contrast, making it strategic to choose labels with high quantum yield and low signal to background ratio (SBR) for untargeted molecules.[22] Spectral separation is also improved when emission spectra are distinct, where separate emission maxima and narrow or distinctly shaped emission spectra are desirable.[4] In contrast to the short Stokes shift fluorophores for bandpass spectral separation, fluorophores with varied length Stokes shifts are ideal for spectral imaging, increasing the number of fluorophores that can be separated using each excitation laser.

Imaging with fluorophore tagged affinity reagents enables versatility in fluorophore choice based on photophysical properties rather than the direct staining pattern. Affinity reagents are typically used with small molecule fluorophores consisting of core scaffolds such as xanthene, rhodamine, BODIPY, cyanine, and oxazine.[9,40] While these fluorophore classes cover a broad range of excitation and emission spectra, they tend to have short Stokes shifts. For example, commercially available BODIPY based fluorophores are mostly limited to those with Stokes shifts of less than 15 nm.[40] AlexaFluor dyes, one of the most popular brands of fluorophores, are based on a variety of scaffolds and have a typical Stokes Shift of 20 nm or less.[40] While short Stokes shifts are ideal for multicolor imaging with bandpass filter configurations, there is opportunity to develop

complementary fluorophores for multicolor microscopy equipped spectral imaging and linear unmixing, particularly fluorophores with varied length Stokes shifts.

BODIPY (boron-dipyrromethene) is a widely utilized fluorophore scaffold due to its advantageous photophysical properties such as its resistance to photobleaching, high quantum yield, and narrow emission spectrum.[10] Furthermore, the BODIPY scaffold is particularly advantageous for novel fluorophore development since its chemistry can be customized using a variety of synthetic routes.[11,12] Libraries originating from various core BODIPY scaffolds have resulted in fluorophores with an array of Stokes shifts.[13-16] While these libraries resulted in successful chemical sensors and probes, the fluorophores did not contain conjugatable chemistry, making them incompatible with tagging affinity reagents. Other BODIPY syntheses have successfully created long Stokes shift fluorophores for bioconjugation, but have been restricted to the near-infrared region.[17]

Herein, we report the first synthesis of a library of BODIPY-based fluorophores specifically designed to generate varied length Stokes shifts while containing chemical moieties compatible with conjugation to affinity reagents for multicolor imaging applications. Our BODIPY-based library was characterized for its SBR and photophysical properties in order to select a subset of fluorophores most appropriate for multicolor microscopy imaging. We also screened our library for organelle specificity in fixed, permeabilized cells and characterized its molecular properties. We identified fluorophores that target the nucleus and nucleolar regions, vesicular structures, and cytosolic regions in fixed cells. Through tagged affinity reagent labeling of five distinct cellular structures, we demonstrated the accurate immunofluorescence labeling and imaging of five colors in a single sample with confocal laser scanning microscopy using spectral imaging and linear unmixing. Unlike previous multicolor imaging applications, our five-color image was attained on spatially overlapping structures using a single laser for excitation and emission spectra distributed over just 60 nm of spectral space.

3.3 RESULTS

3.3.1 Solid Phase Synthesis of BAA Library

A library of BODIPY-based fluorophores was synthesized using solid phase synthesis to add structurally diverse styryl moieties (Scheme 3-1), with the goal to create fluorophores with varied length Stokes shifts for multicolor imaging applications. Commercially available BODIPY FL was loaded onto chlorotrityl chloride polystyrene resin (CTC-PS) through its carboxylic acid moiety (**1**), where the CTC-PS acted as a protecting group for the carboxylic acid.[41] The styryl modification of the BODIPY FL was carried out by reacting the core fluorophore with 79 structurally diverse aromatic aldehydes via Knoevenagel condensation (**b**).[14] Each aromatic aldehyde reaction with BODIPY FL resulted in novel fluorophores with a single styryl modification (**BAA-a**), two styryl modifications (**BAA-b**) or a mixture of the single and double styryl addition (Table S1). The novel BAA fluorophores were cleaved from the CTC-PS resin (**c**) yielding **BAA-a**, **BAA-b** or a mixture of **BAA-a** and **BAA-b**. After purification of the cleaved material by high pressure liquid chromatography (HPLC), a library of 95 novel BAA fluorophores with a minimum of 80% purity (average purity = 99%) was obtained (Table S3-1). 60 BAA fluorophores had one styryl modification and 35 fluorophores had two styryl modifications. NMR on five selected BAA fluorophores revealed single addition of the aromatic aldehyde occurred exclusively at the α-methyl group (Supporting Information).

Scheme 3-1. Synthesis of BAA Library[a]

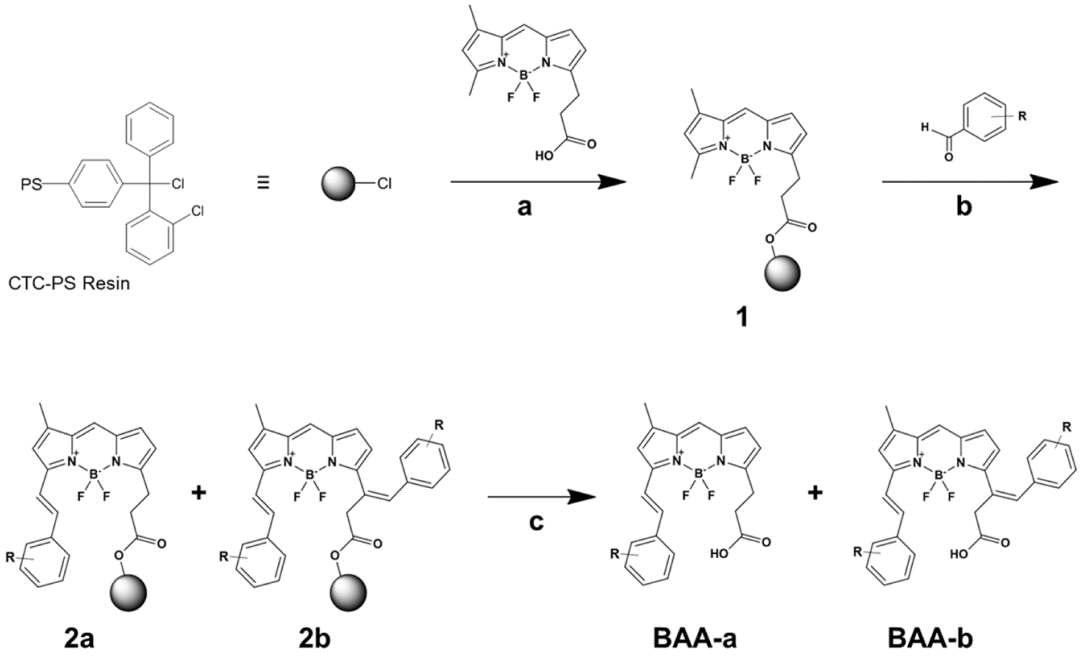

[a]Reagents and Conditions: (a) DCM, DIEA, rt, 20 h; (b) R-CHO (79 aromatic aldehydes, see Table S1, Supporting Information), DMSO-ACN (1:1), pyrrolidine, acetic acid, 85°C, 15 min; (c) TFA-DCM (0.5:99.5), rt, 2 x 10 min.

3.3.2 BAA Library Photophysical Properties

Addition of the aromatic aldehydes to the core BODIPY FL structure ($\lambda_{max\ ABS}$ = 503 nm, $\lambda_{max\ EM}$ = 512 nm) resulted in significantly red-shifted absorbance and emission of all novel BAA fluorophores (Figure 3-1a). The BAA library ranged in maximum absorbance wavelength from 480-614 nm and maximum emission wavelength from 578-714 nm. Of note, most of the BAA fluorophores (84%) had emission wavelengths between 578-610 nm, shifting the emission 75-100 nm from the original compound. The BAA fluorophores ranged in Stokes shifts from 2-58 nm, where the novel fluorophores generally had longer Stokes shifts than BODIPY FL, with an average Stokes shift of 18 nm (Table S3-2). The quantum yields of the BAA fluorophores varied widely, ranging from 0.04 to >0.99 with an average of 0.38 (Figure 3-1b) and tended to be lower than BODIPY FL (0.81). The full-width-at-half-maximum (FWHM) was quantified to determine spectral spread for multicolor microscopy applications. The FWHM of the BAA library had a broad range (30-102 nm) with an average of 44 nm (Figure 3-1c), which was generally wider than BODIPY FL (34 nm).

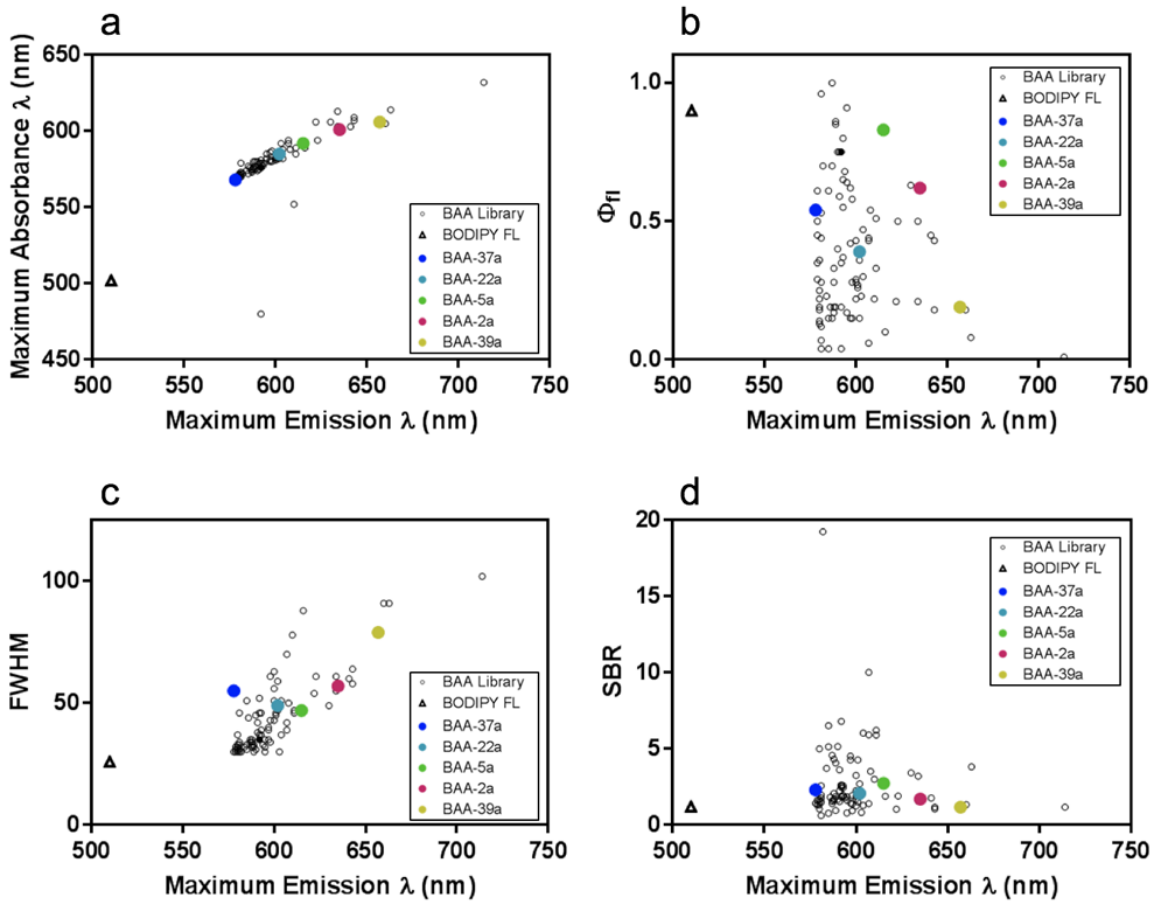

Figure 3-1 Photochemical and signal-to-background ratio (SBR) data for the BAA library compared to BODIPY FL with five selected BAA fluorophores highlighted in color. (a) Maximum absorbance vs. maximum emission wavelength, (b) quantum yield (Φfl) vs. maximum emission wavelength, (c) full-width-at-half-maximum (FWHM) vs. maximum emission wavelength, and (d) SBR vs. maximum emission wavelength.

3.3.3 Organelle Specificity and Signal-to-Background Ratio of BAA Library

The BAA library was screened in permeabilized, fixed U2OS cells at 10 µM to assess organelle specificity of the novel fluorophores (Table S3-3 and S3-4). At the selected concentration, all BAA fluorophores showed cell staining with higher intensity than autofluorescence alone. Interestingly, the specific staining pattern varied across the library (Table S3-3). Three BAA fluorophores were found to localize only to the nucleus and nucleolar regions of the cell including **BAA-2a**, **BAA-30a**, and **BAA-77a** (Figure 3-2a). Vesicular structures were stained by 22 of the BAA fluorophores (Figure 3-2b). Cytosolic staining was seen from 34 of the BAA fluorophores (Figure 3-2c), and the remaining 36 BAA fluorophores localized to a combination of vesicular and cytosolic structures.

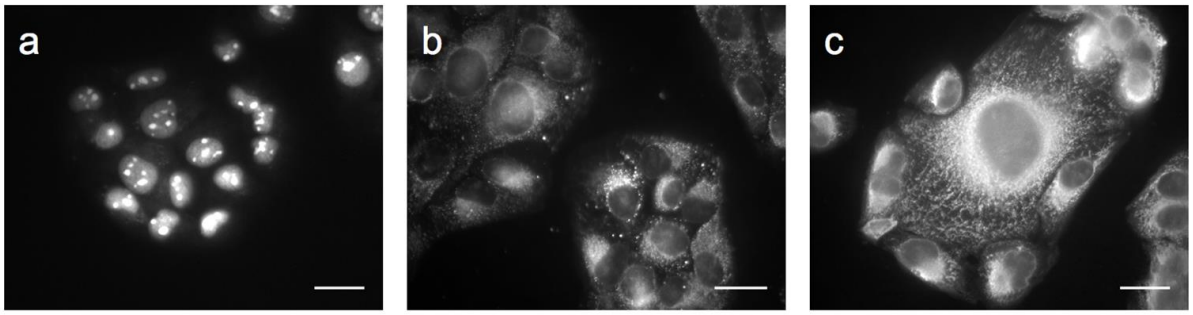

Figure 3-2 Representative images of organelle specificity of BAA fluorophores in permeabilized, fixed U2OS cells. Scale bar = 20 μm. (a) **BAA-2a** localized to nucleus and nucleolar regions, (b) **BAA-10b** localized to vesicular structures and (c) **BAA-1b** localized to cytosolic region.

The BAA library was also screened for fluorescence staining in U2OS cells at 100 nM to determine if nonspecific binding of the BAA fluorophores would be detectable at the fluorophore concentration typical of immunofluorescence staining. The BAA fluorophores had limited staining at 100 nM concentration, where 57% of the compounds had a SBR less than 2 and 73% had a SBR less than 3 (average = 2.65 for all 95 BAA fluorophores) (Figure 3-1d, Table S3-4). In comparison, organelle specificity screening resulted in images with SBR ranging from 9-20, while immunofluorescence images had a minimum SBR of 10.

Molecular properties were calculated for the BAA fluorophores to investigate correlation between the BAA fluorophore structure and organelle staining affinity including the partition coefficient, which is the ratio of the amount of a compound soluble in aqueous phase versus lipophilic phase at equilibrium (LogD), number of rotatable bonds, number of hydrogen bond donors and acceptors (HBD and HBA), and the polar surface area (Table S3-4). Addition of the aromatic aldehydes generated a wide range of distribution coefficients ranging from -4.22 to 7.12, with an average of 2.25, displaying a general increase from BODIPY FL (-2.13). The number of rotatable bonds was also highly variable in the BAA library, ranging from 5-22 with an average of 8.5, with all BAA fluorophores having an increase of at least 3 rotatable bonds over BODIPY FL (rotatable bonds = 2). The number of hydrogen bond donors was similar across the library (1-3, with an average HBD = 1.1) and to BODIPY FL (HBD = 1) while the number of hydrogen bond acceptors showed a fairly large range from 2-12 with an average HBA of 4, differentiating the derivatives from BODIPY FL (HBA = 4) with both higher and lower values. The polar surface area of the BAA fluorophores was also widely variable (45-153, with an average of 72), matching or increasing in polar surface area compared to BODIPY FL (45).

3.3.4 BAA Fluorophores Selected for Immunofluorescence

Five BAA fluorophores were selected to create a multicolor immunofluorescence image with laser scanning confocal microscopy (LSM), including **BAA-37a**, **BAA-22a**, **BAA-5a**, **BAA-2a**, and **BAA-39a** (Figure 3-3a). Density functional theory (DFT) calculations were

used to determine the highest occupied molecular orbital (HOMO) and lowest unoccupied molecular orbital (LUMO) energy levels of the five selected BAA fluorophores, which ranged from 2.36-2.64 (Table 3-1). As expected, BAA fluorophores with higher energy gaps tended to have lower maximum emission wavelengths and smaller Stokes shifts. These five BAA fluorophores covered a range of emission wavelengths and could be optimally excited using a single 561 nm laser. The minimum spectral separation between the five selected BAA fluorophores was 14 nm, facilitating simultaneous detection. The five BAA fluorophores were also selected based on their relatively high quantum yield and narrow FWHM (Figure 3-1) permitting five color simultaneous fluorescence microscopy with a single excitation laser (Figure 3-5).

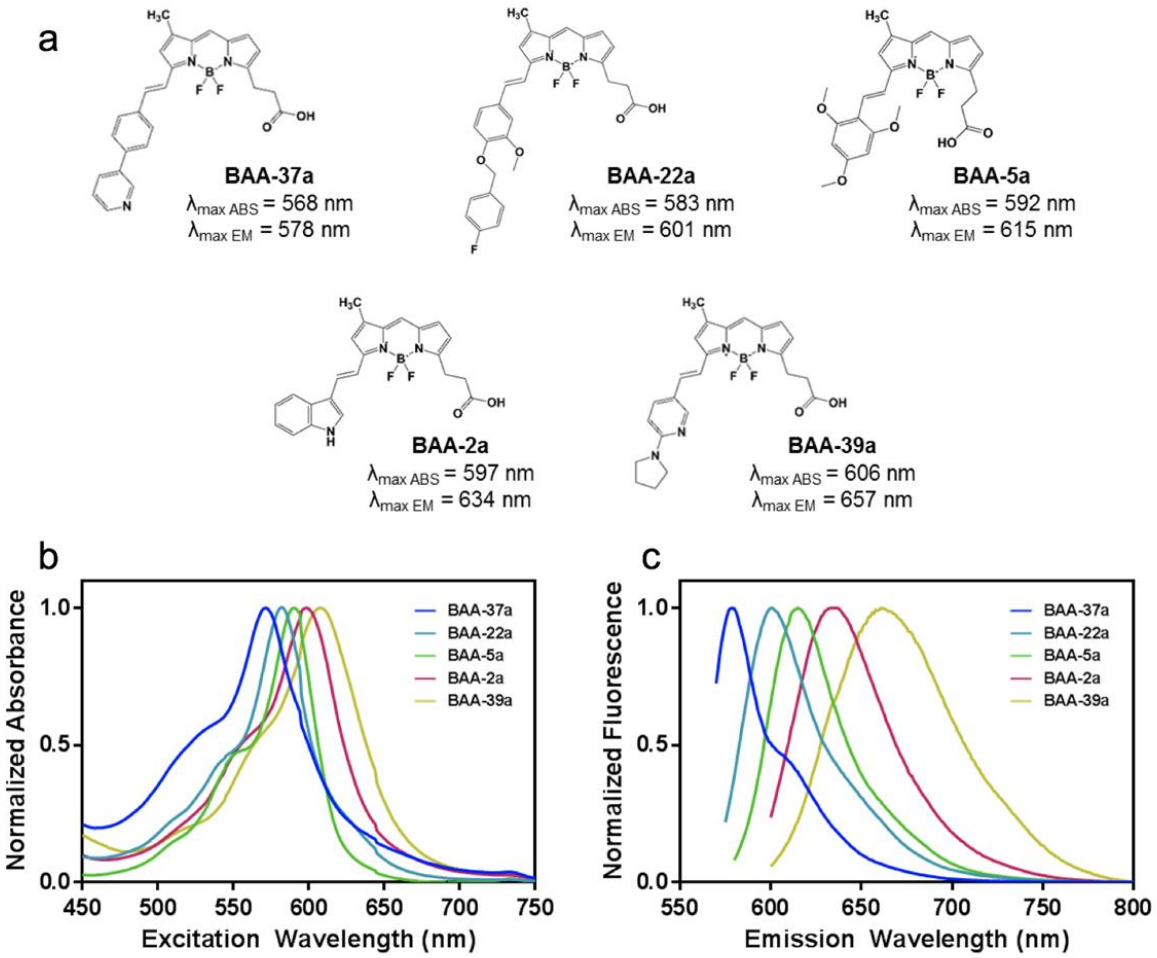

Figure 3-3 (a) Chemical structures of five selected BAA fluorophores with corresponding (b) absorbance spectra and (c) emission spectra.

Table 3-1 Stokes shifts and energy gaps for five selected BAA fluorophores.

Product	λmax ABS (nm)	λmax EM (nm)	Stokes Shift (nm)	HOMO (eV)	LUMO (eV)	Energy Gap (eV)
BAA-37a	568	578	10	-5.37	-2.72	2.64
BAA-22a	585	602	17	-5.27	-2.88	2.39
BAA-5a	592	615	23	-4.76	-2.34	2.42
BAA-2a	597	634	37	-4.87	-2.44	2.43
BAA-39a	606	657	51	-4.83	-2.46	2.36

3.3.5 Multicolor LSM Imaging with BAA Fluorophores

Five cellular structures in fixed U2OS cells were labeled with the selected BAA fluorophores and imaged using LSM. The carboxylic acid moiety of the five selected BAA fluorophores was converted to an N-hydroxysuccinimide (NHS) ester before conjugation to proteins used to target the five structures (Table 3-2). The nuclear membrane was labeled with **BAA-37a,** the mitochondrial membrane was labeled with **BAA-22a**, tubulin was labeled with **BAA-5a**, the extracellular membrane was labeled with **BAA-2a**, and vimentin was labeled with **BAA-39a**.

Each cellular structure was labeled and imaged individually to confirm the accuracy of the immunofluorescence staining (Figure 3-4a-e) and to assess the *in vitro* spectral emission of the five BAA fluorophores for linear unmixing of the multicolor image (Figure 3-4f). The LSM spectral emission data was collected in 8.9 nm steps and was similar to the emission spectral collected in DMSO (Figure 3-2b), with the *in vitro* LSM spectra of **BAA-5a** and **BAA-39a** blue shifted 7 nm and 15 nm, respectively. The five-color image, with all five structures labeled simultaneously, correctly identified each structure upon linear unmixing (Figure 3-5a-f). Two of the structures in the multicolor image, tubulin (Figure 3-5d) and extracellular membrane (Figure 3-5e), appeared to have less contrast in the multicolor image than their corresponding individually labeled images (Figure 3-4c and 3-4d). However, there was little to no cross talk between the channels based on the structures seen in each spectral image (Figure 3-5b-f).

Table 3-2 Cellular targets and proteins used for multicolor microscopy.

Structure	Primary Antibody or Protein	Secondary Antibody	BAA Fluorophore (Extinction Coefficient $M^{-1}cm^{-1}$)	Fluorophore:Protein Conjugation Ratio
Nuclear membrane	anti-lamin A (Abcam, ab8980)	goat anti-mouse IgG3 (msIgG3, Jackson ImmunoReseach, 115-005-209)	BAA-37a (3,500)	4.2:1
Mitochondrial membrane	anti-TOMM20 (Abcam, ab78547)	donkey anti-rabbit IgG (rbIgG, Jackson ImmunoResearch, 711-005-152)	BAA-22a (11,200)	2.4:1
Tubulin	anti-tubulin (Millipore, MAB1864)	donkey anti-rat (ratIgG, Jackson ImmunoResearch, 712-005-153)	BAA-5a (24,700)	4.4:1
Extracellular membrane	Wheat Germ Agglutinin (Vector Labs, L-102)	N/A	BAA-2a (126,200)	0.2:1
Vimentin	anti-vimentin (Millipore, AB5733)	donkey anti-chicken IgG (chIgG, Jackson ImmunoResearch, 703-005-155)	BAA-39a (2,600)	0.9:1

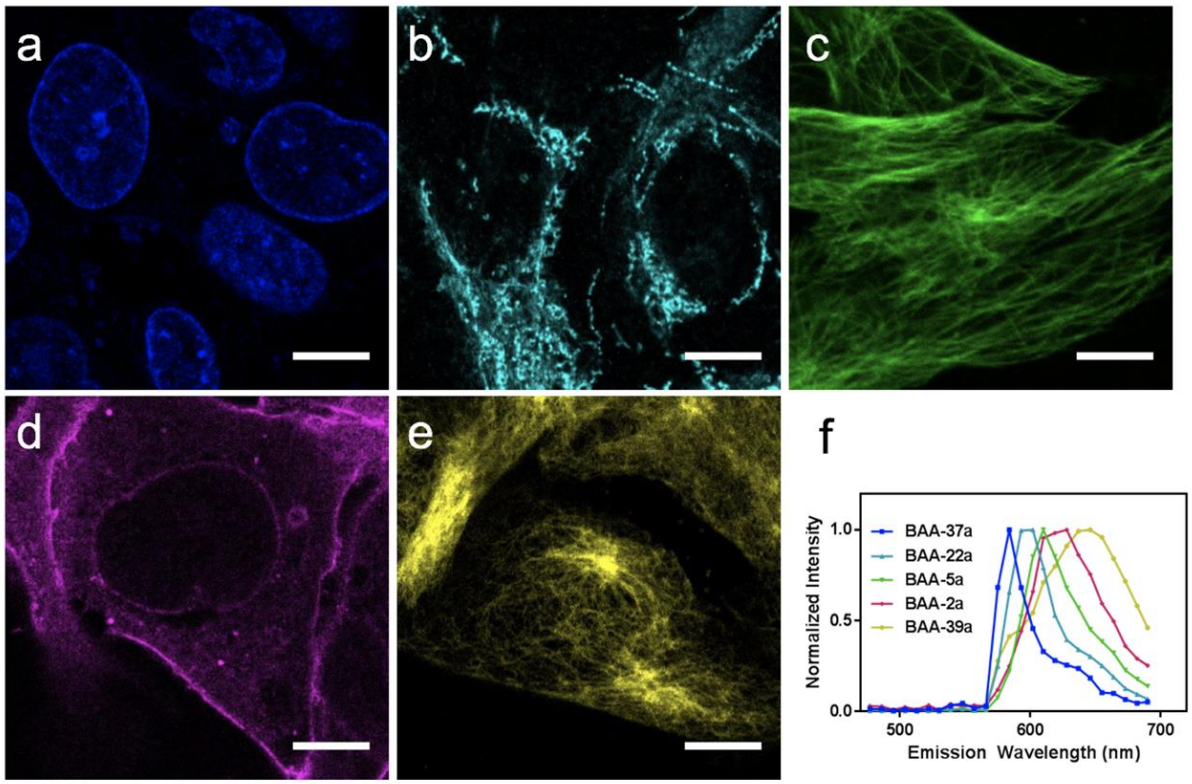

Figure 3-4 Immunofluorescence imaging of cellular structures labeled with individual BAA fluorophores and their LSM spectral data. Scale bar = 10 μm. (a) Nuclear membrane labeled with **BAA-37a**, (b) mitochondrial membrane labeled with **BAA-22a**, (c) tubulin labeled with **BAA-5a**, (d) extracellular membrane labeled with **BAA-2a**, and (e) vimentin labeled with **BAA-39a**.

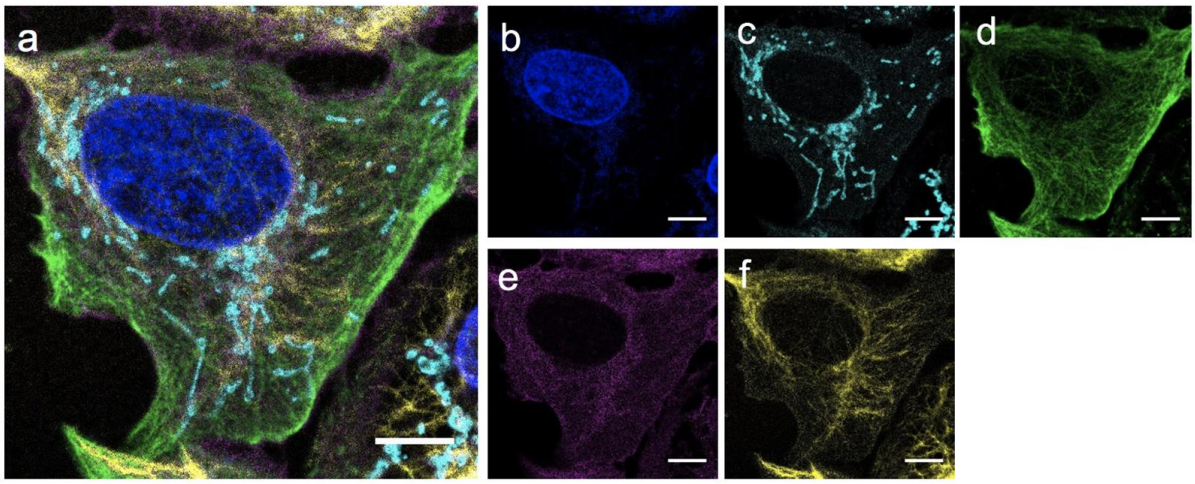

Figure 3-5 (a) Multicolor image created with five selected BAA fluorophores. Individual spectral channels of (b) nuclear membrane labeled with **BAA-37a**, (c) mitochondrial membrane labeled with **BAA-22a**, (d) tubulin labeled with **BAA-5a**, (e) extracellular membrane labeled with **BAA-2a**, and (f) vimentin labeled with **BAA-39a**. Scale bar = 10 μm.

3.4 DISCUSSION

In summary, we designed and developed a library of BODIPY-based fluorophores with varied length Stokes shifts compatible with conjugation to affinity reagents. The diverse styryl modifications of the core BODIPY structure extended its π-conjugation resulting in red-shifted maximum absorbance and emission wavelengths.[42,43] The exact maximum absorbance and emission of each BAA fluorophore was influenced by the electron withdrawing or donating tendency of the aromatic aldehyde used for styryl modification.[44,45] As expected, DFT calculations for the five select BAA fluorophores revealed that compounds with higher maximum absorbance and emission wavelengths tended to have less negative HOMO and LUMO energy levels, as well as longer Stokes shifts due to their smaller energy gaps (Table 3-1).

While the photophysical properties varied among the BAA fluorophores, most compounds were compatible with excitation by the 561 nm laser. This enabled production of a multicolor image utilizing the 561 nm laser as the exclusive excitation source by choosing fluorophores with different length Stokes shifts from our library including, **BAA-37a**, **BAA-22a**, **BAA-5a**, **BAA-2a**, and **BAA-39a**. Multicolor imaging demonstrated simultaneous detection of five cellular structures (Figure 3-5), facilitated by bright, spectrally distinct novel BODIPY fluorophores for detection and spectral separation using linear unmixing. Two of the structures, tubulin labeled with **BAA-5a** and the extracellular membrane labeled with **BAA-2a**, had lower contrast when imaged simultaneously (Figure 3-5d and 3-5e) than when imaged individually (Figure 3-4c and 3-4d), which was likely due to the loss of signal during spectral unmixing as their spectra overlapped considerably in comparison to the other fluorophores (Figure 3-4f). Replacing **BAA-2a** with a slightly more red-shifted fluorophore, such as **BAA-30a**, could potentially improve the image by further increasing the spectral separation.

While we created a multicolor image using five selected BAA fluorophores, additional fluorophores from the BAA library will be useful for future fluorescent imaging applications. Additional or alternative BAA fluorophores could be chosen to image not

only with the 561 nm laser line, but with other common laser lines such as 488 nm, 594 nm and 647 nm. Likewise, BAA fluorophores could be combined with commercially available fluorophores to create alternative color combinations and to increase the number of colors imaged. For example, using a combination of our five selected BODIPY fluorophores and conventional fluorophores, an 8-10 color simultaneous image could be generated.

In screening our BAA fluorophore library for organelle specificity in permeabilized, fixed cells, we found that most fluorophores labeled multiple areas of the cells, while unexpectedly some appeared to have organelle specificity (Figure 3-1, Tables S3-3 and S3-4). We found three BAA fluorophores that labeled the nucleus and nucleolar region, indicating that these potentially have a binding affinity for nucleic acids. We found others that appeared specific to particular vesicles, possibly localizing to the adiposomes, lysosomes or peroxisomes. Additionally, there were BAA fluorophores that appeared specific to a particular structure within the cytosol, possibly localizing to the cytoplasm, endoplasmic reticulum, Golgi complex or mitochondria. The precise location of the BAA fluorophores categorized as vesicle and cytosol is under further study.

Since the BAA fluorophores were synthesized from the same core BODIPY scaffold, differences in the localization can be attributed to their styryl modification. We investigated correlation between the localization of the BAA fluorophores to the three subcellular regions (nucleus and nucleolar, vesicle, and cytosol) and their molecular properties including LogD, number of rotatable bonds, number of hydrogen bond donors and acceptors, and the polar surface area. While the BAA fluorophores showed extensive variation in the values of their molecular properties, correlation between subcellular localization and any single property could not be elucidated. Further modeling is in progress to examine the BAA library structure activity relationship with multiple molecular properties to understand correlation between structure and subcellular localization.

In summary, we designed, synthesized and characterized a BODIPY-based library with applications in multicolor microcopy. We found that specific BAA fluorophores have

potential as organelle specific fluorophores for labeling fixed cells, but overall staining at immunofluorescence concentrations resulted in low SBR ideal for targeted imaging. We demonstrated the application of our BAA fluorophores to generate a five-color image over a narrow 60 nm range with a single laser used for excitation. Establishing spectral imaging with fluorophores in a compact spectral space will advance multicolor imaging, where our novel probes could be combined with conventional short Stokes shift fluorophores to generate an 8-10 color image.

3.5 METHODS

3.5.1 Materials

All commercially available starting materials were used without further purification unless otherwise stated. 4,4-Difluoro-5,7-Dimethyl-4-Bora-3a,4a-Diaza-s-Indacene-3-Propionic Acid (BODIPY FL) was used as the starting material for all novel fluorophore synthesis (Thermo Fisher Scientific, Waltham, MA). All novel BODIPY based fluorophores were synthesized through the addition of aromatic aldehyde building blocks (Thermo Fisher Scientific or Sigma-Aldrich, St. Louis, MO). Solid phase synthesis was performed using 2-Chlorotrityl chloride polystyrene (CTC-PS) 100-200 mesh resin (EMD-Millipore, Billerica, MA). Solvents for synthesis, purification and analysis were purchased at liquid chromatography/mass spectroscopy (LC/MS) purity grade (Thermo Fisher Scientific).

3.5.2 General Synthetic Procedure for BODIPY Aromatic Aldehyde (BAA) Fluorophore Library

BODIPY FL was loaded onto CTC-PS resin as follows: 500 mg of BODIPY FL in 17.2 ml of dichloromethane (DCM) was added to 5 g of CTC-PS resin in 14.9 ml of diisopropylethylamine (DIEA). The mixture was protected from light and mixed on a shaker overnight. The mixture was then washed using the following solvent systems: DCM, dimethyformamide (DMF), methanol (MeOH), DMF, and DMC, with three washes per solvent filtering the CTC-PS resin. BODIPY FL loaded CTC-PS resin was then dried

with ethyl ether, resulting in ~90% BODIPY FL retained on the resin, as quantified by absorbance spectroscopy using the extinction coefficient of BODIPY FL (80,000 $M^{-1}cm^{-1}$). BODIPY FL loaded CTC-PS resin (100 mg in 3 ml of 1:1 dimethysulfoxide (DMSO):acetonitrile (ACN)) and 15 equivalents of the selected aromatic aldehyde (Table S1, 0.45 mmol in 1 ml 1:1 DMSO:ACN) were mixed with 65 equivalents of acetic acid (105 µl, 2 mmol) and 65 equivalents of pyrrolidine (150 µl, 2 mmol) at 85° C for 15 min. The resin was washed 3x with each of the following solvents: DCM, DMF, DCM, DMF, DCM, and DMF, followed by washing 3x with ethyl ether. The synthesized BODIPY aromatic aldehyde (BAA) fluorophores were then cleaved with 0.5% trifluoroacetic acid (TFA) in DCM for 10 min at room temperature. The BAA fluorophores were purified using HPLC (Agilent 1250 Infinity HPLC) with a C18 column (150 mm x 21.2 mm) using solvents A: H_2O-Formic Acid (CH_2O_2): 99.9:0.1 and B: ACN-CH_2O_2: 99.9:0.1, with gradient 90% A to 50% A (6 min), gradient 50% B to 10% B (14 min) at a flowrate of 8 ml/min. The purified samples were lyophilized (Labconco, Kansas City, MO).

3.5.3 BAA Library Structural & Purity Assessment

The mass to charge (m/z) ratio and purity of all BAA fluorophores was assessed by tandem LC/MS (Agilent 6244 TOF LC/MS with diode array detector VL+) using a C18 column (4.6 mm x 50 mm), where purity was determined through area under the curve analysis of the absorbance at 280 nm (Table S3-1). Marvin Sketch was used to calculate physiochemical properties of the BAA library (Table S3-4).[46] Molecular orbital calculations were performed using density functional theory (DFT) at B3LYP/6-31G level. The five BAA fluorophores selected for multicolor microscopy were structurally confirmed using proton (^1H) NMR (Bruker ARK400, Billerica, MA) in DMSO-D6 solvent with 256 scans.

3.5.4 BAA Library Optical Property Measurements

Spectroscopic characterization was performed in DMSO in black polystyrene 96 well plates with clear bottoms (Corning, Corning, NY) using a SpectraMax M5 Microplate reader (Molecular Devices, Sunnyvale, CA). Analysis included solvent corrected

measurement of absorbance spectra from 400-800 nm and calculation of maximum absorbance wavelength, measurement of fluorescence emission spectra using the maximum absorbance for excitation from 10 nm above the excitation to 800 nm, calculation of the maximum fluorescence emission wavelength, measurement of quantum yield, and calculation of the full-width-at half maximum (FWHM) (Table S2). Quantum yields (Φ_{fl}) were determined by comparing the area under the emission spectrum of the BAA fluorophore to a reference fluorophore solution, Fluorescein, Rhodamine B, or Cresyl violet, at three concentrations using equation 3-1, where *Grad* represents the gradient from the plots of integrated fluorescence intensity vs. absorbance at three concentrations and η is the refractive index of the solvent.[47] Fluorescein in 0.1 M sodium hydroxide (NaOH) (Φ_{fl} = 0.91)[48] was used as the reference for all BAA fluorophores with a maximum absorbance of 480-510 nm. For quantum yield measurements using Fluorescein, excitation at 470 nm was used with the emission spectra integrated from 490-800 nm. Rhodamine B in ethanol (Φ_{fl} = 0.70)[49,50] was used as the reference for all BAA fluorophores with a maximum absorbance of 511-595 nm. For quantum yield measurements using Rhodamine B, excitation at 525 nm was used with the emission spectra integrated from 545-800 nm. Cresyl violet in methanol (Φ_{fl} = 0.54)[49] was used as the reference for BAA fluorophores with a maximum absorbance above 595 nm. For quantum yield measurements using Cresyl violet, an excitation at 570 nm was used with the emission spectra integrated from 590-800 nm.

$$\Phi_{fl}^{sample} = \Phi_{fl}^{reference}\left(\frac{Grad^{sample}}{Grad^{reference}}\right)\left(\frac{\eta^{sample}}{\eta^{reference}}\right)^2 \qquad (3\text{-}1)$$

3.5.5 Cell Culture

The U2OS osteosarcoma human cell line was cultured in Dulbecco's Modified Eagle Medium (DMEM) without phenol red (Thermo Fisher Scientific) supplemented with 10% fetal bovine serum (FBS, VWR, Radnor, PA) and 1% Penicillin-Streptomycin-Glutamine (Thermo Fisher Scientific) at 37° C and 5% CO_2. Cells were plated in a 96-well glass

bottom plates (Cellvis, Mountain View, CA) and incubated for 3 days to reach ~50% confluency prior to staining and imaging studies.

3.5.6 BAA Library Staining for *In Vitro* Organelle Specificity and Signal-to-Background Ratio (SBR) Calculations

Cells were pre-extracted with 0.5% Triton X-100 in 1x phosphate buffered saline (PBS) for 20 s, fixed with 0.4% glutaldehyde (GA, Electron Microscopy Science) and 0.25% Triton X-100 in PBS for 90 s, washed again with PBS and finally fixed with 3% GA in PBS for 15 min. Cells were washed with PBS (3 x 5 min), reduced with 10 mM sodium borohydride for 10 min, washed again with PBS (3 x 5 min), and blocked with 5% bovine serum albumin (BSA) in PBS for 10 min. BAA fluorophores were diluted to 10 µM in PBS for organelle screening and 100 nM for SBR screening. The diluted BAA fluorophores were incubated with the permeabilized/fixed cells for 30 min after which the fluorophore was removed and the cells were washed with PBS (3 x 5 min). Cells were counterstained with 4',6-Diamidine-2'-phenylindole dihydrochloride (DAPI) at 1 µg/ml for 5 min and washed with PBS (3 x 5 min) prior to imaging for SBR measurements.

Cell imaging was completed with a Zeiss AxioObserver (Carl Zeiss Microscopy GmbH, Jena, Germany), using a PhotoFluor II (89 North, Burlington, VT) light source and 63x oil immersion objective. Samples were imaged with the optimal bandpass excitation and emission filter sets (Chroma Technology) based the BAA optical property measurements: (1) 470 ± 20 nm excitation and 525 ± 25 nm emission (2) 545 ± 12.5 nm excitation and 605 ± 35 nm emission, or (3) 620 ± 30 nm excitation and 700 ± 37.5 nm emission. Organelle specificity images were collected at exposure times ranging from 1.5-10 sec. Control images of unlabeled cells were collected at the same exposure times to confirm fluorescence was from BAA fluorophore staining and not from autofluorescence alone. Images for SBR analysis were collected at 1.5, 5, and 10 sec exposure times. Two images were obtained for each exposure time, one image to capture the DAPI using 405 ± 20 nm excitation and 470 ± 20 nm emission, and a second image to capture the BAA fluorophore

using its appropriate filter set. Different regions of interest were imaged for each exposure time to ensure photobleaching was not affecting SBR measurements.

Image analysis was performed using QiTissue software (Quantitative Imaging Systems, Pittsburgh, PA). All images were first corrected for camera or scanning sensor bias, as well as dark current introduced at longer exposure times. These values were calculated and subtracted to allow proper computation of the ratios described below. The DAPI images enabled automatic detection of cell nuclei and an estimated location of the surrounding cytoplasm. Regular thresholding would introduce a measurement bias in situations with varied staining results. Instead, non-linear preprocessing, and a-priori knowledge based detection was used to define the organelles, regardless of their variation in intensities. This resulted in a reliable estimate of the area occupied by the target of labeling protocol for each type of image. The calculation then proceeded to determine the average intensity of area occupied (I_o) and the average intensity of the background (I_b) for each sample, and baseline intensity for each filter set *f* with no sample present (I_{zf}). The SBR at each exposure time was calculated as $[I_o - I_{zf}]/[ave(I_{bf}) - I_{zf}]$. The final SBR reported was calculated as the average SBR measured across the three exposure times for each sample.

3.5.7 Protein & Antibody Labeling with BAA Fluorophores

BAA fluorophores 2a, 5a, 22a, 37a, and 39a were selected for multicolor cell imaging studies based on their optical property measurement. These five BAA fluorophores were converted from their carboxylate form to an amine-reactive NHS ester prior for protein conjugation, detailed as follows. BAA fluorophores were diluted into DMF with 2.2 equivalents of 1-[Bis(dimethylamino)methylene]-1H-1,2,3-triazolo[4,5-b]pyridinium 3-oxid hexafluorophosphate (HATU) and 5.8 equivalents of DIEA and mixed for 30 min. Four equivalents of N-hydroxysulfosuccinimide (sulfo-NHS) were added and mixed for an additional 60 min. The reaction was diluted with ethyl acetate (2 ml) and washed with water (500 µl) to separate NHS ester functionalized BAA fluorophore from the reactants. The NHS ester functionalized BAA fluorophores in ethyl acetate were dried by

lyophilization. LC/MS analysis confirmed greater than 90% NHS conversion for each BAA fluorophore.

Five targets were selected for multicolor microscopy and were labeled using BAA fluorophores conjugated to the appropriate proteins (Table 1). Conjugates were made using standard NHS ester reaction conditions, explained as follows. The protein or antibody was buffered exchanged into 1x PBS, pH adjusted to 8.3 with 1 M sodium hydroxide, and mixed with the NHS ester functionalized BAA fluorophore in a 3:1 fluorophore to protein/antibody molar ratio. The mixture was rocked gently at room temperature protected from light for 3 h. The conjugation reactions were purified using fast protein liquid chromatography (FPLC, NGC Quest 10 Plus Chromatography System, Bio-Rad, Hercules, CA) by size exclusion (P6 gel filtration column, 40 mm x 12.6 mm, Bio-Rad). Final fluorophore concentration, protein concentration and conjugation ratios were determined using absorbance spectroscopy (Table 3-1).

3.5.8 Immunofluorescence Staining of Cellular Structures

Live cells were incubated with **BAA-2a**-WGA to label the cell membrane at 20 µg/ml WGA in PBS for ~10 s before adding paraformaldehyde (PFA, Electron Microscopy Science) to a final concentration of 2% PFA and incubating for 10 min at 37° C and 5% CO_2. The media/fixative mixture was exchanged with fresh 2% PFA and incubated for an additional 20 min at 37° C and 5% CO_2. Cells were pre-extracted with 0.5% Triton X-100 in PBS for 20 s, fixed with 0.4% GA and 0.25% Triton X-100 in PBS for 90 s, washed with PBS and finally fixed with 3% GA in PBS for 15 min. Cells were then incubated with primary antibodies in 5% BSA for overnight at 4° C protected from light at 10 $\mu g ml^{-1}$ anti-lamin A, 10 $\mu g ml^{-1}$ anti-TOMM20, 10 $\mu g ml^{-1}$ anti-tubulin, and 6.6 $\mu g ml^{-1}$ anti-vimentin. Cells were washed with PBS (3 x 5 min) then incubated with 30 $\mu g ml^{-1}$ **BAA-37a**-msIgG3, 2 $\mu g ml^{-1}$ **BAA-22a**-rbIgG, 20 $\mu g ml^{-1}$ **BAA-5a**-ratIgG, and 50 $\mu g ml^{-1}$ **BAA-39a**-chIgG in 5% BSA for 30 min at room temperature protected from light. The stained cells were then washed with PBS (3 x 5 min) and post-fixed with 4% PFA in PBS for 10 min before a final PBS wash. For images with single BAA fluorophores, cells without **BAA-2a**-WGA were used.

3.5.9 Confocal Laser Scanning Microscopy

Images were acquired using a Zeiss LSM 880 with Airyscan using a plan-apochromatic 63x (NA = 1.4) oil immersion objective. Images were collected in lambda mode with the following settings: laser 561 nm (DPSS 561-10), 0.05%; beam splitter: MBS 458/561; filter: 410-695 nm; pixel dwell: 48.8 µs, average: line 1; master gain: 900; pinhole size: 60 um; and acquisition area: 1384 x 1384 pixels, 16 bit. Spectral data from 410-695 nm was acquired using samples labeled with individual BAA fluorophores. Zen imaging software (Zeiss) was used for spectral unmixing and FIJI ImageJ was used to process the final images.[51]

3.6 SUPPLEMENT

Supplemental Table S3-1 Chemical structures and purity data for BAA library.

Product	Aromatic Aldehyde	Final Structure	m/z calc	m/z exp	RT (min)	Purity (%)
BAA-1b	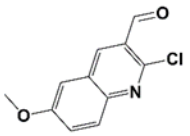	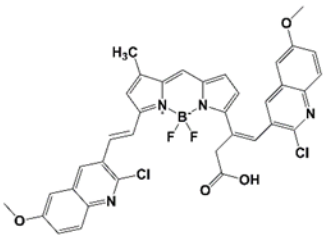	698.15	699.15	7.83	92
BAA-2a	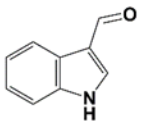	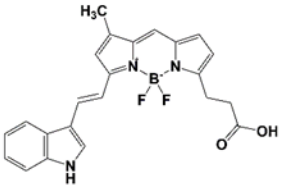	419.16	400.16[a]	7.66	>99
BAA-3a	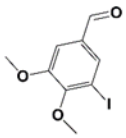	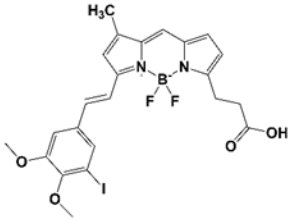	566.07	567.95	8.07	98
BAA-3b	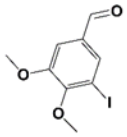	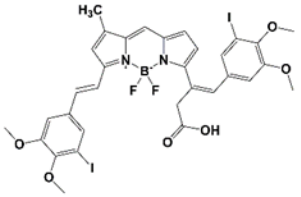	840.02	863.25[b]	8.21	97
BAA-4a	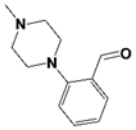	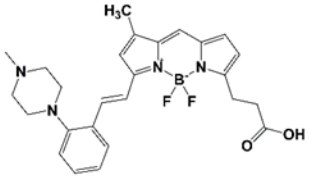	478.24	479.24	6.02	>99
BAA-5a	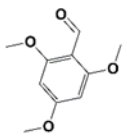	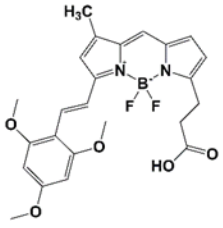	470.18	471.19	8.26	>99

Product	Aromatic Aldehyde	Final Structure	m/z calc	m/z exp	RT (min)	Purity (%)
BAA-6a	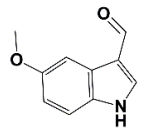	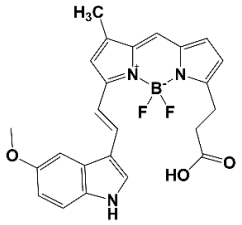	449.17	472.18[b]	7.69	82
BAA-7a	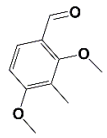	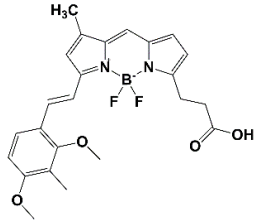	454.19	477.27[b]	8.64	83
BAA-7b	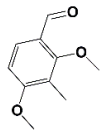	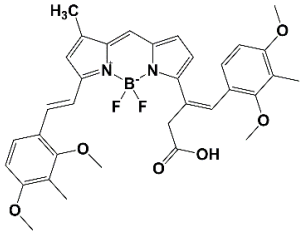	616.26	617.26	7.32	88
BAA-8a	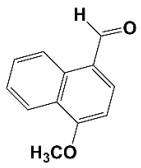	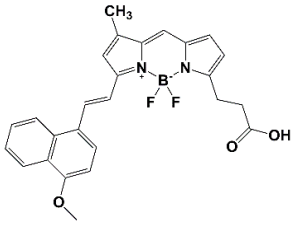	460.18	461.19	8.31	80
BAA-9a	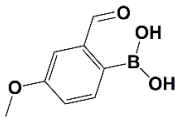	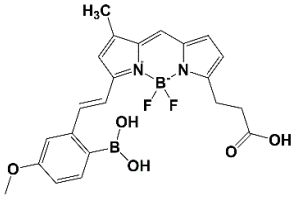	454.17	455.13	8.15	92
BAA-10b	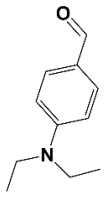	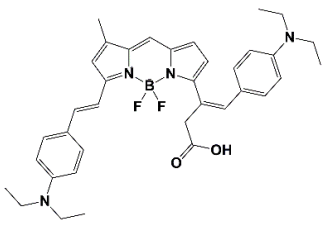	610.33	611.35	9.45	>99
BAA-11a	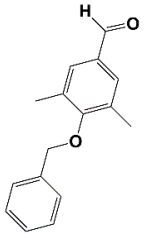	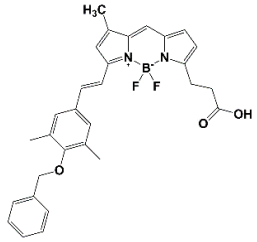	514.22	515.22	8.98	91

Product	Aromatic Aldehyde	Final Structure	m/z calc	m/z exp	RT (min)	Purity (%)
BAA-12a	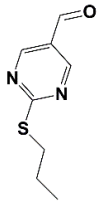	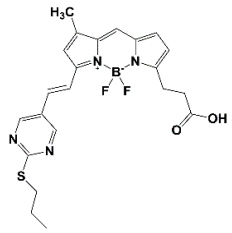	456.16	474.19[c]	7.69	88
BAA-13a	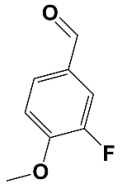	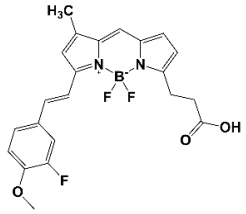	428.15	429.15	7.28	90
BAA-14a	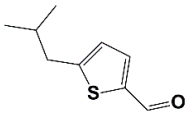	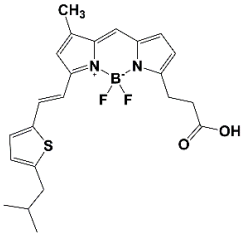	442.17	465.16[b]	9.153	83
BAA-15a	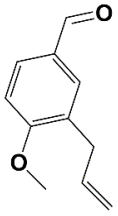	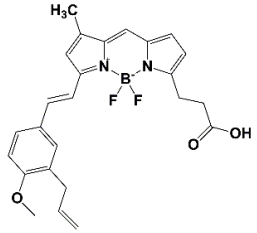	450.19	451.19	8.83	96
BAA-16a	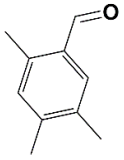	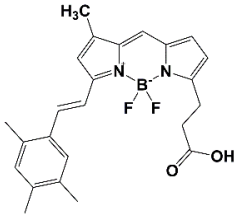	422.2	445.19[b]	9.08	98
BAA-17a	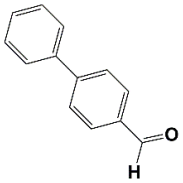	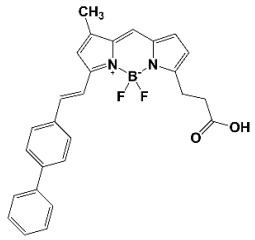	456.18	479.17[b]	9.09	85
BAA-18a	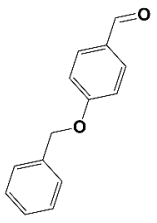	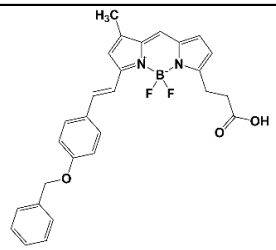	486.19	509.18[b]	8.94	92

Product	Aromatic Aldehyde	Final Structure	m/z calc	m/z exp	RT (min)	Purity (%)
BAA-19a	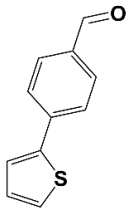	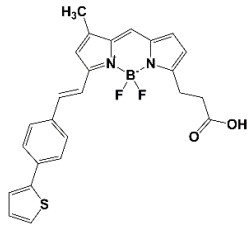	462.14	485.13[b]	8.94	96
BAA-20a	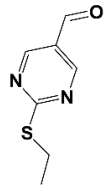	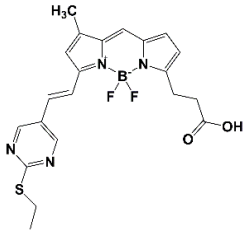	442.14	443.15	8.07	98
BAA-21a	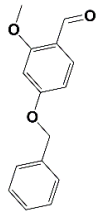	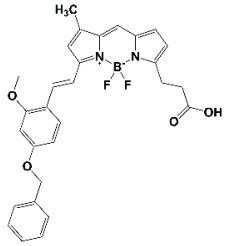	516.2	497.21[a]	9.13	95
BAA-21b	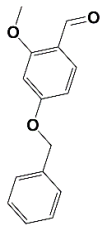	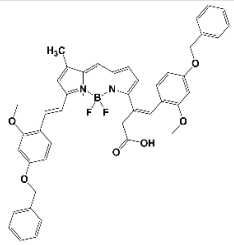	740.29	741.29	7.82	92
BAA-22a	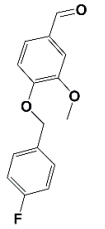	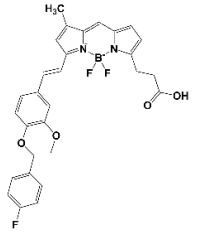	534.19	515.20[a]	8.65	94
BAA-22b	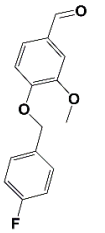	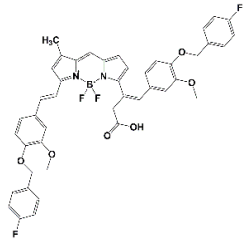	776.27	777.28	7.51	90
BAA-23a	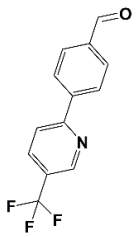	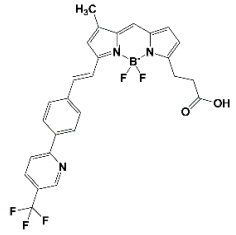	525.16	526.18	9.05	>99

Product	Aromatic Aldehyde	Final Structure	m/z calc	m/z exp	RT (min)	Purity (%)
BAA-23b	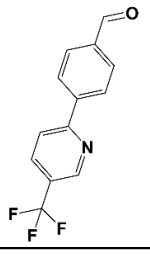	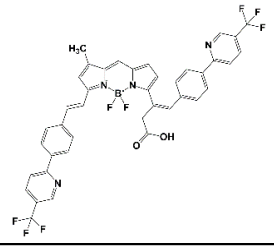	758.21	739.13[a]	7.93	89
BAA-24b	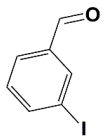	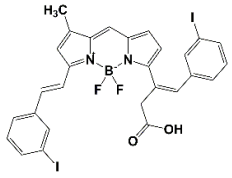	719.98	700.98[a]	7.46	94
BAA-25a	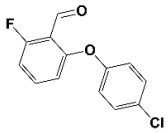	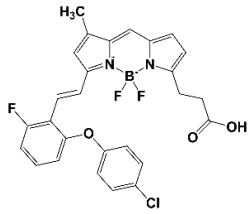	524.73	547.12[b]	9.30	93
BAA-25b	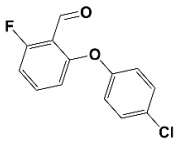	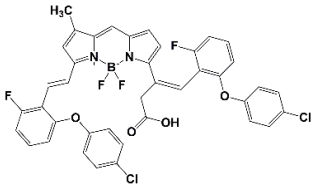	756.14	757.15	7.88	95
BAA-26b	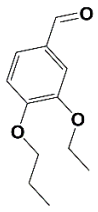	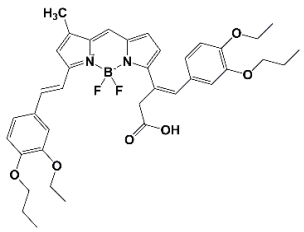	672.32	673.33	7.56	98
BAA-27b	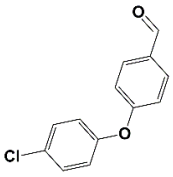	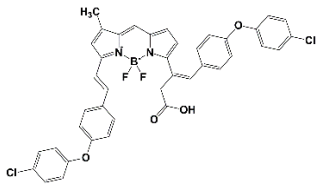	720.16	683.22[d]	7.19	97
BAA-28a	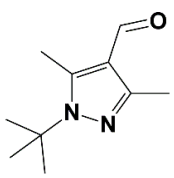	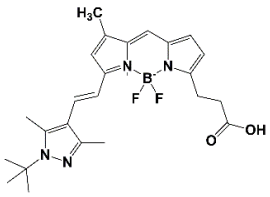	454.24	435.28[a]	6.69	88

Product	Aromatic Aldehyde	Final Structure	m/z calc	m/z exp	RT (min)	Purity (%)
BAA-28b	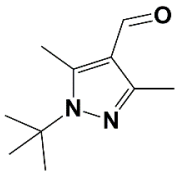	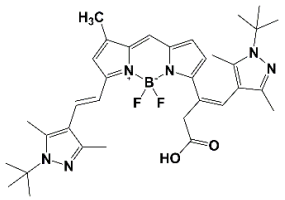	616.35	617.37	6.99	97
BAA-29b	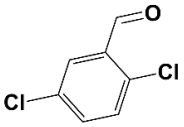	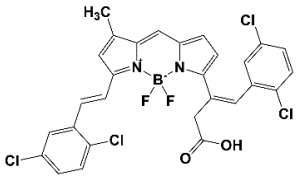	604.03	605.03	8.14	86
BAA-30a	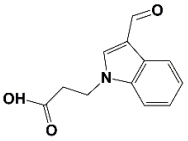	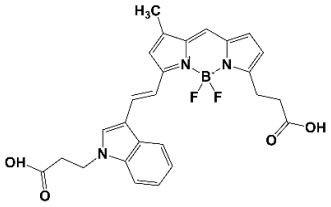	491.18	492.19	7.41	96
BAA-31b	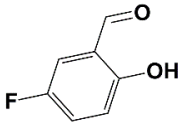	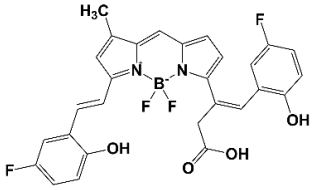	536.28	497.15[d]	6.34	94
BAA-32a	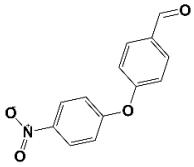	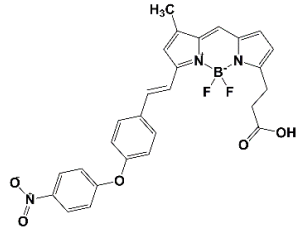	517.16	478.15[d]	8.77	>99
BAA-33a	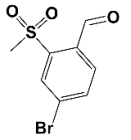	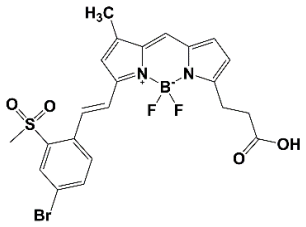	536.04	559.02[b]	7.94	98
BAA-34b	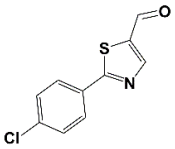	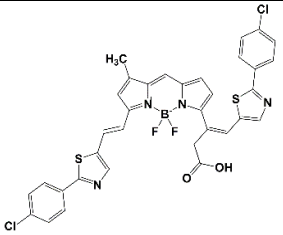	702.07	683.06[a]	7.69	94

Product	Aromatic Aldehyde	Final Structure	m/z calc	m/z exp	RT (min)	Purity (%)
BAA-35b	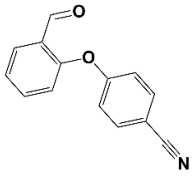	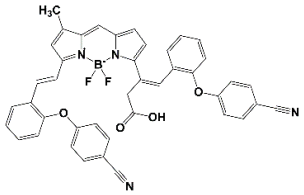	702.22	703.15	8.49	86
BAA-36b	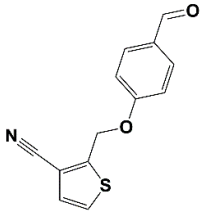	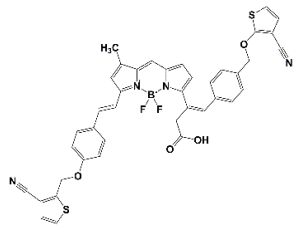	742.17	743.18	8.16	94
BAA-37a	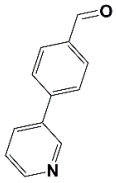	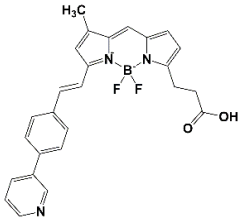	457.18	438.18[a]	5.75	88
BAA-37b	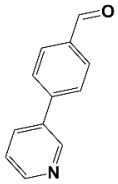	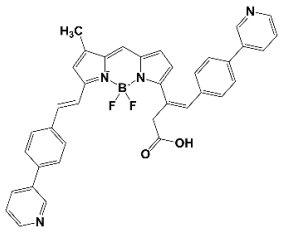	622.24	623.24	5.78	>99
BAA-38a	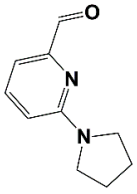	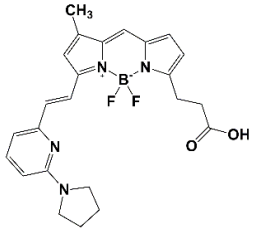	450.2	451.21	6.28	99
BAA-39a[g]	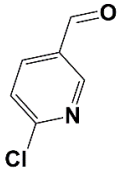	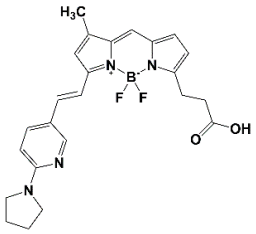	415.11	451.21[g]	5.99	94
BAA-40b	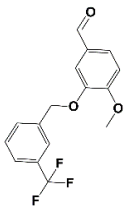	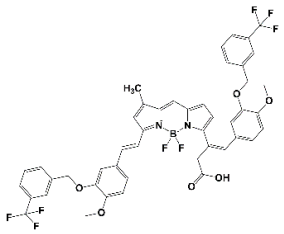	876.26	877.27	7.96	89

Product	Aromatic Aldehyde	Final Structure	m/z calc	m/z exp	RT (min)	Purity (%)
BAA-41b	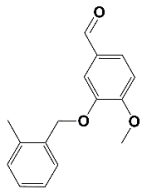	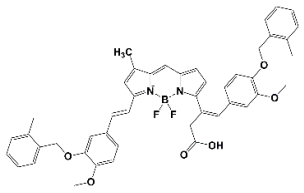	768.32	769.33	7.61	94
BAA-42a	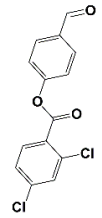	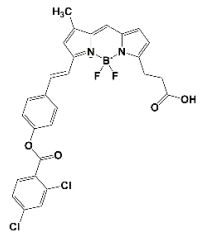	568.09	501.17[e]	6.17	82
BAA-43a	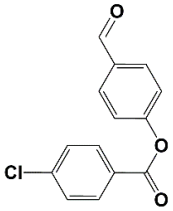	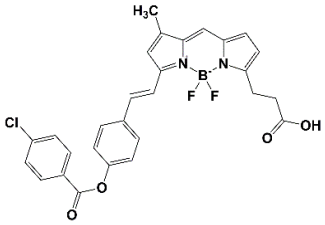	534.13	501.17[f]	6.13	94
BAA-44b	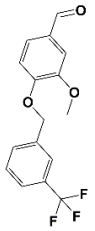	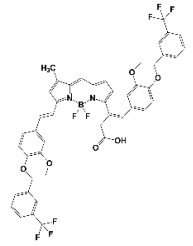	876.26	877.27	8.15	92
BAA-45a	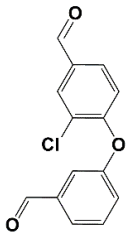	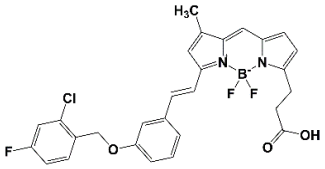	538.75	562.14[b]	9.29	>99
BAA-45b	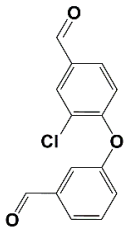	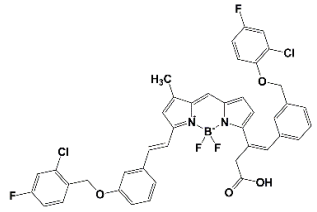	784.17	785.17	8.24	96
BAA-46b	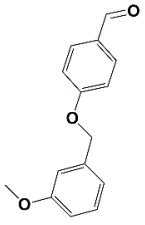	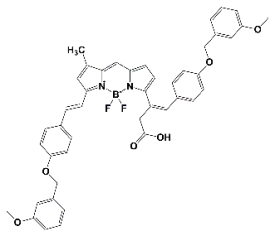	740.29	741.28	7.69	94

Product	Aromatic Aldehyde	Final Structure	m/z calc	m/z exp	RT (min)	Purity (%)
BAA-47a	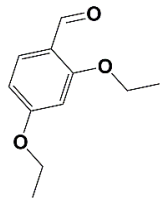	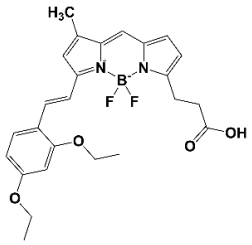	468.2	491.20[b]	8.62	94
BAA-48a	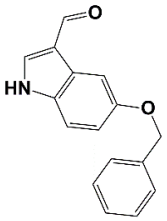	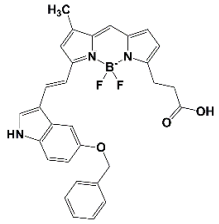	525.2	548.19[b]	8.24	>99
BAA-49b	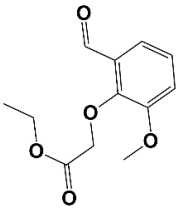	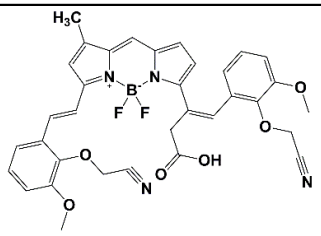	638.21	619.21[a]	6.58	>99
BAA-50a	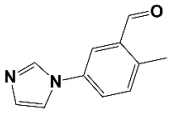	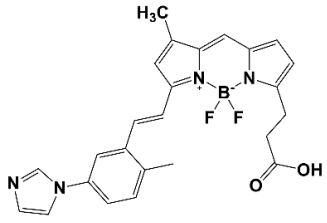	460.19	483.18[b]	8.07	>99
BAA-50b	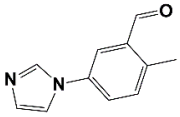	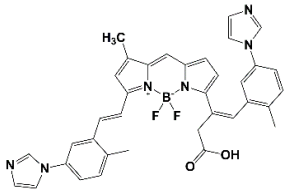	628.26	629.25	6.94	>99
BAA-51a	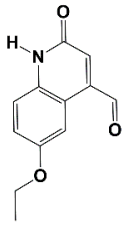	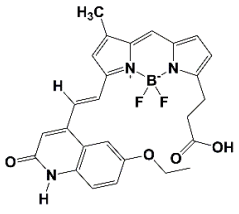	491.18	514.16[b]	7.59	89
BAA-52a	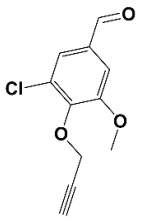	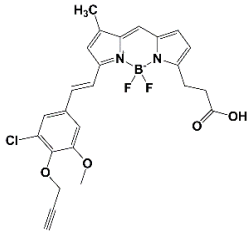	498.13	499.12	7.86	83

Product	Aromatic Aldehyde	Final Structure	m/z calc	m/z exp	RT (min)	Purity (%)
BAA-53a	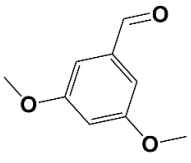	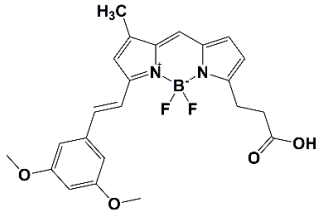	440.17	441.17	7.57	>99
BAA-54a	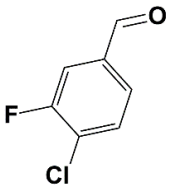	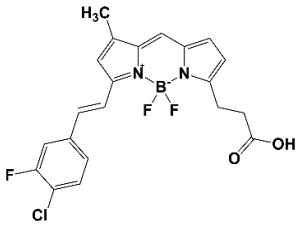	432.1	433.09	7.98	89
BAA-55a	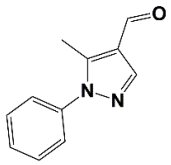	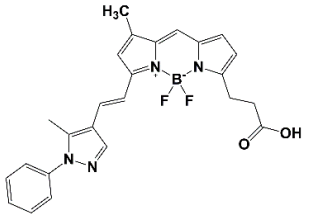	460.19	461.18	7.30	>99
BAA-55b	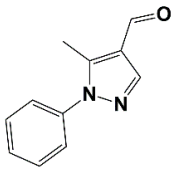	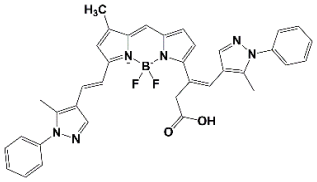	628.26	629.26	6.89	89
BAA-56a	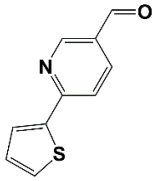	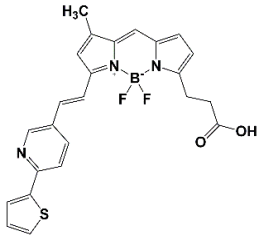	463.13	464.13	5.87	>99
BAA-56b	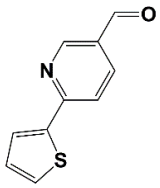	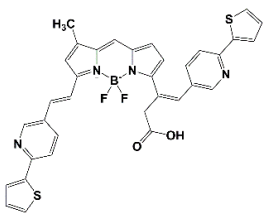	634.15	635.15	7.84	84
BAA-57a	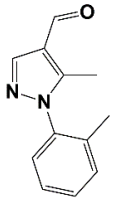	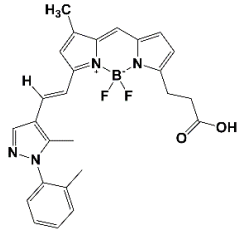	474.2	475.21	6.10	85

Product	Aromatic Aldehyde	Final Structure	m/z calc	m/z exp	RT (min)	Purity (%)
BAA-57b	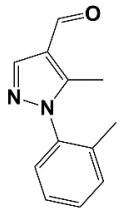	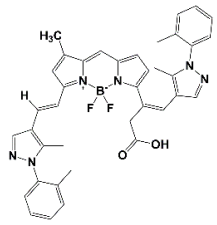	656.29	657.30	8.01	>99
BAA-58a	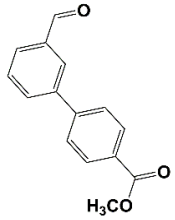	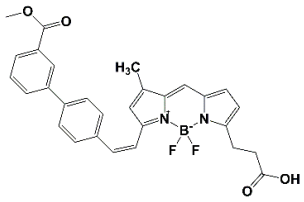	514.19	515.18	8.20	>99
BAA-59a	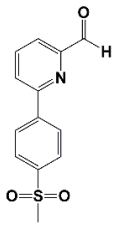	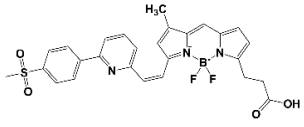	535.15	553.16[c]	7.37	96
BAA-60b	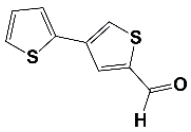	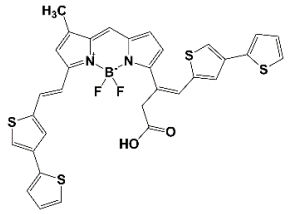	644.07	645.08	8.11	99
BAA-61a	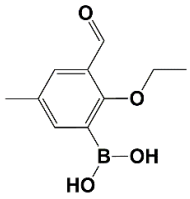	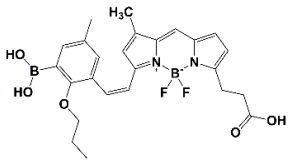	496.22	497.21	7.32	98
BAA-62a	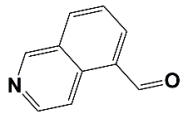	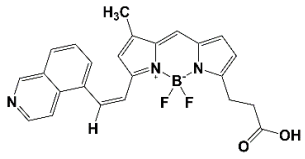	431.16	449.16[c]	6.81	>99
BAA-63a	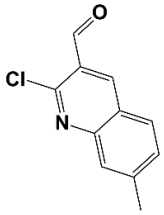	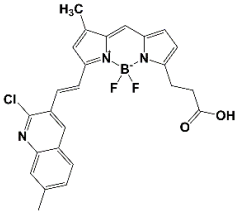	479.14	502.15[b]	7.05	93

Product	Aromatic Aldehyde	Final Structure	m/z calc	m/z exp	RT (min)	Purity (%)
BAA-64a	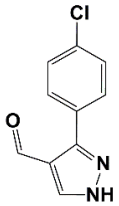	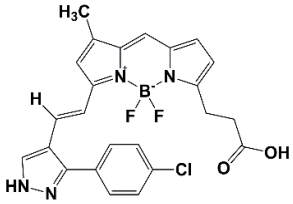	480.13	481.11	7.50	91
BAA-65a	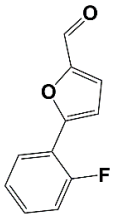	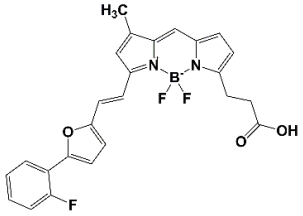	464.15	427.14[d]	8.82	88
BAA-66a	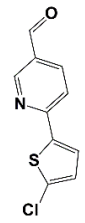	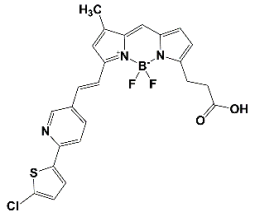	497.09	498.10	9.09	93
BAA-67a	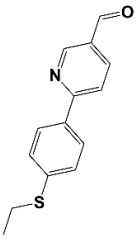	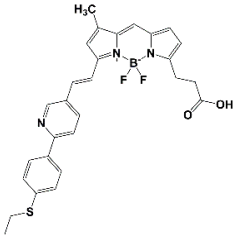	517.18	518.18	9.02	92
BAA-68a	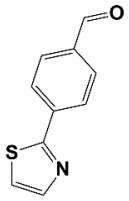	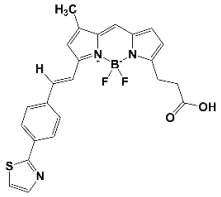	463.13	464.14	8.27	>99
BAA-69a	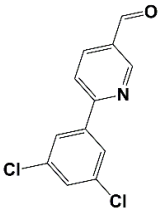	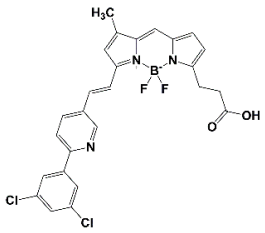	525.1	526.09	9.08	>99
BAA-70a	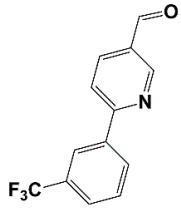	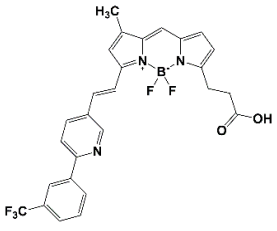	525.16	526.18	8.95	99

Product	Aromatic Aldehyde	Final Structure	m/z calc	m/z exp	RT (min)	Purity (%)
BAA-71a	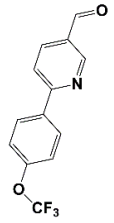	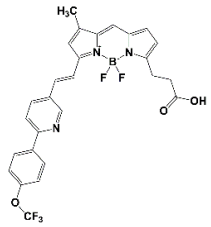	541.16	542.17	9.06	>99
BAA-72a	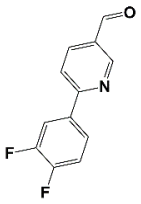	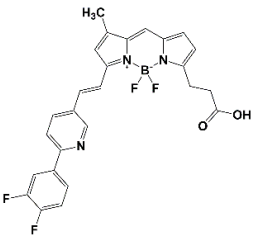	493.16	511.17[c]	8.13	98
BAA-73a	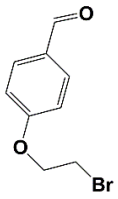	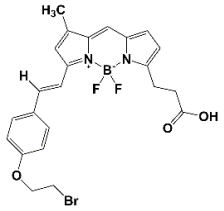	502.09	503.08	7.95	>99
BAA-74a	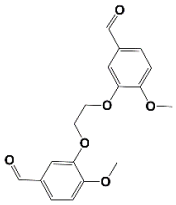	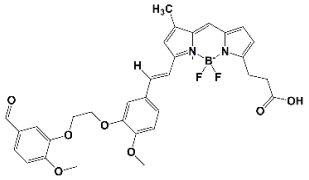	604.22	627.21[b]	8.02	92
BAA-74b	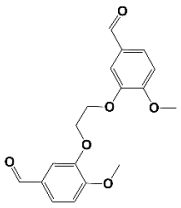	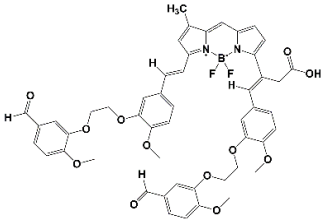	916.32	897.32[a]	7.01	94
BAA-75a	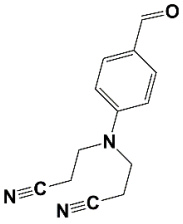	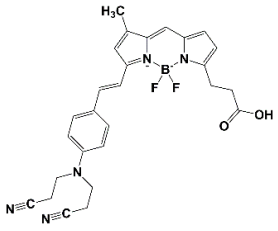	501.21	482.22[a]	10.99	>99
BAA-75b	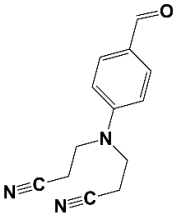	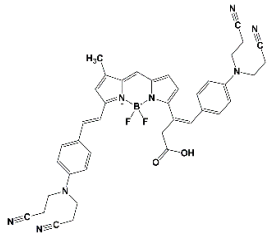	710.31	711.32	6.38	94

Product	Aromatic Aldehyde	Final Structure	m/z calc	m/z exp	RT (min)	Purity (%)
BAA-76a	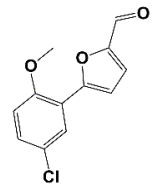	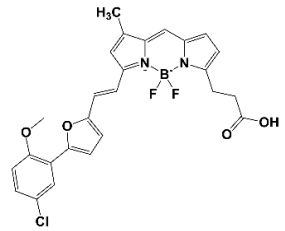	510.13	491.13[a]	90.31	98
BAA-77a	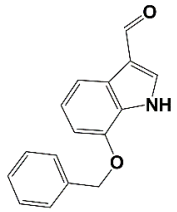	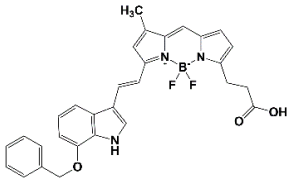	525.2	506.21[a]	8.52	99
BAA-78a	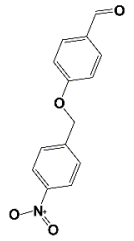	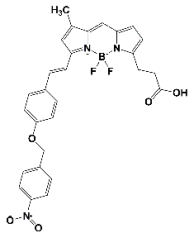	531.18	512.18[a]	8.72	>99
BAA-78b	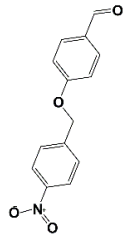	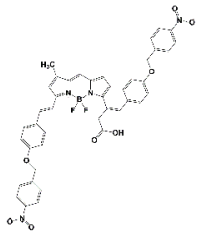	770.24	771.24	7.73	98
BAA-79a	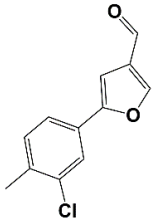	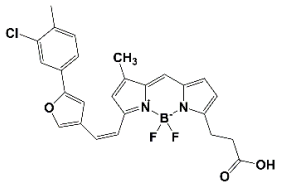	494.14	457.13[d]	9.421	91

Supplemental Table S3-2 Spectroscopic properties of BAA library.

Product	λmax ABS (nm)	λmax EM (nm)	Stokes Shift (nm)	Φ_{fl}	FWHM
BAA-1b	580	597	17	0.62	40
BAA-2a	601	635	34	0.62	57
BAA-3a	569	579	10	0.61	31
BAA-3b	574	587	13	0.70	34
BAA-4a	581	600	19	0.43	56
BAA-5a	592	615	23	0.83	47
BAA-6a	609	643	34	0.18	64
BAA-7a	582	600	18	0.29	63
BAA-7b	581	600	19	0.43	56
BAA-8a	594	623	29	0.50	61
BAA-9a	569	579	10	0.35	32
BAA-10b	632	714	82	0.01	102
BAA-11a	575	589	14	0.86	33
BAA-12a	589	616	27	0.10	88
BAA-13a	576	586	10	0.19	44
BAA-14a	594	607	13	0.44	70
BAA-15a	581	597	16	0.42	39
BAA-16a	552	610	58	0.22	78
BAA-17a	579	591	12	0.59	42
BAA-18a	577	593	16	0.65	37
BAA-19a	582	595	13	0.64	35
BAA-20a	577	585	8	0.15	31
BAA-21a	585	611	26	0.51	46
BAA-21b	588	608	20	0.54	50
BAA-22a	585	602	17	0.39	49
BAA-22b	582	601	19	0.27	46
BAA-23a	592	603	11	0.23	30
BAA-23b	580	588	8	0.19	32
BAA-24b	570	579	9	0.29	32
BAA-25a	571	580	9	0.19	32
BAA-25b	572	580	8	0.18	32
BAA-26b	582	604	22	0.30	51
BAA-27b	575	588	13	0.33	35
BAA-28a	480	592	112	0.04	52
BAA-28b	580	598	18	0.58	43
BAA-29b	569	580	11	0.13	37
BAA-30a	607	643	36	0.43	58

Product	λmax ABS (nm)	λmax EM (nm)	Stokes Shift (nm)	Φ_{fl}	FWHM
BAA-31b	576	588	12	0.28	34
BAA-32a	574	584	10	0.23	32
BAA-33a	575	587	12	0.15	35
BAA-34b	570	581	11	0.96	31
BAA-35b	571	580	9	0.25	32
BAA-36b	579	592	13	0.35	37
BAA-37a	568	578	10	0.54	55
BAA-37b	569	578	9	0.55	30
BAA-38a	579	581	2	0.07	33
BAA-39a	606	657	51	0.19	79
BAA-40b	583	601	18	0.26	45
BAA-41b	582	602	20	0.36	47
BAA-42a	570	580	10	0.36	30
BAA-43a	569	579	10	0.45	31
BAA-44b	582	600	18	0.28	43
BAA-45b	570	579	9	0.50	30
BAA-45a	571	580	9	0.22	31
BAA-46b	572	585	13	0.61	33
BAA-47a	589	611	22	0.33	47
BAA-48a	603	641	38	0.45	60
BAA-49b	571	580	9	0.14	33
BAA-50a	571	581	10	0.28	33
BAA-50b	572	581	9	0.12	34
BAA-51a	594	607	13	0.06	42
BAA-52a	577	585	8	0.04	51
BAA-53a	570	581	11	0.44	30
BAA-54a	573	581	8	0.04	46
BAA-55a	576	592	16	0.75	35
BAA-55b	575	591	16	0.75	38
BAA-56a	585	595	10	0.91	32
BAA-56b	586	597	11	0.15	35
BAA-57a	574	590	16	0.75	45
BAA-57b	575	591	16	0.75	38
BAA-58a	572	582	10	0.70	30
BAA-59a	571	581	10	0.53	30
BAA-60b	588	604	16	0.47	37
BAA-61a	573	587	14	>0.99	35
BAA-62a	579	594	15	0.68	33
BAA-63a	592	607	15	0.43	39

Product	λmax ABS (nm)	λmax EM (nm)	Stokes Shift (nm)	Φ_{fl}	FWHM
BAA-64a	576	593	17	0.80	37
BAA-65a	606	622	16	0.21	54
BAA-66a	587	598	11	0.28	34
BAA-67a	587	598	11	0.15	61
BAA-68a	585	595	10	0.17	30
BAA-69a	577	589	12	0.85	30
BAA-70a	580	588	8	0.17	33
BAA-71a	580	589	9	0.19	32
BAA-72a	580	590	10	0.40	31
BAA-73a	579	593	14	0.55	46
BAA-74a	584	602	18	0.15	59
BAA-74b	583	600	17	0.22	51
BAA-75a	614	663	49	0.08	91
BAA-75b	605	660	55	0.18	91
BAA-76a	613	634	21	0.21	55
BAA-77a	603	634	31	0.50	61
BAA-78a	581	592	11	0.19	46
BAA-78b	579	593	14	0.37	39
BAA-79a	606	630	24	0.63	49

Supplemental Table S3-3 Organelle specificity of BAA Library in fixed U2OS cells.

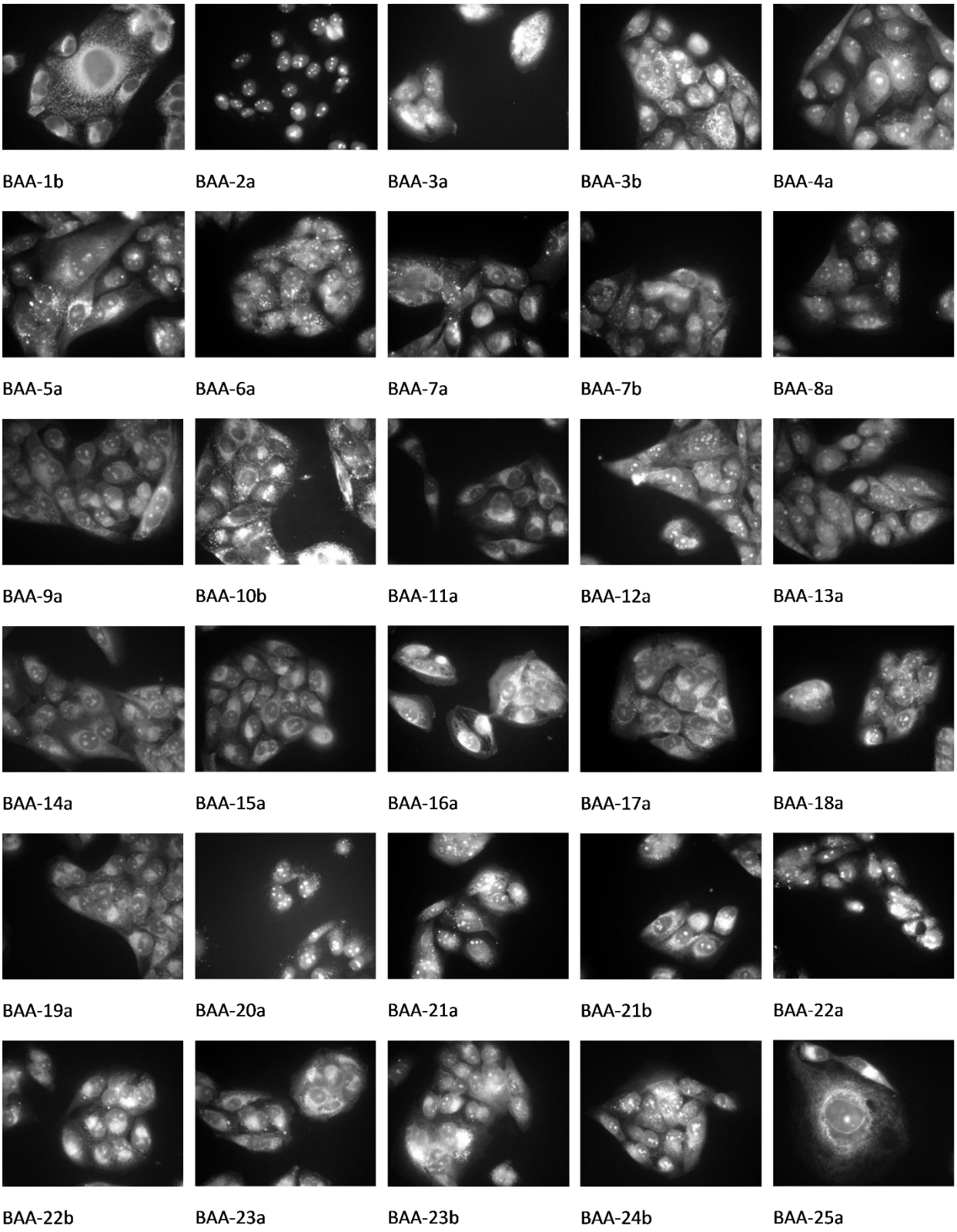

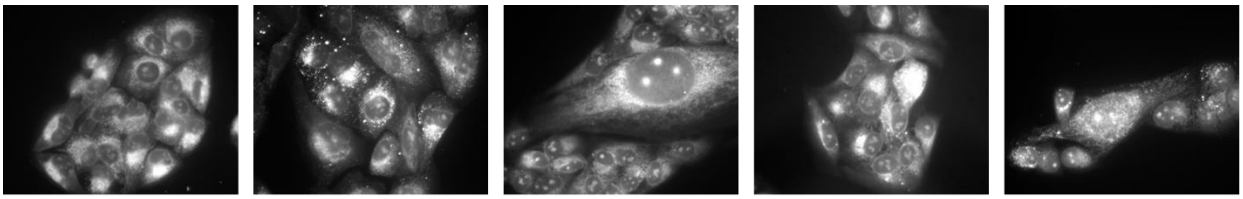

BAA-25b BAA-26b BAA-27b BAA-28a BAA28-b

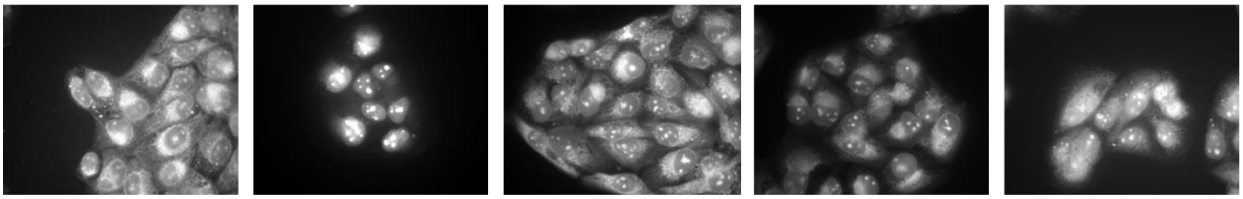

BAA-29b BAA-30a BAA-31b BAA-32a BAA-33a

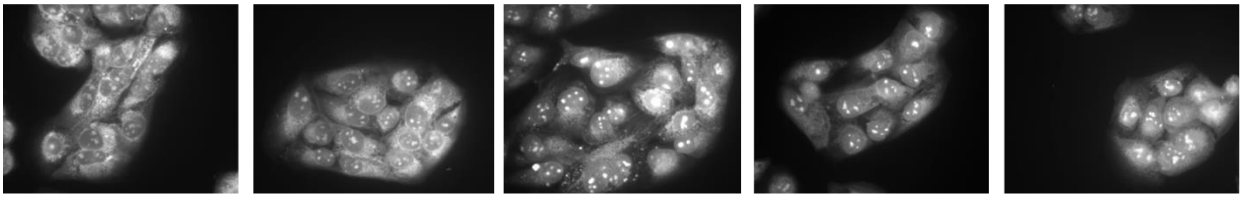

BAA-34b BAA-35b BAA-36b BAA-37a BAA-37b

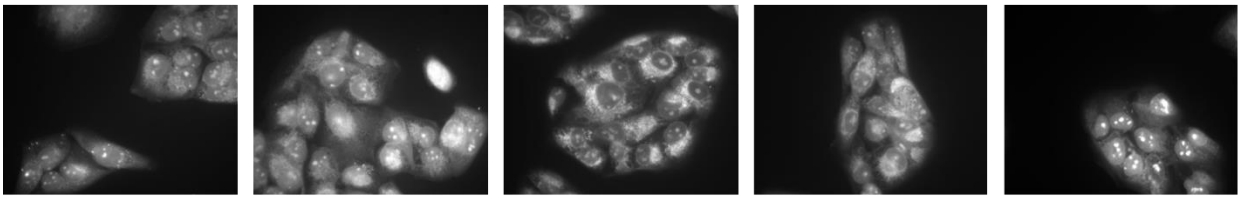

BAA-38a BAA-39a BAA-40b BAA-41b BAA-42a

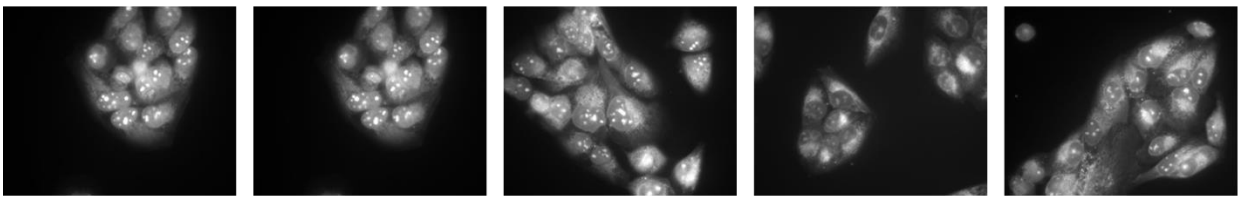

BAA-43a BAA-44b BAA-45a BAA-45b BAA-46b

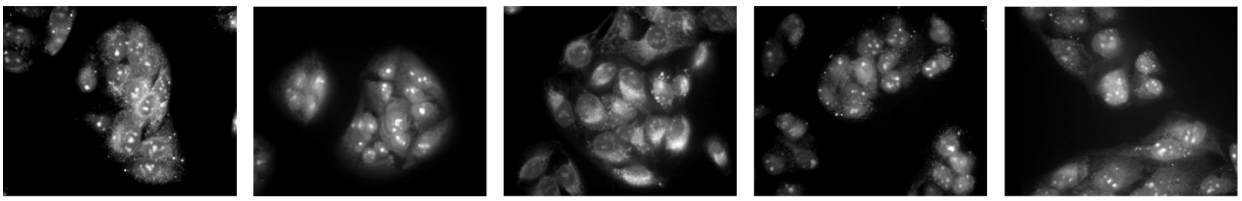

BAA-47a BAA-48a BAA-49b BAA-50a BAA-50b

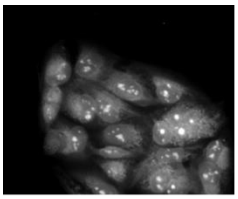

BAA-51a

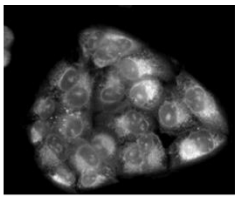

BAA-52a

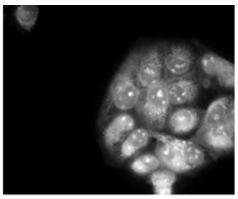

BAA-53a

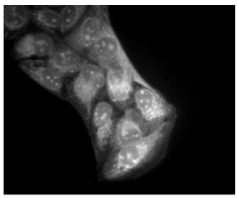

BAA-54a

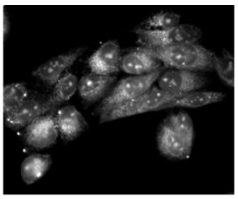

BAA-55a

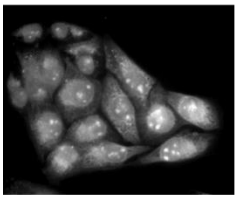

BAA-55b

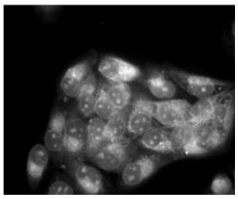

BAA-56a

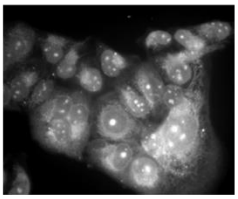

BAA-56b

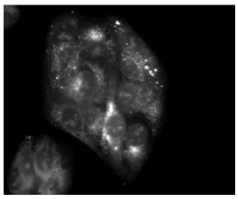

BAA-57a

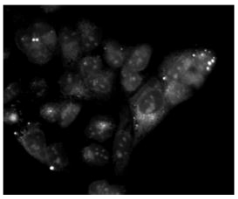

BAA-57b

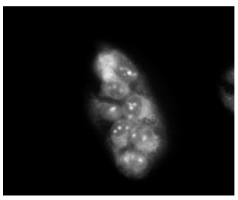

BAA-58a

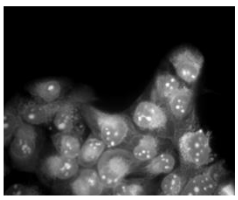

BAA-59a

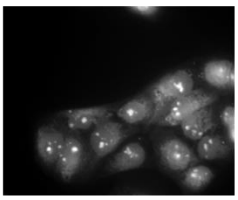

BAA-60b

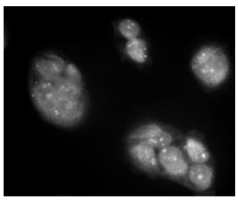

BAA-61a

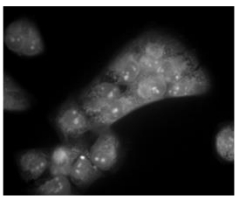

BAA-62a

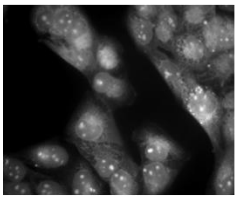

BAA-63a

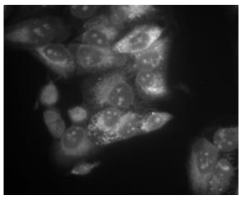

BAA-64a

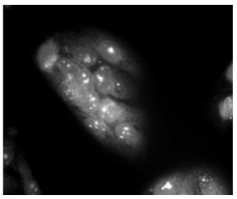

BAA-65a

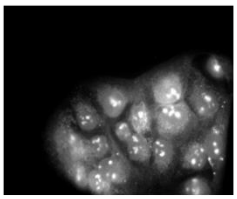

BAA-66a

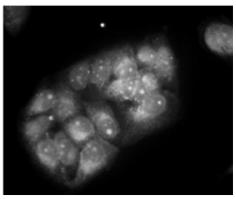

BAA-67a

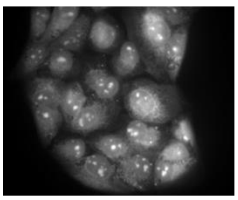

BAA-68a

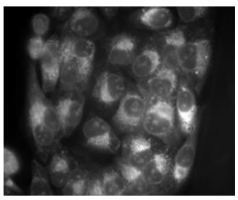

BAA-69a

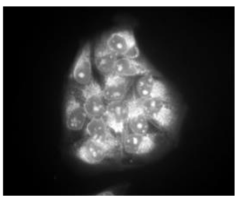

BAA-70a

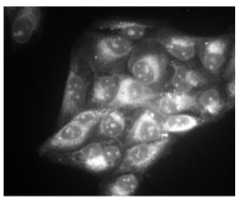

BAA-71a

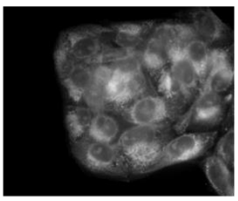

BAA-72a

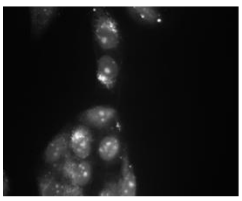

BAA-73a

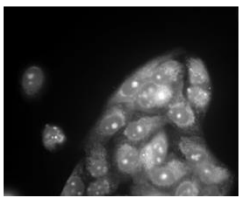

BAA-74a

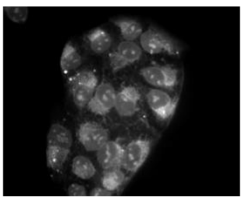

BAA-74b

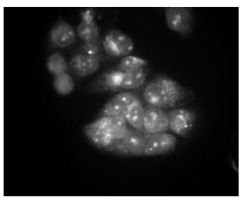

BAA-75a

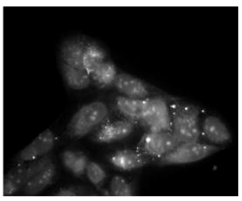

BAA-75b

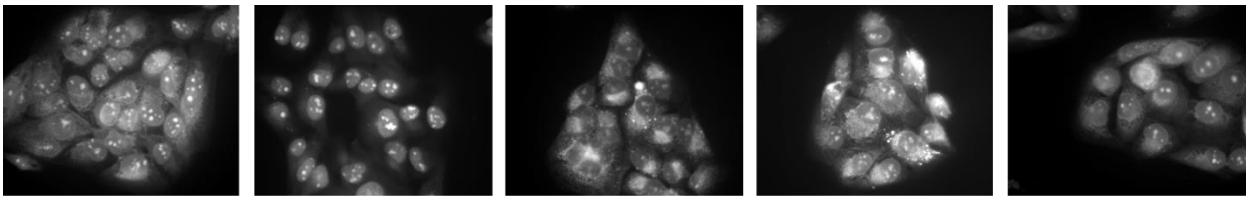

BAA-76a BAA-77a BAA-78a BAA-78b BAA-79a

Images are 168 µm by 135 µm with contrast optimized for each dye to show cellular structure.

Supplemental Table S3-4 Molecular properties, organelle specificity, and signal-to-background ratio for BAA library.

Product	LogD @ pH 7.4	Rotatable Bonds	H Bond Donor	H Bond Acceptor	Polar Surface Area	Cell Organelle Specificity	Signal to Background Ratio
BAA-1b	4.20	8	1	6	89.48	c	4.52
BAA-2a	0.54	5	2	4	61.03	n	1.71
BAA-3a	3.72	10	1	6	82.16	c, v	2.19
BAA-3b	0.92	7	1	4	63.70	v	1.41
BAA-4a	-0.04	6	1	4	51.72	c,v	1.26
BAA-5a	1.24	12	1	8	100.62	v	2.74
BAA-6a	0.29	6	2	3	70.26	c,v	1.06
BAA-7a	0.40	7	1	4	63.70	v	1.73
BAA-7b	2.68	10	1	6	82.16	c,v	1.89
BAA-8a	1.19	6	1	3	54.47	v	1.91
BAA-9a	-0.24	7	3	5	94.93	c,v	1.63
BAA-10b	4.64	12	1	4	51.72	v	1.17
BAA-11a	2.90	8	1	3	54.47	c	4.08
BAA-12a	0.34	8	1	4	71.02	c	1.89
BAA-13a	0.32	6	1	3	54.47	c	1.83
BAA-14a	2.00	7	1	2	45.24	c	1.41
BAA-15a	1.23	8	1	3	54.47	c,v	4.28
BAA-16a	1.84	5	1	2	45.24	c	3.01
BAA-17a	2.12	6	1	2	45.24	c	2.25
BAA-18a	1.96	8	1	3	54.47	c,v	2.59
BAA-19a	1.54	6	1	2	45.24	c	0.79
BAA-20a	-0.13	7	1	4	71.02	v	5.14
BAA-21a	1.71	9	1	4	63.70	v	6.23
BAA-21b	5.30	14	1	6	82.16	c	3.52
BAA-22a	1.85	9	1	4	63.70	c,v	2.07
BAA-22b	5.57	14	1	6	82.16	c,v	4.27
BAA-23a	2.09	7	1	3	58.13	v	0.82
BAA-23b	6.06	10	1	4	71.02	c,v	1.71
BAA-24b	4.73	6	1	2	45.24	c,v	1.33
BAA-25a	2.52	7	1	2	54.47	c	1.33
BAA-25b	6.93	10	1	2	63.70	c	1.52
BAA-26b	4.05	16	1	6	82.16	v	1.29
BAA-27b	6.65	10	1	2	63.70	c,v	4.33
BAA-28a	-0.27	6	1	3	63.06	v	1.86
BAA-28b	1.34	8	1	4	80.88	v	1.37
BAA-29b	4.83	6	1	2	45.24	c,v	1.06

Product	LogD @ pH 7.4	Rotatable Bonds	H Bond Donor	H Bond Acceptor	Polar Surface Area	Cell Organelle Specificity	Signal to Background Ratio
BAA-30a	-4.22	8	2	5	85.75	n	1.17
BAA-31b	2.44	6	3	4	85.70	c,v	1.61
BAA-32a	1.82	8	1	4	97.61	c	3.73
BAA-33a	0.00	6	1	4	79.38	c,v	1.57
BAA-34b	5.19	8	1	4	71.02	c	2.57
BAA-35b	5.24	10	1	4	111.28	c	1.51
BAA-36b	4.85	12	1	6	111.28	c,v	2.48
BAA-37a	0.81	6	1	3	58.13	c	2.31
BAA-37b	3.50	8	1	4	71.02	c	1.42
BAA-38a	0.68	6	1	4	61.37	c,v	1.50
BAA-39a	0.39	6	1	4	61.37	c	1.18
BAA-40b	7.06	16	1	6	82.16	c	1.52
BAA-41b	6.23	14	1	6	82.16	c	1.94
BAA-42a	3.30	8	1	3	71.54	c	1.69
BAA-43a	2.78	8	1	3	71.54	c	2.16
BAA-44b	7.06	16	1	6	82.16	c	3.26
BAA-45b	7.12	12	1	4	63.70	c	2.34
BAA-45a	2.62	8	1	3	54.47	c	5.01
BAA-46b	5.30	14	1	6	82.16	c	6.52
BAA-47a	0.62	9	1	4	63.70	v	5.90
BAA-48a	2.06	8	2	3	70.26	c	1.77
BAA-49b	0.50	12	1	8	129.74	c	1.00
BAA-50a	0.52	6	1	3	63.06	v	1.97
BAA-50b	2.92	8	1	4	80.88	c,v	1.50
BAA-51a	-0.02	7	2	4	83.57	c	10.02
BAA-52a	0.72	8	1	4	63.70	c	0.77
BAA-53a	-0.07	7	1	4	63.70	c,v	0.63
BAA-54a	1.10	5	1	2	45.24	c,v	0.69
BAA-55a	0.41	6	1	3	63.06	v	2.61
BAA-55b	2.69	8	1	4	80.88	c	1.54
BAA-56a	0.62	6	1	5	58.13	c,v	1.63
BAA-56b	3.13	8	1	6	71.02	c,v	1.44
BAA-57a	0.87	6	1	3	63.06	v	1.67
BAA-57b	3.63	8	1	4	80.88	v	3.63
BAA-58a	2.27	8	1	3	71.54	c	19.25
BAA-59a	0.26	7	1	5	92.27	c	1.77
BAA-60b	4.60	8	1	2	45.24	v	6.04
BAA-61a	1.02	9	3	5	94.93	c,v	4.57
BAA-62a	0.13	5	1	3	58.13	c,v	1.79

Product	LogD @ pH 7.4	Rotatable Bonds	H Bond Donor	H Bond Acceptor	Polar Surface Area	Cell Organelle Specificity	Signal to Background Ratio
BAA-63a	1.88	5	1	3	58.13	c	5.92
BAA-64a	1.37	6	2	3	73.92	c,v	1.95
BAA-65a	0.97	6	1	2	58.38	c,v	1.04
BAA-66a	1.07	6	1	3	58.13	c,v	0.94
BAA-67a	2.10	8	1	3	58.13	v	1.94
BAA-68a	0.98	6	1	3	58.13	v	1.86
BAA-69a	2.24	6	1	3	58.13	c,v	0.96
BAA-70a	2.09	7	1	3	58.13	c,v	2.08
BAA-71a	2.89	8	1	4	67.36	c,v	1.88
BAA-72a	1.49	6	1	3	58.13	c,v	5.15
BAA-73a	0.95	8	1	3	54.47	v	1.90
BAA-74a	0.97	13	1	7	99.23	c,v	2.70
BAA-74b	3.82	22	1	12	153.22	c,v	2.25
BAA-75a	-0.18	10	1	5	96.06	v	3.83
BAA-75b	1.52	16	1	8	146.88	v	1.34
BAA-76a	1.10	7	1	3	67.61	c,v	1.58
BAA-77a	2.06	8	2	3	70.26	n	3.21
BAA-78a	1.92	9	1	5	97.61	c,v	6.81
BAA-78b	5.71	14	1	8	149.98	c,v	2.44
BAA-79a	2.06	6	1	2	58.38	c	3.43

Formal charge for all compounds was 0. Organelle specificity of BAA compounds localized to cytosol (c), vesicles (v), and nucleolar (n).

a. BAA-37a

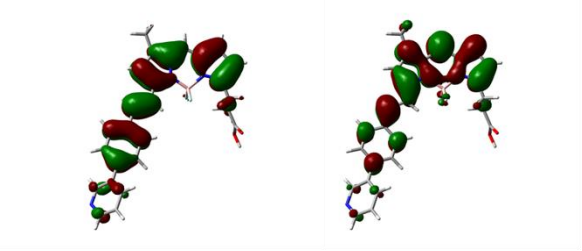

b. BAA-22a

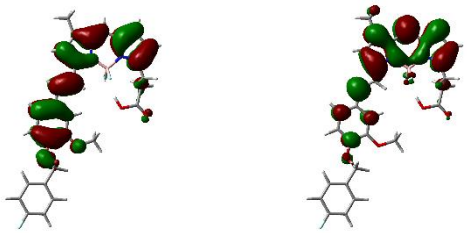

c. BAA-5a

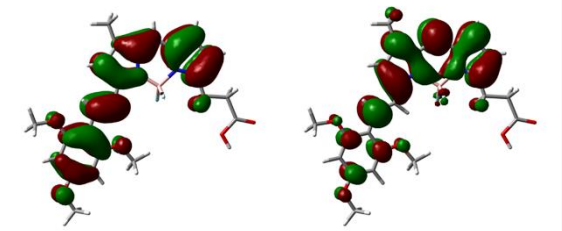

d. BAA-2a

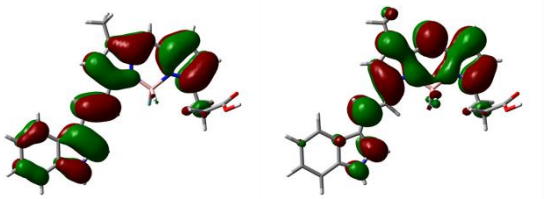

e. BAA-39a

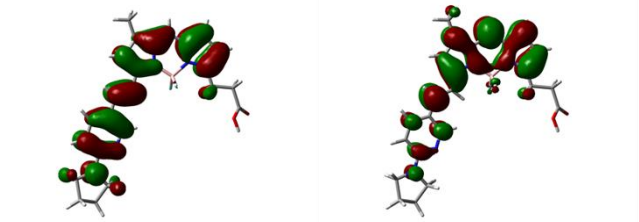

Supplemental Figure S3-1 HOMO and LUMO molecular orbitals, left and right respectively, of the five selected BAA compounds. (a) **BAA-37a** (b) **BAA-22a** (c) **BAA-5a** (d) **BAA-2a** (e) **BAA-39a**.

NMR Data

BAA-37a: ^{1}H NMR (400 MHz, DMSO-D6): δ 2.33 (s, 3H), 2.52-2.56 (m, 2H), 3.11 (t, 2H, *J* = 7.8 Hz), 6.46 (d, 1H, *J* = 4.0 Hz), 7.05 (s, 1H), 7.15 (d, 1H, *J* = 4.0 Hz), 7.49 – 7.56 (m, 2H), 7.60 (t, 1H, *J* = 7.7 Hz), 7.69-7.80 (m, 4H), 7.88 (t, 1H, *J* = 1.7 Hz), 8.13 (ddd, 1H, *J* = 8.0, 2.5, 1.6 Hz) 8.62 (dd, 1H, *J* = 4.8, 1.6 Hz), 8.94 (dd, 1H, *J* = 2.5, 0.9 Hz).

BAA-22a: ^{1}H NMR (400 MHz, DMSO-D6): δ 2.31 (s, 3H), 2.65-2.71 (m, 2H), 3.09 (t, 2H, *J* = 7.8 Hz), 3.84 (s, 3H), 5.13 (s, 2H), 6.40 (d, 1H, *J* = 4.0 Hz), 7.02 (s, 1H), 7.07 (d, 1H, *J* = 4.0 Hz), 7.13-7.33 (m, 5H,), 7.48-7.68 (m, 5H).

BAA-5a: ^{1}H NMR (400 MHz, DMSO-D6): δ 2.29 (s, 3H), 2.59-2.64 (m, 2H), 3.09 (t, 2H, *J* = 7.7 Hz), 3.88 (d, 9H, *J* = 13.3 Hz), 6.32 (s, 2H), 6.33 (d, 1H, *J* = 4.1 Hz), 6.92 (s, 1H), 6.97 (d, 1H, *J* = 4.0 Hz), 7.09 (s, 1H), 7.51 (s, 1H), 7.72 (d, 1H, *J* = 16.4 Hz), 7.85 (d, 1H, *J* = 16.4 Hz).

BAA-2a: ^{1}H NMR (400 MHz, DMSO-D6): δ 2.31 (s, 3H), 2.61 (t, 2H, *J* = 7.8 Hz), 3.12 (t, 2H, *J* = 7.8 Hz), 6.30 (d, 1H, *J* = 3.9 Hz), 6.93 (d, 1H, *J* = 3.9 Hz), 7.09 (s, 1H), 7.20-7.34 (m, 2H), 7.37-7.57 (m, 3H), 7.89-8.00 (m, 3H), 11.96 (s, 1H).

BAA-39a: ^{1}H NMR (400 MHz, DMSO-D6): δ 1.96 (p, 6H), 2.29 (s, 3H), 2.41 (t, 2H, *J* = 8.0), 3.06, (t, 2H, *J* = 8.0 Hz), 3.46, (m, 2H), 6.35 (d, 1H, *J* = 4.0 Hz), 6.57 (d, 1H, *J* = 9.0 Hz), 6.99 (d, 1H, *J* = 3.9 Hz), 7.02 (s, 1H), 7.18 (d, 1H, *J* = 16.2 Hz), 7.51 (s, 1H), 7.59 (d, 1H, *J* = 16.2 Hz), 7.84 (dd, 1H, *J* = 9.0, 2.5 Hz), 8.25 (d, 1H, *J* = 2.5 Hz).

CHAPTER 4: Methodology for Quantitative Characterization of Fluorophore Photoswitching to Predict Superresolution Microscopy Image Quality[6]

[6]Bittel, A. M. Nickerson, N., Saldivar, I.S., Dolman, N.J., Nan, X., & Gibbs, S.L. *Methodology for Quantitative Characterization of Fluorophore Photoswitching to Predict Superresolution Microscopy Image Quality*. Sci Rep 6, 29687, doi:10.1038/srep29687 (2016).

4.1 ABSTRACT

Single-molecule localization microscopy (SMLM) image quality and resolution strongly depend on the photoswitching properties of fluorophores used for sample labeling. Development of fluorophores with optimized photoswitching will considerably improve SMLM spatial and spectral resolution. Currently, evaluating fluorophore photoswitching requires protein-conjugation before assessment mandating specific fluorophore functionality, which is a major hurdle for systematic characterization. Herein, we validated polyvinyl alcohol (PVA) as a single-molecule environment to efficiently quantify the photoswitching properties of fluorophores and identified photoswitching properties predictive of quality SMLM images. We demonstrated that the same fluorophore photoswitching properties measured in PVA films and using antibody adsorption, a protein-conjugation environment analogous to labeled cells, were significantly correlated to microtubule width and continuity, surrogate measures of SMLM image quality. Defining PVA as a fluorophore photoswitching screening platform will facilitate SMLM fluorophore development and optimal image buffer assessment through facile and accurate photoswitching property characterization, which translates to SMLM fluorophore performance *in vitro*.

4.2 INTRODUCTION

Superresolution microscopy (SRM) has enabled fluorescence imaging at unprecedented spatial resolution.[5,23,38] Although a number of SRM techniques exist, single-molecule localization microscopy (SMLM) has gained in popularity due to its relative ease of instrumentation and compatibility with current labeling approaches for biological samples.[52,53] Two common SMLM techniques are stochastic optical reconstruction microscopy (STORM)[5,54,55] and photoactivated localization microscopy (PALM),[23,31] which enable visualization with ~10-20 nm resolution; however, resolution depends strongly upon the performance of the fluorophore used for sample labeling.[32,35,56,57]

SMLM requires dense labeling of features of interest with photoswitchable fluorophores that have the ability to stochastically switch between the fluorescent “on” state where photons are emitted and the nonfluorescent “off” or dark state.[28,29] Although the exact photoswitching mechanism is unknown for all fluorophore scaffolds, switching between the fluorescent on and off states is largely attributed to manipulation of the reductive and oxidative status of the imaging environment.[28,58,59] Subdiffractive localization of individual fluorophores throughout a series of images via activation of a stochastic, small population of fluorophores in the on state facilitates reconstruction of a superresolution image.[30] Thus, the photoswitching ability of the fluorescent labels is crucial to the quality of SMLM.

Currently utilized fluorophores largely consist of commercially available probes that have been demonstrated to photoswitch or be photoactivatable under certain imaging conditions.[2,35,60] However such probes are not designed to provide the optimal photoswitching as it is a disadvantage for conventional fluorescence microscopy, presenting an opportunity for photoswitching improvement. The most widely used fluorophores for SMLM include AlexaFluor647 and Cy5, which can achieve ~20 nm resolution, yet the majority of commercial fluorophores identified as the top SMLM candidates reach resolutions of only 30-40 nm at best.[2,35,54] Furthermore, as SMLM progresses to imaging multi-protein cellular complexes with multicolor SMLM, photoswitchable fluorophores with relatively narrow excitation and emission spectra will

be required to minimize crosstalk.[2,35] Advancing the spatial and spectral resolution of SMLM will be realized through the synthesis of fluorophores specifically designed to photoswitch or photoactivate with ideal spectral properties for multicolor imaging. The chemical space to be investigated for development of ideal photoswitchable fluorophores in addition to the numerous imaging buffer formulations that significantly impact photoswitching behavior present a pressing need for a robust and efficient method to characterize fluorophore utility for SMLM.

A common approach to assess fluorophore photoswitching is through *in vitro* labeling of a known cellular structure within fixed cells with descriptive image evaluation of the rendered SMLM image as this closely reflects most SMLM fluorophore applications.[2,35,61] However, the quality of the resulting image is often influenced by more than just fluorophore photoswitching properties. SMLM image quality can also reflect labeling issues arising from nonspecific binding or insufficient labeling density rather than the photoswitching ability of the fluorophore. Descriptive image evaluation of SMLM image quality is subjective and thus not readily comparable between fluorophores. Additionally, *in vitro* evaluation requires the fluorophore of interest to contain a readily conjugatable group, such as an N-hydroxysuccinimide (NHS) ester, maleimide or azide, for conjugation to a targeting molecule where the type of chemical attachment to the labeling protein may affect fluorophore photoswitching. Thus, *in vitro* evaluation of photoswitching requires additional fluorophore synthetic steps for conjugation, convolves the fluorophore photoswitching properties with labeling density and nonspecific background, and may be affected by the selected protein attachment strategy making direct assessment of fluorophore photoswitching time consuming and largely descriptive instead of quantitative.

An alternative approach is studying fluorophore photophysical properties sans cells by spatially isolating and immobilizing single molecules. Such single-molecule systems include fluorophore adsorption to coverglass through protein-conjugation[2,62-65] and fluorophores fixed in various polymer films.[66-72] Protein adsorption may more closely represent the environment utilized for biological SMLM imaging than polymer films while

minimizing sample preparation time in comparison to *in vitro* evaluation. However, protein adsorption still requires addition of a readily conjugatable group on the fluorophore of interest, which may affect photoswitching properties. By contrast, polymer films enable isolation of fluorophores devoid of conjugatable groups, which has significant utility for screening of novel fluorophores as a photoswitch as well as isolation of the photoswitching properties from conjugation strategy. While fluorophore photoswitching performance evaluated via protein adsorption has been shown to qualitatively correlate to *in vitro* applications,[2] it has not been established how the more advantageous polymer film isolation method compares, nor how photoswitching properties quantitatively compare to SMLM image quality.

In this study, we compared the polymer film and the protein adsorption single-molecule systems for their ability to predict *in vitro* SMLM image quality within fixed cells through measurement of photoswitching properties. SMLM images ranging in quality were acquired of microtubules labeled *in vitro* with eight commercial fluorophores. Photoswitching properties of the eight fluorophores were then obtained using dilute fluorophores dried into a polyvinyl alcohol (PVA) film and fluorophore-conjugated antibodies adsorbed to coverglass as the two single-molecule isolation platforms. Through statistical analysis, we identified the photoswitching properties measured using each isolation platform that correlate to, and ultimately predict, SMLM image quality. We demonstrated PVA films were efficacious and robust in evaluating fluorophores for SMLM *in vitro* applications and hence, provide the necessary screening system for SMLM fluorophore development.

4.3 RESULTS

4.3.1 SMLM Image Quality Varies with Photoswitchable Fluorophore Label

We established *in vitro* SMLM performance of selected fluorophores through quantitative assessment of the structure of microtubules labeled with indirect immunofluorescence in fixed cells. Eight commercially available fluorophores were used: three blue absorbing

fluorophores, Fluorescein, ATTO 488 (ATTO488), and BODIPY™ FL (BODIPY FL); two green absorbing fluorophores, Cy™3B (Cy3B), and Alexa Fluor™ 568 (AlexaFluor568); and three red absorbing fluorophores, Cy™5 (Cy5), Alexa Fluor™ 647 (AlexaFluor647), and ATTO 680 (ATTO680). These eight fluorophores covered the ultraviolet to red region of the light spectrum and represented four classic fluorophore scaffolds including xanthene, BODIPY, cyanine, and oxazine. Microtubule labeling was completed with equal concentrations of primary antibody and fluorophore concentration conjugated to secondary antibody to maintain equal labeling density across the different fluorophores. Images of all fluorophores were collected under constant imaging buffer, image capture settings, and fluence rate within an excitation laser line.

Microtubule structures were visible in all rendered images with image quality varying in fluorophore homogeneity (Figure 4-1), measured width (Figure 4-2a), and measured continuity (Figure 4-2b) of the labeled structure. AlexaFluor647, Cy5, and ATTO488 provided the most homogeneous rendered microtubule structures, followed by AlexaFluor568, Fluorescein, BODIPY FL, and ATTO680. Cy3B had the worst fluorophore homogeneity across the microtubule structure and the lack of Cy3B fluorophores rendered required the quadrupling of image contrast to aid in visualization of the displayed images (Figure 4-1a and 4-1b). The range in SMLM image quality was expected as the chosen imaging conditions were not optimized for each fluorophore, but rather kept constant to enable differences in resulting image quality to be attributed to the photoswitching properties of the selected fluorophore. SMLM image quality using the selected fluorophores could be improved for future studies by tailoring the imaging buffer and acquisition settings for each fluorophore.[32,73]

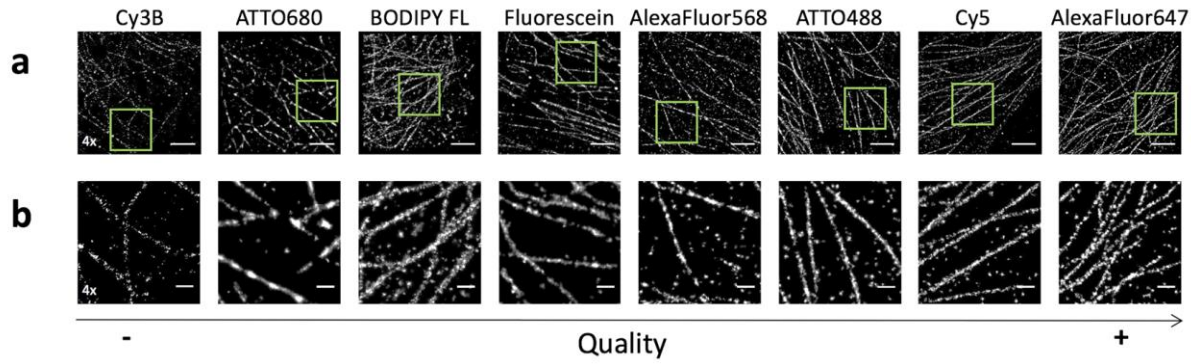

Figure 4-1 SMLM imaging of microtubules *in vitro* via indirect immunofluorescence. (a) Rendered SMLM images of microtubules (scale bar = 2 μm) with (b) magnified boxes to demonstrate reconstructed microtubule detail (scale bar = 0.5 μm). Panels labeled with "4x" are displayed with four times the brightness in comparison to other panels. Rendered images were organized by increasing observed quality from left to right: Cy3B, ATTO680, BODIPY FL, Fluorescein, AlexaFluor568, ATTO488, Cy5, and AlexaFluor647.

SMLM image quality of the rendered microtubules resulting from each fluorophore was quantified by measuring the average width (Figure 4-2a) and continuity (Figure 4-2b). The width was measured as the full width at half maximum (FWHM) of the microtubule structure and the continuity was defined as the photons detected per nm^2 of the measured microtubule. As expected, the average microtubule width measurements closely aligned with the observed quality of the rendered images (Figure 4-1a, 4-1b and 4-2a). The fluorophores with the narrowest average microtubule widths, AlexaFluor647 (51.3 ± 12.6 nm), Cy5 (60.2 ± 15.3 nm), and ATTO488 (62.9 ± 10.6 nm) had the highest quality microtubule images. These widths closely aligned with the expected 55 nm FWHM width, which are wider than the reported 25 nm width of microtubules as measured by electron crystallography due to the primary and secondary antibodies used for indirect immunofluorescence labeling.[2,56,74,75] Microtubule images of lower quality had larger widths including AlexaFluor568 (67.4 ± 20.7 nm), Fluorescein (76.1 ± 14.0 nm) and BODIPY FL (80.9 ± 23.1 nm). The poorest quality SRM images demonstrated the widest microtubules, which were found to be ATTO680 (83.1 ± 17.6 nm) and Cy3B (83.7 ± 37.3 nm) herein. The large microtubule width standard deviations reflect the inconsistent detection of fluorophores across even the most continuous microtubules within the SMLM image, which was likely attributed to their poor photoswitching properties and relatively low signal to background ratio (SBR). The average continuity measurements (Figure 4-2b) also varied between fluorophores and showed a similar trend to observed image quality. Continuity was greatest for ATTO488 (1.48 ± 0.26 photons/nm^2), AlexaFluor568 (1.35 ± 0.42 photons/nm^2), Cy5 (1.20 ± 0.31 photons/nm^2), and AlexaFluor647 (1.16 ± 0.29 photons/nm^2). Fluorescein (1.11 ± 0.22 photons/nm^2), ATTO680 (1.07 ± 0.23 photons/nm^2), and BODIPY FL (0.97 ± 0.28 photons/nm^2) demonstrated mid-level continuity, while Cy3B (0.52 ± 0.24 photons/nm^2) showed the lowest average signal intensity and thus the least microtubule continuity. SMLM microtubule width and continuity measurements were used to identify correlation of image quality to photoswitching properties measured using each single-molecule isolation system.

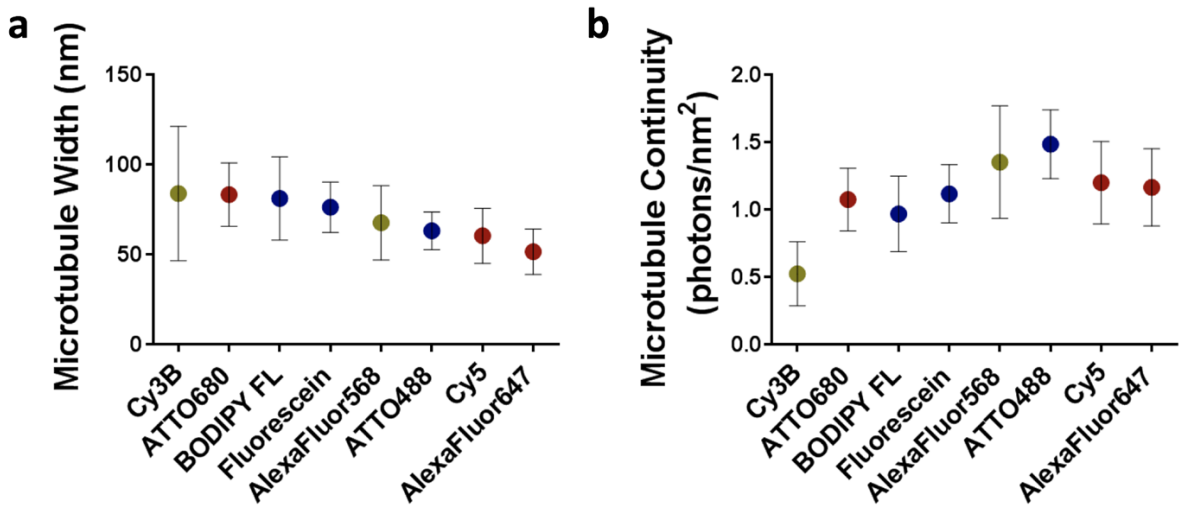

Figure 4-2 Calculated (a) average microtubule width and (b) average continuity of microtubules for each fluorophore, organized by observed quality. Average width and continuity measurements are graphed as the mean ± standard deviation of n=15 measurements per image of the corresponding fluorophore. Images were collected at the following fluence rates: 0.28 $kWcm^{-2}$ for the 488 nm laser line (blue points), 0.49 $kWcm^{-2}$ for the 561 nm laser line (green points) and 1.11 $kWcm^{-2}$ for the 647 nm laser line (red points).

4.3.2 Correlation of SMLM Image Quality to Fluorophore Photoswitching Properties

The photoswitching properties of the eight fluorophores were measured using both the antibody adsorption and PVA film single-molecule isolation systems (Table 4-1 and Figure 4-3a-f). Previous studies of a variety of commercially available photoswitchable fluorophores[36,76-80] have shown that SMLM image quality is influenced by photoswitchable fluorophore photon output and the amount of time each fluorophore spends in the fluorescent on and off states.[2,81,82] Herein, we quantified six photoswitching properties for the spatially isolated fluorophores where four properties characterized photon output and two properties characterized time in the fluorescent on and off states. Measurements were collected in triplicate to assess photoswitching property reproducibility over three fluence rates within each excitation laser line. Measurements across the three fluence rates were used to assess the relationship between photoswitching behavior in each single-molecule isolation system and fluence rate. Measurements collected at the highest fluence rate were used for photoswitching property correlation analysis, as this was the same fluence rate used to acquire the SMLM microtubule images.

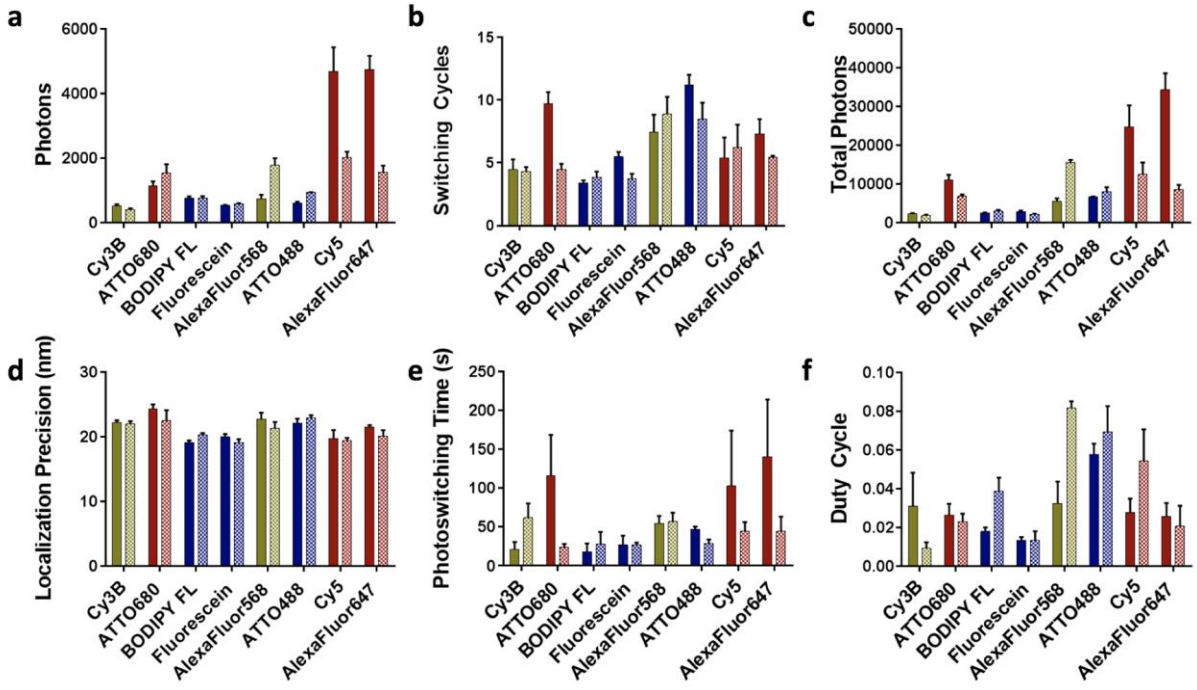

Figure 4-3 Photoswitching properties of antibody adsorption (solid bars) and PVA film (patterned bars) isolated fluorophores. Average photoswitching properties including (a) photons per switching cycle, (b) number of switching cycles, (c) total photons, (d) localization precision, (e) photoswitching time, and (f) duty cycle are demonstrated. Average photoswitching properties represented the mean ± standard deviation of n=3 SMLM imaging series for each fluorophore. Photoswitching property measurements were collected at fluence rates equivalent to those utilized for imaging: 0.28 $kWcm^{-2}$ for the 488 nm laser line (blue bars), 0.49 $kWcm^{-2}$ for the 561 nm laser line (green bars) and 1.11 $kWcm^{-2}$ for the 647 nm laser line (red bars).

Table 4-1 Photoswitching properties of 8 fluorophores isolated via antibody adsorption and PVA methods.

	Fluorophore		Photons	Switching Cycles	Total Photons	Localization Precision (nm)	Photoswitching Time (s)	Duty Cycle
Antibody Adsorption	Cy3B	low Φ	169 ± 26	9.2 ± 1.6	1,535 ± 116	26.6 ± 0.8	50 ± 2	0.0348 ± 0.0099
		mid Φ	288 ± 12	6.5 ± 0.9	1,871 ± 190	25.1 ± 0.1	45 ± 17	0.0286 ± 0.0048
		high Φ	515 ± 50	4.5 ± 0.8	2,265 ± 229	22.2 ± 0.4	21 ± 9	0.0311 ± 0.0172
	ATTO680	low Φ	477 ± 34	12.9 ± 0.6	6,143 ± 721	28.7 ± 1.9	150 ± 51	0.0230 ± 0.0049
		mid Φ	721 ± 60	11.4 ± 0.9	8,283 ± 1,278	25.6 ± 0.6	164 ± 31	0.0187 ± 0.0017
		high Φ	1,136 ± 139	9.7 ± 0.9	11,002 ± 1,362	24.4 ± 0.7	116 ± 52	0.0263 ± 0.0059
	BODIPY FL	low Φ	294 ± 13	4.9 ± 0.3	1,456 ± 140	22.7 ± 0.6	34 ± 14	0.0111 ± 0.0021
		mid Φ	570 ± 198	4.0 ± 0.6	2,221 ± 520	20.3 ± 1.1	23 ± 7	0.0207 ± 0.0079
		high Φ	756 ± 57	3.4 ± 0.2	2,555 ± 106	19.2 ± 0.3	18 ± 11	0.0179 ± 0.0021
	Fluorescein	low Φ	240 ± 16	7.6 ± 0.3	1,837 ± 184	22.1 ± 0.6	50 ± 8	0.0198 ± 0.0041
		mid Φ	444 ± 32	7.7 ± 1.0	3,415 ± 197	20.5 ± 0.7	35 ± 7	0.0123 ± 0.0039
		high Φ	531 ± 21	5.5 ± 0.4	2,908 ± 207	20.0 ± 0.5	27 ± 12	0.0133 ± 0.0017
	AlexaFluor568	low Φ	206 ± 34	15.2 ± 1.9	3,126 ± 670	27.0 ± 0.6	85 ± 18	0.0338 ± 0.0008
		mid Φ	389 ± 97	10.1 ± 2.4	3,796 ± 368	25.0 ± 0.3	60 ± 12	0.0324 ± 0.0027
		high Φ	739 ± 124	7.5 ± 1.4	5,438 ± 854	22.7 ± 1.0	55 ± 9	0.0324 ± 0.0113
	ATTO488	low Φ	205 ± 12	20.4 ± 4.3	4,158 ± 763	30.4 ± 1.1	70 ± 14	0.0487 ± 0.0088
		mid Φ	374 ± 39	16.9 ± 2.4	6,362 ± 1,542	26.0 ± 0.6	69 ± 20	0.0657 ± 0.0065
		high Φ	595 ± 53	11.2 ± 0.8	6,638 ± 97	22.2 ± 0.7	47 ± 3	0.0576 ± 0.0056
	Cy5	low Φ	1,606 ± 675	11.0 ± 2.5	17,174 ± 7,080	23.0 ± 0.9	68 ± 29	0.0728 ± 0.0091
		mid Φ	2,643 ± 115	9.0 ± 1.7	23,808 ± 3,788	22.2 ± 0.6	129 ± 36	0.0396 ± 0.0058
		high Φ	4,682 ± 749	5.4 ± 1.6	24,635 ± 5,635	19.8 ± 1.3	103 ± 71	0.0275 ± 0.0074
	AlexaFluor647	low Φ	1,255 ± 115	12.6 ± 1.9	15,913 ± 3,740	22.7 ± 1.4	103 ± 48	0.0399 ± 0.0064
		mid Φ	1,663 ± 74	12.2 ± 1.5	20,205 ± 1,827	21.5 ± 1.0	151 ± 71	0.0304 ± 0.0030
		high Φ	4,742 ± 427	7.3 ± 1.2	34,309 ± 4,253	21.5 ± 0.3	140 ± 74	0.0257 ± 0.0069
PVA	Cy3B	low Φ	133 ± 4	8.0 ± 1.8	1,065 ± 225	26.5 ± 1.4	77 ± 15	0.0138 ± 0.0058
		mid Φ	230 ± 27	5.6 ± 0.8	1,269 ± 181	23.8 ± 0.9	42 ± 16	0.0127 ± 0.0026
		high Φ	405 ± 40	4.3 ± 0.3	1,756 ± 293	22.0 ± 0.4	62 ± 19	0.0093 ± 0.0031
	ATTO680	low Φ	555 ± 106	11.7 ± 2.4	6,576 ± 2,096	26.7 ± 1.1	85 ± 49	0.0364 ± 0.0101
		mid Φ	912 ± 103	8.0 ± 1.3	7,249 ± 1,002	24.9 ± 0.8	39 ± 7	0.0270 ± 0.0071
		high Φ	1,536 ± 275	4.5 ± 0.5	6,762 ± 526	22.5 ± 1.6	24 ± 4	0.0231 ± 0.0040
	BODIPY FL	low Φ	247 ± 9	8.2 ± 0.8	2,020 ± 208	25.9 ± 1.5	36 ± 15	0.0525 ± 0.0101
		mid Φ	434 ± 21	5.9 ± 0.4	2,561 ± 200	23.0 ± 0.4	26 ± 10	0.0486 ± 0.0176
		high Φ	758 ± 60	3.9 ± 0.4	2,926 ± 361	20.3 ± 0.3	28 ± 15	0.0387 ± 0.0070
	Fluorescein	low Φ	277 ± 7	6.5 ± 0.3	1,797 ± 71	21.8 ± 0.6	30 ± 11	0.0134 ± 0.0027
		mid Φ	439 ± 29	4.7 ± 0.6	2,086 ± 340	20.3 ± 0.7	39 ± 21	0.0099 ± 0.0046
		high Φ	579 ± 23	3.7 ± 0.4	2,146 ± 158	19.1 ± 0.5	27 ± 3	0.0134 ± 0.0046
	AlexaFluor568	low Φ	447 ± 66	18.7 ± 1.7	8,392 ± 1,793	27.3 ± 0.3	100 ± 4	0.0563 ± 0.0070
		mid Φ	1,309 ± 232	14.3 ± 2.5	14,482 ± 788	25.1 ± 0.2	71 ± 16	0.0785 ± 0.0170
		high Φ	1,772 ± 227	8.9 ± 1.4	15,506 ± 699	21.3 ± 1.0	57 ± 11	0.0815 ± 0.0036
	ATTO488	low Φ	340 ± 22	20.8 ± 3.8	7,053 ± 1,106	29.9 ± 2.5	55 ± 11	0.0734 ± 0.0161
		mid Φ	619 ± 35	12.4 ± 0.5	7,681 ± 255	25.6 ± 0.2	36 ± 0	0.0955 ± 0.0099
		high Φ	940 ± 7	8.5 ± 1.3	7,962 ± 1,177	22.9 ± 0.4	29 ± 5	0.0693 ± 0.0133
	Cy5	low Φ	670 ± 146	10.0 ± 2.4	6,711 ± 2,334	22.7 ± 0.6	55 ± 8	0.0346 ± 0.0074
		mid Φ	1,317 ± 204	7.7 ± 0.6	10,125 ± 1,048	21.4 ± 1.1	45 ± 14	0.0459 ± 0.0083
		high Φ	2,021 ± 175	6.2 ± 1.8	12,417 ± 3,118	19.5 ± 0.4	45 ± 11	0.0543 ± 0.0163
	AlexaFluor647	low Φ	374 ± 37	14.2 ± 2.4	5,248 ± 445	26.2 ± 1.8	141 ± 17	0.0138 ± 0.0022
		mid Φ	1,137 ± 261	6.8 ± 1.9	7,377 ± 1,006	21.0 ± 1.1	80 ± 21	0.0151 ± 0.0019
		high Φ	1,566 ± 201	5.4 ± 0.1	8,506 ± 1,270	20.2 ± 0.9	45 ± 19	0.0205 ± 0.0107

Results are mean ± standard deviation; N = 3 SMLM movies for each fluorophore, with at least 100 particles analyzed in each movie. Fluence rate is represented by Φ. BODIPY FL, Fluorescein, and ATTO488 and were excited with the 488 nm laser line, with low Φ = 0.08, mid Φ = 0.14, and high Φ = 0.28 kW cm^{-2}. Cy3B and AlexaFluor568 were excited with the 561 nm laser line, with low Φ = 0.12, mid Φ = 0.26, and high Φ = 0.49 kW cm-2. ATTO680, Cy5, and AlexaFluor647 were excited with the 647 nm laser line, with low Φ = 0.30, mid Φ = 0.58, and high Φ = 1.11 kW cm^{-2}.

Of the six measured photoswitching properties, four characterized single-molecule photon output including: (1) photons per switching cycle, which represented the intensity of each molecule per fluorescent on cycle (Supplementary Figure S4-1a), (2) number of switching cycles, which were the number of transitions from the dark off state to the fluorescent on state and were counted when photons were emitted above a set threshold (Supplementary Figure S4-1b), (3) total photons, which were calculated as the photons per switching cycle multiplied by the number of switching cycles, and (4) localization precision, which reflected the deviation in the x and y position of the location of the maximum intensity of each molecule's switching cycle.[83] The remaining two photoswitching properties characterized time in the fluorescent on and off states including: (5) photoswitching time, which reflected the length of time a molecule photoswitched before photobleaching occurred (Supplementary Figure S1b), and (6) duty cycle, which described the fraction of time the molecule was on during the entire collected video.

Trends were seen when comparing the image quality of the eight selected fluorophores (Figure 4-1) to their photoswitching property data (Figure 4-3 and Table 4-1). Fluorophores with higher quality images tended to have higher photons per switching cycle, a greater number of switching cycles, higher total photons, and higher duty cycles. Statistically significant correlations were identified using Spearman two-tail correlation tests[84] with significance reported as $p < 0.05$, which validated our observations. Both the antibody adsorption and PVA film systems produced total photon output results that correlated to SMLM image quality (Table 4-2) represented by the width (Antibody method: $p = 0.037$ and PVA method: $p = 0.046$). These findings agreed with previous studies that showed that SMLM image quality was improved by higher photon output as well as theoretical localization-precision-based calculations.[16,18,19] Additionally, both the antibody adsorption and PVA film systems produced duty cycle results that correlated to continuity measurements (Antibody method: $p = 0.028$ and PVA method: $p = 0.037$) (Table 4-2). Other photoswitching properties statistically correlated with continuity but the exact property varied based on the fluorophore isolation method used. Using the antibody adsorption method the localization precision correlated to continuity ($p = 0.046$). Using

the PVA film isolation method, the switching cycles ($p = 0.022$) and total photons ($p = 0.028$) correlated to continuity (Table 4-2).

Table 4-2 P value results: photoswitching properties correlated to image quality via width and continuity for antibody adsorption and PVA single-molecule systems.

	Width		Continuity	
Photoswitching Property	Antibody	PVA	Antibody	PVA
Photons	0.132	0.069	0.501	0.096
Switching Cycles	0.501	0.171	0.327	**0.022** *
Total Photons	**0.037** *	**0.046** *	0.882	**0.028** *
Localization Precision	0.428	0.389	**0.046** *	0.882
Photoswitching Time	0.151	0.752	0.840	0.793
Duty Cycle	0.840	0.299	**0.028** *	**0.037** *

P values calculated via two-tailed Spearman correlation, with *p < 0.05.

4.3.3 Equivalent Fluorophore Photoswitching Property Measurements Using Antibody Adsorption and PVA Film Fixation Methods

The antibody adsorption fluorophore isolation method recapitulated established photoswitching property measurements collected using similar fixation techniques.[2,35] Comparing photons per switching cycle and number of switching cycles with the previously published literature demonstrated similar trends with our antibody isolated fluorophore photoswitching data. Both studies demonstrated similar photon output for the blue fluorophores ATTO488 and Fluorescein. When comparing photon output of the green fluorophores, AlexaFluor568 had higher photon output than Cy3B, similar to previously published results. Both studies also demonstrated a similar trend for the red fluorophores where AlexaFluor647 and Cy5 showed higher photon output than ATTO680.[2] Switching cycles were also comparable between the two studies, where ATTO488 had more switching cycles than Fluorescein for the blue fluorophores and Cy3B showed a similar number of switching cycles to AlexaFluor568 for the green fluorophores. The only anomaly between our photoswitching property data and the previously published results was in the switching cycle number for the red fluorophores. While both studies reported AlexaFluor647 had more switching cycles than Cy5, Dempsey *et al.* reported ATTO680 had the fewest switching cycles, while we measured the greatest number of switching cycles from ATTO680 across the red fluorophores.[2] Of note, the exact numerical values for photons per switching cycle and number of switching cycles between our study and previously published work did differ as would be expected from collecting photoswitching property data using different instrument configurations. The difference in switching cycle number across the red fluorophores was most likely due to differences in illumination fluence between the two studies, which strongly affect number of switching cycles. Even with some slight discrepancies, our antibody fluorophore isolation data demonstrated very similar photoswitching properties to previously published literature, validating our assay for photoswitching property evaluation. Of note, we did not directly compare duty cycle to the previously published study as our calculation represented an average over the entire collected dataset rather than a subset of frames that excluded the initial photobleach step. The inclusion of data collected during the initial photobleaching

step in our duty cycle calculation resulted in higher absolute numerical values than previously reported.[2] Localization precision was also not directly compared to previous studies, as it has not previously been calculated for a suite of fluorophores.

The validated antibody adsorption photoswitching properties were compared to the PVA film isolated photoswitching properties to determine the similarity of the fluorophore photoswitching performance in these different environments. All six measured photoswitching properties showed correlation based on similarity in values and trends across the eight fluorophores between the antibody adsorption and PVA film isolation methods at the high fluence rate (Table 4-1), which was used to collect the SRM images utilized to assess image quality. Localization precision had the strongest correlation with antibody adsorption values closely matching PVA film values for all eight fluorophores tested (Figure 4-3d). Photons per switching cycle (Figure 4-3a), number of switching cycles (Figure 4-3b), and total photons (Figure 4-3c) also showed strong correlation between the antibody adsorption and PVA film photoswitching property data. Duty cycle (Figure 4-3f) and photoswitching time (Figure 4-3e) were less strongly correlated between the two different fluorophore isolation methods. Overall, the antibody and PVA fluorophore isolation methods demonstrated strongly correlated photoswitching properties, which was further demonstrated by the fact that the total photons measured using each method statistically correlated to microtubule width and that the duty cycle measured for each method statistically correlated to microtubule continuity (Table 4-2).

Correlations seen between the photoswitching properties measured with both the antibody adsorption and PVA film isolation methods at the highest fluence rate translated to trends seen across all three fluence rates (Figure 4-4). Localization precision (Figure 4-4d and 4-4j) and switching events (Figure 4-4b and 4-4h) demonstrated the strongest correlation at the highest fluence rate. Photons (Figure 4-4a and 4-4g) and total photons (Figure 4-4c and 4-4i) trended similarly for both the antibody adsorption and PVA film isolation methods. Photoswitching time (Figure 4-4e and 4-4k) and duty cycle (Figure 4-4f and 4-4l) showed little relationship to fluence rate.

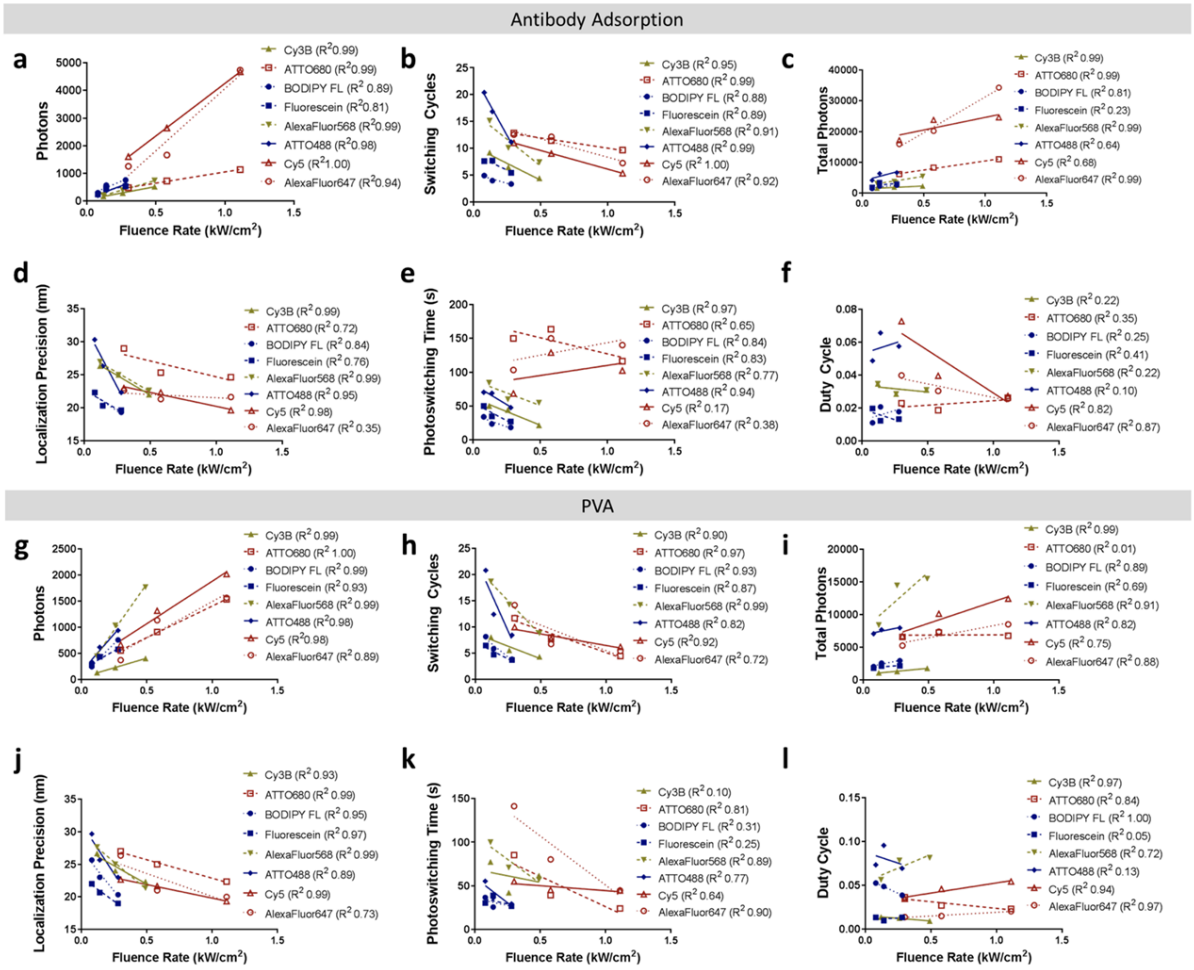

Figure 4-4 Correlation of photoswitching properties and fluence rate for antibody adsorption (a-f) and PVA (g-l) isolated fluorophores. Linear regression analysis of each average photoswitching property versus fluence rate was completed and R^2 values were calculated (see key for values) for (a,g) photons per switching cycle, (b,h) switching cycles, (c,i) total photons, (d,j) localization precision, (e,k) photoswitching time, and (f,l) duty cycle. Mean photoswitching properties for n=3 SMLM imaging series for each fluorophore are displayed.

4.3.4 Effect of Excitation Fluence Rate on Photoswitching Properties

Correlative relationships were observed between select photoswitching properties and fluence rate using both the antibody adsorption and PVA film single-molecule systems (Figure 4-4). Linear regressions were calculated using the average value (n=3 SMLM image series/fluorophore) for each photoswitching property at each fluence rate to quantify the degree of correlation using R^2 values. Photons per switching cycle (Antibody R^2 = 0.81-1.0, PVA R^2 = 0.89-1.0) and number of switching cycles (Antibody R^2 = 0.88-1.0, PVA R^2 = 0.72-0.99) were strongly correlated with fluence rate, where increased fluence rate resulted in greater photon output and fewer switching cycles. Total photons (Antibody R^2 = 0.23-0.99, PVA R^2 = 0.01-0.99) and localization precision (Antibody R^2 = 0.35-0.99, PVA R^2 = 0.73-0.99) showed general positive correlation with fluence rate, however neither property was as strongly correlated as photons per switching cycle or number of switching cycles. Photoswitching time and duty cycle were largely unaffected by fluence rate (Figure 4-4e, 4-4f, 4-4k and 4-4l).

4.3.5 Intersample Stability of Photoswitching Property Measurements

The reported photoswitching properties represented mean and standard deviation calculated from triplicate imaging series collected for each fluorophore at three fluence rates (Table 4-1 and Supplementary Figure S4-2, S4-3). The coefficient of variation (CV) was less than 1 for all fluorophores across the computed photoswitching properties, demonstrating that the photoswitching property measurements were reproducible using both the antibody adsorption and PVA film fluorophore isolation methods. Some properties had lower standard deviation than others exhibiting better reproducibility. For both the antibody adsorption and PVA film fixation methods the least variable photoswitching property was localization precision (CV < 0.1 for all fluorophores), followed by photons with CVs ranging 0.03 – 0.4. The most variable photoswitching properties was photoswitching time with CVs ranging up to 0.7. However, overall both fluorophore isolation methods provided robust, reproducible measurements of the defined photoswitching properties.

4.4 DISCUSSION

In summary, we developed a methodology to correlate fluorophore photoswitching properties to SMLM image quality using two single molecule isolation systems. We examined PVA film as a method for facile characterization of fluorophores developed for SMLM or optimization of imaging buffer systems, where the photoswitching properties of fluorophores measured using both PVA film and the previously utilized antibody adsorption method were correlated with SMLM image quality (Figure 4-1 and 4-2). While prior studies have characterized photoswitching,[2,29,35] our study is the first to demonstrate a statistically significant correlation between SMLM image quality and photoswitching properties including total photons and duty cycle (Table 4-2). We found microtubule width was statistically correlated with total photon output using both the antibody absorption and PVA film fluorophore isolation methods, while duty cycle was significantly correlated to microtubule continuity using both fluorophore isolation methods (Table 4-2 and Figure 4-3). Interestingly, previous studies have demonstrated strong correlation between photons per switching cycle and SRM image quality. In the current study, total photons was significantly correlated to image quality rather than photons per switching cycle, which is likely explained by the different photophysical environments provided by the antibody adsorption and PVA film isolation methods. Although the imaging buffer utilized in both fluorophore isolation systems contained oxygen scavengers, the PVA film may have further reduced oxygen permeation into the system, thus affecting photoswitching physics,[54,63,85] potentially accounting for the differences seen in photon output per switching cycle and the number of switching cycles compared with the antibody adsorption method. However, the calculation of total photon output as the product of these two photoswitching properties recapitulated the relationship seen in the antibody adsorption fluorophore isolation method, where significant correlation was demonstrated between image quality and overall photon output (Table 4-2).

Interestingly, we found that fluorophores resulting in higher quality images had higher duty cycle than those of lower quality SRM images, which is in contradiction to previous

studies where shorter duty cycle was thought to improve SRM image quality.[2] We hypothesize that higher duty cycle was significantly correlated with image quality in our study because of the difference in duty cycle calculation. In our study, duty cycle was calculated over the entire collected photoswitching analysis video, where images were collected as soon as the laser was turned on and thus, no pre-photobleaching step was included. Therefore, our higher duty cycle measurements represent individual fluorophore molecules that were less susceptible to photobleaching. Thus, higher duty cycles reflected fluorophore molecules spending more time in the fluorescent on state. While higher duty cycles could enhance imaging by improving the ability to detect individual fluorophore molecules, it could potentially be detrimental for fluorophores to have high cycles as it increases the chances of detected fluorophore overlap, which degrades SMLM image quality.[86] The low fluorophore density used for photoswitching property analysis in this study were well below the threshold where fluorophore overlap would affect accurate quantification of photoswitching property measurements, explaining the strong imaging quality correlation to the higher duty cycle photoswitching property in both the antibody absorption and PVA fluorophore isolation methods.

We also found that the photon output related photoswitching properties measured using both fluorophore isolation methods correlated to fluence rate, while the fluorescent on and off time parameters showed little correlation with fluence rate. While previous studies observed that the fluence rate used to excite photoswitchable fluorophores affects SMLM image quality,[2,87] the clear impact of fluence rate on photoswitching properties and image quality was demonstrated here. We found a strong correlation between photons per switching cycle and number of switching cycles as well as general positive correlation between fluence rate, total photons and localization precision. Higher quality SMLM images were achieved with fluorophores having higher total photons and duty cycle (Figure 4-1 and 4-3). Therefore, the highest fluence rate tested for each laser line was found to be the best for SMLM imaging, and hence most effective for future screening of developed fluorophores for SMLM. Importantly, similarities in photoswitching property rankings and response to fluence rate will enable either fluorophore isolation method to be used for accurate fluorophore evaluation and comparison. Lastly, we also quantified

the repeatability of photoswitching measurements in both the antibody adsorption and PVA film based systems, demonstrating a robust platform for screening developed fluorophores for SMLM using single-molecule isolation (Figure 4-3 and Table 4-1).

Herein, we demonstrate that PVA is a facile fluorophore isolation method that can be used to screen fluorophores or imaging buffer conditions to predict SMLM image quality based on the quantification of total photon output and duty cycle. The PVA film method eliminates the functionality hurdle in screening novel fluorophores, facilitating a potentially high throughput approach for large studies. The utilization of PVA film fluorophore isolation system, provides the necessary means to evaluate and guide future fluorophore development, as well as screen for optimal image buffer conditions, to improve the spatial and spectral resolution of SRM through quantification of photoswitching properties that predict SRM image quality.

4.5 METHODS

4.5.1 Fluorophores

The eight fluorophores utilized in this study were obtained commercially in their succinimidyl ester form including Fluorescein, BODIPY FL, AlexaFluor568, AlexaFluor647 (Thermo Fisher Scientific), ATTO488, ATTO680 (ATTO-TEC), Cy3B and Cy5 (GE Healthcare Life Sciences).

4.5.2 Fluorophore-labeled Antibodies

Each fluorophore was conjugated to donkey anti-mouse antibody (Jackson ImmunoResearch) for SMLM microtubule imaging and single-molecule photoswitching property measurements. The antibody was buffered exchanged into 1x phosphate buffered saline (PBS) and pH adjusted to 8.0 with 35 mM disodium phosphate. The conjugation reactions were set up with fluorophore and antibody mixed in a 5:1 molar ratio for SMLM microtubule imaging and 1:1 molar ratio for single-molecule

photoswitching property measurements. The fluorophore-antibody conjugation reactions were rocked gently at room temperature protected from light for 3 hr and were concentrated in 10 kDa MWCO spin filters followed by purification using a 7 kDa desalting column. The fluorophore to antibody-labeling conjugation ratios ranged from 1.1:1 to 2.3:1 for SMLM microtubule imaging and ranged from 0.4:1 to 0.5:1 for single-molecule photoswitching property measurements, which were determined using an absorbance spectrometer (SpectraMax M5 Microplate Reader).

4.5.3 Single-Molecule Localization Super Resolution Microscope Configuration

Imaging was completed on a Nikon ECLIPSE Ti-U inverted microscope equipped with a 60x oil immersion objective (NA=1.49) using total internal reflection fluorescence configuration of the light path. Excitation laser lines included 488-nm (Coherent), 561-nm (Opto Engine LLC), and 647-nm (Coherent), with images collected through a 525/45, 605/64, or 708/75 nm single-bandpass filter (Semrock Inc.), respectively. An EMCCD camera (Andor Technology) recorded images in a 512 x 512 pixel area at 107 nm/pixel, with a 100 ms exposure time and a gain setting of 300 via via Micro-Manager.[88,89] Images of single molecules were processed with modified custom-written Matlab scripts (Mathworks)[90] and microtubule images were processed with the ThunderSTORM[91] plugin for ImageJ. Processing conditions were kept constant across all 8 selected fluorophores.

4.5.4 Imaging Buffer

Tris-buffered saline (TN buffer, 50 mM Tris pH 8.0 and 10 mM NaCl) with oxygen scavenger components including 0.5 $mgml^{-1}$ glucose oxidase, 40 μgml^{-1} catalase (Sigma Aldrich), and 10% w/v glucose, as well as the reducing component 10 mM β-mercaptoethylamine, were utilized for all imaging and photoswitching property measurements.[2,8]

4.5.5 SMLM Microtubule Images

Cell culture. U2OS cells were cultured in Dulbecco's Modified Eagle media without phenol red supplemented with 10% FBS and 1% Penicillin-Streptomycin-Glutamine at 37° C and 5% CO_2. LabTek 8-well coverglass chambers were washed with SparKLEEN (5 min), milli-Q water (3 x 5 min), 1 M NaOH (90 min), and milli-Q water (3 x 5 min) prior to plating cells at ~80,000 cells per well. Cells were incubated for 2 days to reach ~75% confluency.

Immunofluorescence labeling. Cells were preextracted with 0.5% Triton X-100 in PEM (100 mM PIPES buffer pH 7.0, 1 mM EGTA and 1 mM $MgCl_2$) for 20 s, fixed with 0.4% glutaraldehyde (Electron Microscopy Science) and 0.25% Triton X-100 in PEM for 90 s, washed with PBS before fixing with 3% glutaraldehyde in PEM 15 min. Cells were washed with PBS (3 x 5 min), then reduced with 10 mM sodium borohydride for 10 min, washed again with PBS (3 x 5 min), and blocked with 5% bovine serum albumin (BSA) in PBS. Cells were incubated with bovine alpha-tubulin mouse primary antibody (Thermo Fisher Scientific) at 2 $\mu g ml^{-1}$ in BSA/Triton for 4 h at room temperature and washed with PBS (3 x 5 min). Lastly, cells were incubated with fluorophore-labeled donkey anti-mouse secondary antibody at 25 µM fluorophore concentration across the eight fluorophores in 5% BSA for 30 min at room temperature protected from light and washed with PBS (3 x 5 mins).[61]

Imaging. A mixture of 200 µl imaging buffer and 2 µl gold nanoparticles (BBI International) fiducial markers was added to the labeled cells prior to imaging. Images were collected at a frame rate of 10 Hz for 10,000 frames. Samples labeled with Fluorescein, ATTO488, or BODIPY FL were excited using 488-nm laser line (0.28 $kWcm^{-2}$). Samples labeled with Cy3B or AlexaFluor568 were excited by the 561-nm laser line (0.49 $kWcm^{-2}$). Samples labeled with Cy5, AlexaFluor647, or ATTO680 were excited by the 647-nm laser line (1.11 $kWcm^{-2}$).

Microtubule quantitation. The image quality of the rendered SMLM images was quantitated based on the microtubule width and continuity, which were measured at 15

representative points per image where labeling was most complete and the structure was well defined. The width was calculated by taking the FWHM from line profiles summed over 13 nm lengths of the microtubule structure. The continuity was reported as the photon density of microtubules per square nanometer. Continuity was calculated as the summed photons detected along a 670 nm length sections of microtubules using the calculated width to determine the measured microtubule area in nm^2.

4.5.6 Single-Molecule Fixation

Single-molecule samples were fixed in 96-well glass bottom plates with #1.5 coverglass bottom (In Vitro Scientific), washed as detailed for the LabTek plates above. Single-molecule isolation was performed using two fixation methods: antibody adsorption and PVA film formation. For the antibody adsorption method, 100 µl of fluorophore-labeled antibody diluted to a final concentration of $1x10^{-10}$ M fluorophore in 1x PBS was used per well. Antibody solutions were incubated for 16 h at room temperature sealed and protected from light, then washed and stored in PBS at 4° C. For the PVA film method, fluorophores were diluted to a final concentration of $5x10^{-9}$ M in 1 wt% PVA (72,000 MW) and 50 µl was used per well before drying in a fume hood overnight.

4.5.7 Single-Molecule Photoswitching Measurements

All measurements were carried out in the imaging buffer described above. For adsorbed antibody samples, storage PBS was aspirated prior to the addition of imaging buffer. For PVA film samples, the dried PVA films were quickly flushed with PBS 3x to remove any molecules not isolated by the dried film prior to addition of imaging buffer. PVA film measurements were collected between 10 and 60 minutes after adding the imaging buffer to allow for adequate penetration of the buffer into the solid film, but prior to any compromise of the film by rehydration that could allow for molecule drift out of the PVA matrix.

Each sample was imaged three times in three different regions of the 96-well plate at each of the selected fluence rates termed low, mid and high for each laser line.

Fluorescein, ATTO488 and BODIPY FL were excited with a 488-nm laser line at fluence rates of 0.08, 0.14, and 0.28 $kWcm^{-2}$. Cy3B and AlexaFluor568 were excited with a 561-nm laser line at fluence rates of 0.12, 0.26, and 0.49 $kWcm^{-2}$. Cy5, AlexaFluor647, and ATTO680 were excited with a 647-nm laser line at fluence rates of 0.30, 0.58, and 1.11 $kWcm^{-2}$. Imaging videos were collected for 5,000 frames at 10 Hz.

4.5.8 Single-Molecule Data Analysis

Single molecules were identified as fluorescent signals detected above a threshold 6 times root mean square (RMS) of the average detected signal. Molecules were tracked positionally throughout the 5,000-frame image series while recording the x and y coordinates of their point-spread function. A minimum of 100 molecules were identified in each 5,000-frame image series. Photoswitching properties were quantitated as follows.

Photons per switching cycle. The number of photons emitted per switching cycle was calculated algebraically by summing the fluorescence emission signal collected over consecutive frames from a single molecule that was above 6 times RMS, minus the baseline intensity. This was considered a single switching cycle. The summed signal (analog digital units, ADU) was converted to photons using the camera's reported analog-to-digital conversion factor (DCF, electrons/ADU), quantum efficiency (QE), and the acquisition gain setting (gain) as follows: photons = ADU x DCF x 1/QE x 1/gain.

Switching Cycles. The number of switching cycles was determined by counting the instances a tracked particle emitted photons above 6 times RMS, reflecting how often the molecule transitioned from the off to the on state.

Total Photons. The total photon values were calculated by multiplying the photons per switching cycle by the number of switching cycle, resulting in the total photons a single molecule emitted throughout the image series.

Localization Precision. The lateral localization precision, σ_{xy}, was determined using the standard deviation of the x (σ_x) and y (σ_y) coordinates recorded for each molecule throughout the 5,000-frame image series calculated as $\sigma_{xy} = (\sigma_x^2 + \sigma_y^2)^{1/2}$.

Photoswitching Time. The photoswitching time was calculated as the amount of time in seconds a single molecule photoswitched during the entire 5,000-frame image series. This was calculated as the time difference between the first switching cycle and the last switching cycle. Results were calculated only for molecules that had their initial cycle during the first 100 s to prevent truncating photoswitching time calculations for molecules that started blinking at a later time point in the image series.

Duty Cycle. The duty cycle represents the fraction of time fluorophores emit photons during the 500 s acquisition time. Duty cycle was calculated as the number of frames the fluorophore was considered on (above the set threshold of RMS 6) divided by the total number of frames.

4.5.9 Statistical Analysis of Photoswitching Properties

Statistical analysis was completed using GraphPad Prism (GraphPad Software). To determine the correlation of each photoswitching property to image quality, a spearman two-tail correlation test[84] was completed comparing the set of average widths (n=15/fluorophore, 8 fluorophores) and the set of average continuity (n=15/fluorophore, 8 fluorophores) to the average of each photoswitching property (n=3/fluorophore, 8 fluorophores) (Table 4-2). This test was conducted on data from both the antibody adsorption and PVA film fixation methods. Correlation was reported as significant for $p<0.05$.

To study the relationship between fluence rate and photoswitching properties, linear regressions were completed using the average value (n=3 SMLM image series/fluorophore) for a particular photoswitching property at each fluence rate. Computed R^2 values, defined as the coefficient of determination, were reported to

characterize the correlation between photoswitching property and fluence rate. R^2 values closer to 1 indicate a more linear relationship while R^2 values closer to 0 indicate a less linear relationship.[92]

To study the intersample stability of photoswitching property measurements, the coefficient of variance (CV) was calculated by dividing the standard deviation of the triplicate measurements by the mean of the triplicate measurements.

4.6 ACKNOWLEDGEMENTS

We would like to thank Drs. Tao Huang and Li-Jung Lin for experimental assistance. This study was supported in part by a collaborative research agreement between Thermo Fisher Scientific and Oregon Health and Science University.

4.7 SUPPLEMENT

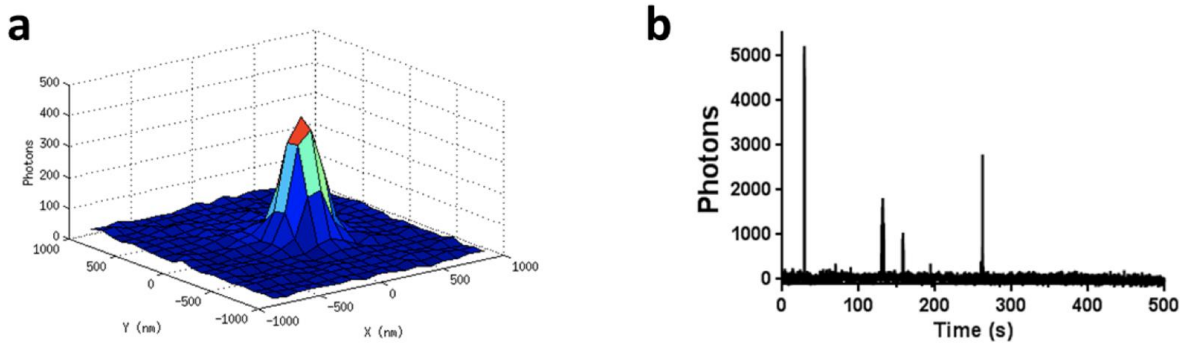

Supplemental Figure S4-1 Representative single molecule data to demonstrate photoswitching property calculations. Photoswitching data characterizing a single molecule of AlexaFluor568 fixed in PVA film, measured at the high fluence rate (Φ = 0.49 kWcm-2) are shown. (a) The intensity of a single molecule in its fluorescent on state in one frame. (b) Intensity tracked throughout the entire 500 s imaging series. Switching events represented the number of spikes in intensity over a set threshold. Photoswitching time represented the time from the first switching event to the last switching event.

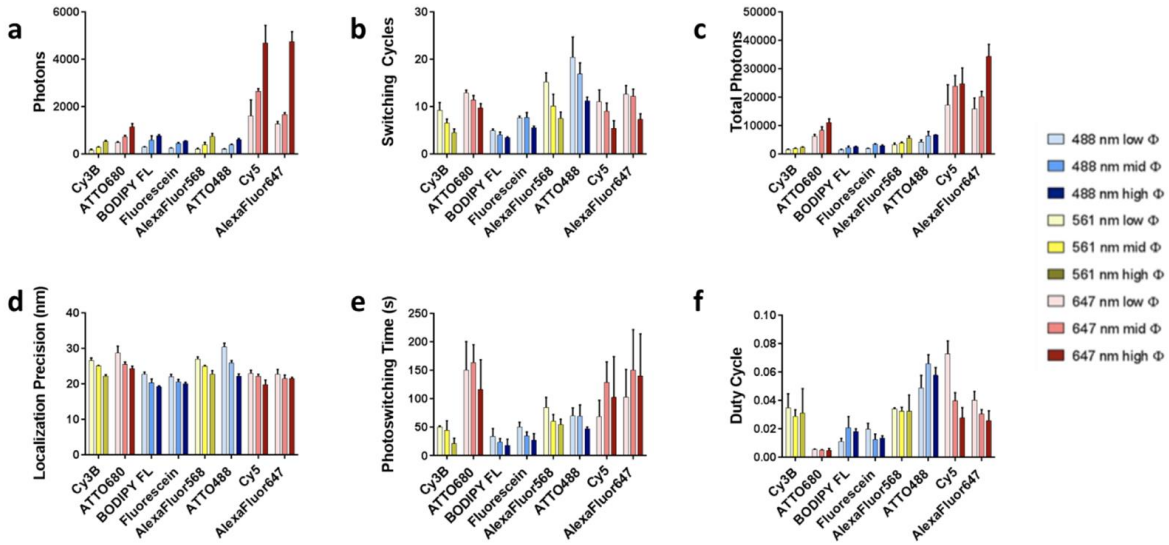

Supplemental Figure S4-2 Photoswitching properties of antibody adsorption isolated fluorophores over a range of fluence rates. A low, mid and high fluence rate (Φ) were selected for each laser line and utilized to measure photoswitching properties including (a) photons per switching cycle, (b) number of switching cycles, (c) total photons, (d) localization precision, (e) photoswitching time, and (f) duty cycle. Average photoswitching properties represent the mean ± standard deviation of N=3 single molecule localization SRM imaging series for each fluorophore.

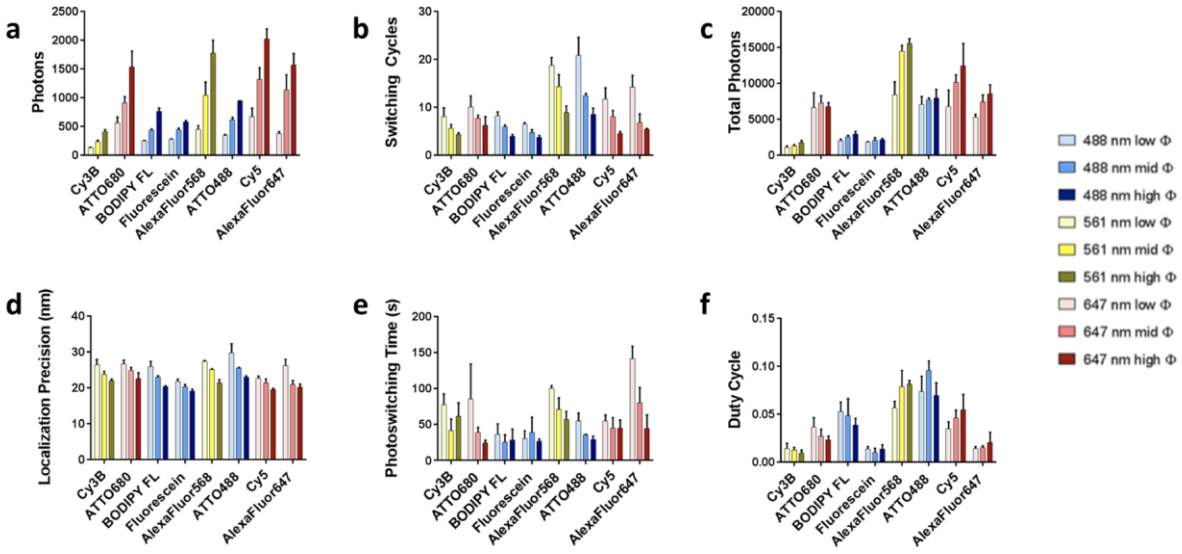

Supplemental Figure S4-3 Photoswitching properties of PVA film isolated fluorophores over a range of fluence rates. A low, mid and high fluence rate (Φ) were selected for each laser line and utilized to measure photoswitching properties including (a) photons per switching cycle, (b) number of switching cycles, (c) total photons, (d) localization precision, (e) photoswitching time, and (f) duty cycle. Average photoswitching properties represent the mean ± standard deviation of N=3 single molecule localization SRM imaging series for each fluorophore.

CHAPTER 5: Screening Imaging Buffers for BODIPY-Based Photoswitchable Fluorophores[§]

[§]Bittel, A.M., Saldivar, I.S., Dolman, N.J., Nan, X., & Gibbs, S.L. *Superresolution Microscopy with Novel BODIPY-Based Fluorophores.* Will submit for publication July 2017.

5.1 ABSTRACT

Single-molecule localization microscopy (SMLM) is a fluorescence microscopy technique able to achieve resolution of ~10-20 nm with photoswitchable fluorophores. Small molecule organic fluorophores are a popular choice for SMLM, however they require suitable imaging buffer conditions to promote photoswitching. While imaging buffers have been thoroughly examined for the routinely used fluorophores scaffolds including cyanine, rhodamine, and oxazine, optimal conditions have not been found for the BODIPY scaffold, precluding its routine use for SMLM. Herein, we screened common imaging buffer conditions including seven redox reagents with five additives, resulting in 35 overall imaging buffer conditions to identify compatible combinations for BODIPY based fluorophores. We found BODIPY FL produced high quality SMLM images with several imaging buffers with two redox conditions where 10 mM MEA (2-mercaptoethylamine) and 100 mM MEA were optimal. Advantageously, these imaging buffers also resulted in high quality SMLM imaging with the conventionally used Alexa Fluor 647, paving the way for multicolor imaging studies using BODIPY based probes with fluorophores routinely used for SMLM imaging.

5.2 INTRODUCTION

Single-molecule localization microscopy (SMLM) is one of several super resolution microcopy (SRM) techniques that enable fluorescence imaging below the diffraction limit

of light (~250 nm).[5,23] SMLM is able to achieve resolution on the scale of ~10-20 nm through the use of photoswitchable fluorophores that stochastically switch between the fluorescent “on” state and the nonfluorescent “off” state.[93] Photoswitching enables the accurate localization of individual fluorophores to be tracked during the collection of many images, which are then reconstructed to form a single SRM image with ~10-20 nm resolution.

Photoswitchable fluorophores consist of small molecule organic fluorophores, which are used with the SMLM technique stochastic optical reconstruction microscopy (STORM),[5,32,54] and fluorescent proteins, which are used with photoactivated localization microscopy (PALM) technique.[23,31] Small molecule organic fluorophores are advantageous for SMLM because they are brighter than fluorescent proteins and offer more options for multicolor SMLM imaging studies than fluorescent proteins. However, commercially available small molecule organic fluorophores do not innately photoswitch, and the required photoswitching must be driven by imaging conditions, particularly selection of an appropriate imaging buffer.

Imaging buffers have been studied thoroughly with the small molecule organic fluorophore scaffolds including cyanine, oxazine, and rhodamine, and have revealed that different conditions are optimal for each chemical scaffold.[2] For example, ascorbic acid (AA) and methyl viologen (MV) have often been used as reducing and oxidizing agents, respectively. Cyanine based fluorophores photoswitch best when there is more AA than MV,[36] while oxazine based fluorophore photoswitching is improved when there are equal amounts of AA and MV.[80] Additionally, additives have been shown to further enhance photoswitching, such as tris(2-carboxyethyl)phosphine (TCEP)[37] and cyclooctatetraene (COT)[7] for cyanine, and sodium borohydride ($NaBH_4$) for rhodamine and oxazine.[94] However, even with the many imaging buffers options that have been investigated for SMLM, little is known about the optimal conditions for the BODIPY fluorophore scaffold. Importantly, BODIPY-based fluorophores have strong potential to provide additional fluorophore options for SMLM since they encompass a range of spectral properties. Commercially available BODIPY fluorophores emit at various wavelengths throughout the

visible range with short Stokes shifts,[1] and recently BODIPY-based fluorophores have been developed with varied length Stokes shifts,[39] potentially permitting SMLM imaging of additional colors in a single sample.

Herein, we evaluated common imaging buffers and additives, resulting in a total of 35 tested conditions to identify optimal photoswitching conditions for the BODIPY fluorophore scaffold using BODIPY FL as our model fluorophore. We also measured the cyanine based fluorophore, AlexaFluor647 (AF647) for comparison since it is one of the most widely used fluorophores for SMLM.[2,32,54] Through screening single molecules isolated in PVA, we found multiple buffer conditions that resulted in photoswitching of BODIPY FL. SMLM imaging of *in vitro* microtubules confirmed the imaging buffer conditions of 10 mM MEA and 100 mM MEA, both with oxygen scavenger, worked best for BODIPY FL by producing high quality SMLM images.

5.3 RESULTS AND DISCUSSION

5.3.1 Imaging buffer effect on photoswitching properties of single molecules

BODIPY FL and AF647 were diluted and dried in PVA to isolate single molecules before evaluating their photoswitching properties in the presence of various imaging buffer conditions and additives. The imaging buffers consisted of 7 redox reagents including **(1)** 500 µM AA and 500 µM MV, **(2)** 500 µM AA, **(3)** 500 µM MV, **(4)** 10 mM MEA, **(5)** 100 mM MEA, **(6)** 143 mM βME, and **(7)** 5 mM catechol, with five different additive conditions including, **(i)** 2 mM COT, **(ii)** 10 mM TCEP, **(iii)** 5 mM 3CP, **(iv)** $NaBH_4$ treatment, as well as **(v)** no additive, all with the oxygen scavenger GLOX. Qualitative photoswitching quality was assessed during image series collection (Table 5-1). Single molecules ranged widely in the frequency of their switching, with some buffers resulting in little to no switching while others resulted in switching that occurred throughout the entire image series. Additionally, there were vast differences in intensity of the switching in comparison to the background, where some buffers promoted higher photon output per switching event. Based on qualitative observations, the highest quality switching conditions were similar for both

BODIPY FL and AF647, and included the four oxidizing conditions **(1)** 500 µM AA and 500 µM MV, **(4)** 10 mM MEA, **(5)** 100 mM MEA, and **(6)** 143 mM βME, with three of the additive conditions including **(i)** 2 mM COT, **(iii)** 5 mM 3CP, and **(v)** no additive.

Table 5-1 Imaging buffer conditions and qualitative observed switching quality. BODIPY FL and AF647 were screened in PVA with various imaging buffer conditions. Observed switching quality of single molecules is indicated by (-): little/no switching; (+): some switching; (++): switching through most of the image series; and (+++): bright switching throughout the image series.

Buffer		Observed Blinking Quality	
Reducing and/or Oxidizing Agent	Additive	BODIPY FL	AF647
1) 500 µM MV, 500 µM AA	i) 2 mM COT	++	++
	ii) 10 mM TCEP	+	-
	iii) 5 mM 3CP	++	++
	iv) NaBH4, 10mM for 5 min	++	++
	v) none	+	++
2) 500 µM AA	i) 2 mM COT	+	++
	ii) 10 mM TCEP	-	-
	iii) 5 mM 3CP	+	+
	iv) NaBH4, 10mM for 5 min	-	+
	v) none	-	++
3) 500 µM MV	i) 2 mM COT	++	++
	ii) 10 mM TCEP	-	+
	iii) 5 mM 3CP	++	+
	iv) NaBH4, 10mM for 5 min	-	-
	v) none	-	++
4) 10 mM MEA	i) 2 mM COT	+	++
	ii) 10 mM TCEP	-	-
	iii) 5 mM 3CP	++	+++
	iv) NaBH4, 10mM for 5 min	++	-
	v) none	+++	+++
5) 100 mM MEA	i) 2 mM COT	++	+++
	ii) 10 mM TCEP	-	+
	iii) 5 mM 3CP	++	+++
	iv) NaBH4, 10mM for 5 min	+	++
	v) none	+++	+++
6) 143 mM βME	i) 2 mM COT	++	++
	ii) 10 mM TCEP	-	++
	iii) 5 mM 3CP	-	+
	iv) NaBH4, 10mM for 5 min	+	++
	v) none	+++	++
7) 5 mM Catechol	i) 2 mM COT	+	+
	ii) 10 mM TCEP	-	-
	iii) 5 mM 3CP	+	-
	iv) NaBH4, 10mM for 5 min	-	+
	v) none	+	+

Photoswitching properties were calculated for these aforementioned highest quality switching conditions (Figure 5-1). Photoswitching properties were not calculated for the lower quality imaging buffer and additive conditions, as they were not relevant to SMLM imaging. Interestingly, some of the lowest quality imaging buffer and additive conditions had an extremely low population of switching events, or in some cases no switching events that could be reliably detected above background. Additionally, some imaging buffer and additive conditions did not result in photoswitching, but were perpetually in the "on" state until eventual photobleaching, resulting in a misleading representation of those imaging series by photoswitching properties alone. For the high quality imaging buffer and additive condition image series that were further analyzed, four photoswitching properties were calculated including total photons, duty cycle, number of switching cycles, and localization precision, which has been previously demonstrated to significantly correlate with high quality SMLM images.[6]

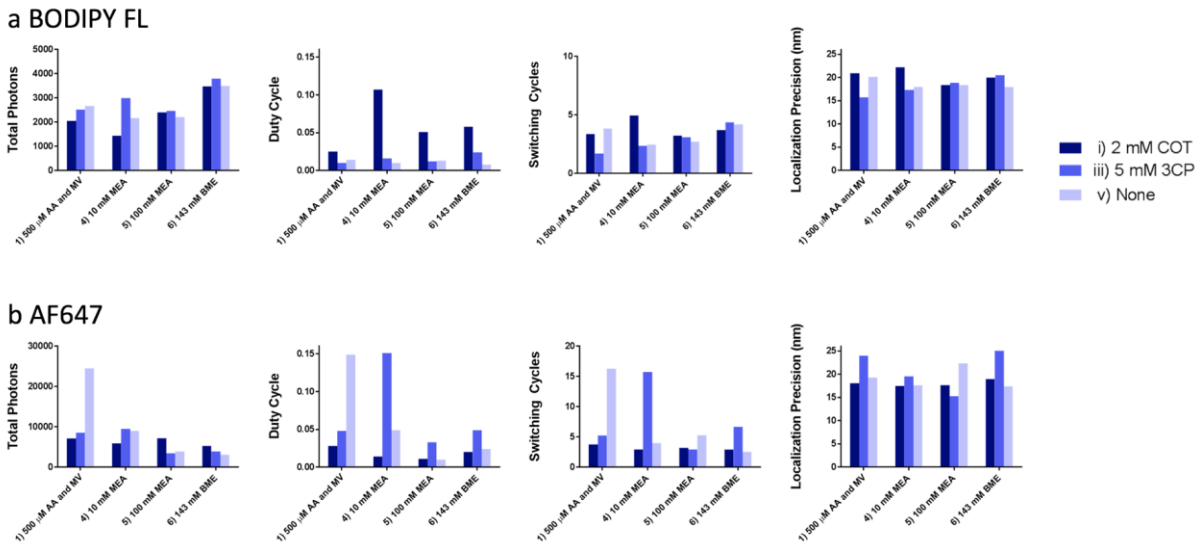

Figure 5-1 Photoswitching properties of single molecules in PVA including total photons, duty cycle, switching cycles, and localization precision. The data was grouped by reducing/oxidizing reagent, noted on the x-axis, with the additives indicated by the color bars coded in the key. (a) BODIPY FL and (b) AF647.

BODIPY FL had the highest total photon output with 143 mM βME with additives **(i)**, **(iii)** and **(v)**, ranging from 3,500-3,800 total photons, while the other redox systems had lower total photon output ranging from 1,400-3,000 photons (Figure 5-1a). AF647 emitted the highest total photons with the redox reagents 500 µm AA and 500 µM MV with additives **(i)**, **(iii)** and **(v)**, ranging from 7,100-25,000 photons, and 10 mM MEA with the additives **(i)**, **(iii)** and **(v)**, ranging from 5,900-9,600 photons (Figure 5-1b). Interestingly, no additive demonstrated a consistent influence on the total photon output for either BODIPY FL or AF647. Of note, the additive 2 mM COT clearly increased the duty cycle across all four redox conditions for BODIPY FL, where duty cycle was highest with 10 mM MEA. The additive 5 mM 3CP resulted in the highest duty cycle in three out four of the redox conditions for AF647. Likewise, BODIPY FL also had the highest number of switching events with the 2 mM COT additive combined with 10 mM MEA while AF647 had nearly the highest number of switching cycles with 5 mM 3CP combined with 10 mM MEA. Localization precision ranged similarly for BODIPY FL (17.9-22.2 nm) and AF647 (15.3-25.0 nm), with no consistent trends across redox reagents or additives.

Overall, there was no single imaging buffer condition and additive for either BODIPY FL or AF647 that optimized values across all four measured photoswitching properties. However, the additive 2 mM COT resulted in the highest duty cycle and switching cycles for BODIPY FL, while the additive 5 mM 3CP resulted the highest duty cycle and nearly the highest switching cycles for AF647. Select imaging buffers were further examined using SMLM imaging of microtubules to elucidate optimal formulations for high quality SMLM images.

5.3.2 High quality SMLM images of microtubules obtained with multiple imaging buffer and additive conditions

Imaging buffer conditions evaluated by SMLM imaging of *in vitro* microtubules included **(4)** 10 mM MEA with **(v)** no additive, **(5)** 100 mM MEA with **(v)** no additive, **(6)** 143 mM βME with **(v)** no additive, **(5)** 100 mM MEA with **(iii)** 5 mM 3CP, and **(5)** 100 mM MEA with **(i)** 2 mM COT (Figure 5-2). While all buffers produced images of distinct microtubule

structures, there were differences in image quality. BODIPY FL microtubule images had the best single-to-noise (SNR) using 10 mM MEA, 100 mM MEA, and 143 mM βME, all with no additive, and the worst SNR with 100 mM MEA with the 2 mM COT additive (Figure 5-2a). Interestingly, the 100 mM MEA with the 2 mM COT additive provided the highest duty cycle and switching cycles for BODIPY FL on single molecules in PVA, but this did not necessarily translate to image quality based on the microtubule images. AF647 clearly had the highest image quality when imaged in 100 mM MEA with the 2 mM COT additive, matching previous observations with COT.[75] However, high quality SMLM images were also rendered for AF647 using 10 mM MEA and 100 mM MEA without additive (Figure 5-2b).

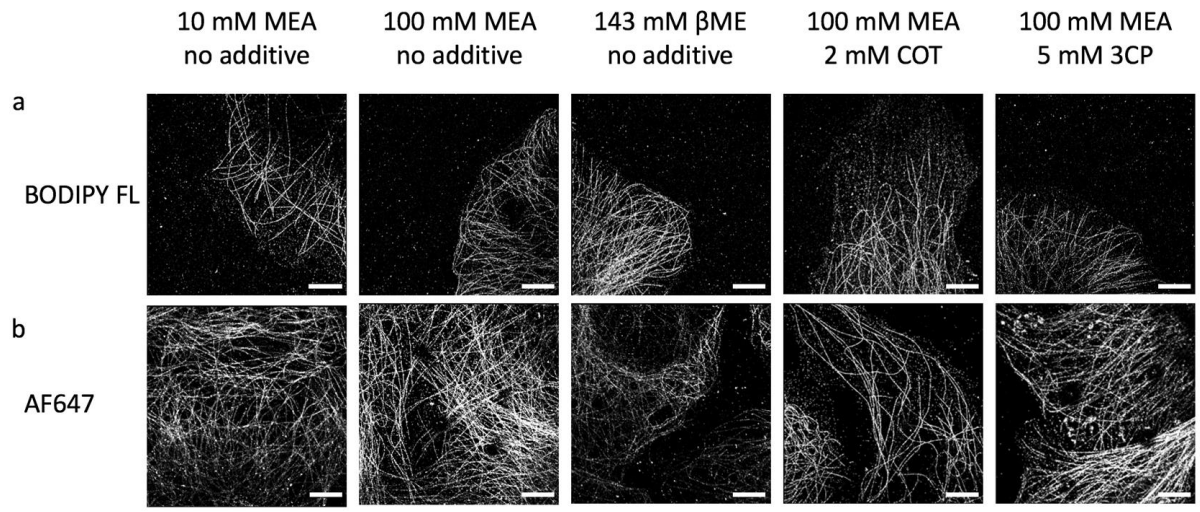

Figure 5-2 SMLM imaging of microtubules *in vitro* via indirect immunofluorescence in fixed cells with various imaging buffer conditions labeled by immunofluorescence with (a) BODIPY FL and (b) AF647. (scale bar = 5 μm)

In summary, the imaging buffers selected based on PVA screening of photoswitching properties all resulted in clear SMLM images of microtubule structures, further validating the fluorophore photoswitching property screening methodology. However, the best images did not precisely align with the photoswitching properties, which could indicate that there is a finite limitation to the PVA screening approach, in that it can undoubtedly identify conditions that will produce quality images, however the best imaging conditions cannot necessarily be identify based on photoswitching properties alone and require imaging studies for full validation. Overall, the photoswitching screening methodology provide utility as it enabled assessment of 35 unique imaging conditions on single molecules to be pared down to 5 successful conditions for final assessment by microtubule imaging studies.

Identification of multiple imaging buffer conditions that result in high quality SMLM images is advantageous as it provides flexibility when choosing buffer conditions to accommodate multiple fluorophores. Conveniently, the best buffer conditions for BODIPY FL, which were 10 mM MEA, 100 mM MEA, and 143 mM βME, all with no additive, included buffers commonly used with other scaffolds,[2,35] making integration of BODIPY-based fluorophores into current SMLM protocols and multicolor experiments feasible. Specifically, since BODIPY FL and AF647 both resulted in high quality SMLM images using 10 mM MEA and 100 mM MEA with no additive, multicolor experiments could be completed using either of these imaging buffer formulations. When AF647 is used individually for SMLM imaging, high quality images resulted from using of the COT additive.

5.4 CONCLUSION

In summary, we evaluated a range of imaging buffer conditions with BODIPY FL and AF647, including seven redox reagent combinations with five additive conditions, resulting in 35 imaging buffer conditions evaluated in total. As expected, image series collected in PVA clearly demonstrated that imaging buffer conditions strongly influenced fluorophore photoswitching. Select conditions were further evaluated by SMLM imaging

of microtubules, which revealed several imaging buffer conditions that resulted in high quality images with both BODIPY FL and AF647, including overlapping conditions of 10 mM MEA and 100 mM MEA without additive. Identification of image buffer conditions that result in high quality BODIPY-based fluorophores opens up an entire new class of fluorophores for use with SMLM.

5.5 METHODS

5.5.1 Single-Molecule Localization Microscopy Configuration

Imaging was completed on a Nikon ECLIPSE Ti-U inverted microscope equipped with a Nikon 60x oil immersion objective (NA = 1.49) using total internal reflection fluorescence configuration of the light path (Nikon Inc., Melville, NY). Excitation was completed using 488-nm and 647-nm lasers (Coherent, Santa Clara, CA), with images collected through a 525/45 nm or 708/75 nm single-bandpass filter (Semrock Inc., Rochester, NY), respectively. The 488-nm laser was used at a fluence rate of 0.28 $kWcm^{-2}$ and the 647-nm laser was used at fluence rate of 1.11 $kWcm^{-2}$. An EMCCD camera was used to (Andor Technology, Concord, MA) recorded images in a 256 × 256 pixel area at 107 nm/pixel, with a 100 ms exposure time and an EM gain setting of 300 using Micro-Manager.[89]

5.5.2 Imaging Buffers

All imaging buffers were prepared in tris-buffered saline (TN buffer, 50 mM tris pH 8 and 10 mM NaCl) with GLOX as the oxygen scavenger (0.5 $mgml^{-1}$ glucose oxidase (Sigma Aldrich, St. Louis, MO), 40 μgml^{-1} catalase (Sigma Aldrich), and 10% w/v glucose). Seven redox conditions were tested including, **(1)** 500 µM ascorbic acid (AA, Thermo Fisher Scientific) with 500 µM methyl viologen hydrate (MV, Thermo Fisher Scientific, Waltham, MA), **(2)** 500 µM AA, **(3)** 500 µM MV, **(4)** 10 mM 2-mercaptoethylamine HCl (MEA, Thermo Fisher Scientific), **(5)** 100 mM MEA, **(6)** 143 mM 2-mercaptoethanol (βME, Thermo Fisher Scientific), and **(7)** 5 mM catechol (Thermo Fisher Scientific). With each

redox condition tested, five additives were screened including, **(i)** 2 mM cyclooctatetraene (COT, Thermo Fisher Scientific), **(ii)** 10 mM tris(2-carboxyethyl)phosphine (TCEP, Thermo Fisher Scientific), **(iii)** 5 mM 3-(Carboxy)-2,2,5,5-tetramethyl-1-pyrrolidinyloxy (3CP, Thermo Fisher Scientific), **(iv)** sodium borohydride ($NaBH_4$, Sigma Aldrich), where the sample was incubated with 10 mM $NaBH_4$ in Milli-Q water for 5 min, washed with TN buffer, then imaged with the remaining redox buffer, and **(v)** no additive. See Table 5-1 for all imaging buffer conditions and additive combinations tested. GLOX oxygen scavenger, redox agent, and additive were mixed and added to the sample 10-30 min before imaging in a sealed plated.

5.5.3 Single-molecule Photoswitching Measurements

BODIPY FL and AlexaFluor 647 (AF647) were obtained in their N-hydroxysuccinimide (NHS) ester form (Thermo Fisher Scientific, Waltham, MA) and prepared as 10 mM stocks with dimethyl sulfoxide. Fluorophores were diluted to 5 nM in 1% polyvinyl alcohol (PVA, 72,000 MW, MP Biomedicals, Newport Beach, CA) and 50 µl was placed per well of a 96-well glass bottom plate (Cellvis, Mountain View, CA), and dried under vacuum overnight. Wells were flushed three times with 1x phosphate buffered saline (PBS) before adding imaging buffer. Images were collected for 5,000 frames with BODIPY FL excited using the 488-nm laser and AF647 excited using the 647-nm laser. Images were processed with custom Matlab scripts to quantify photoswitching properties including, total photons, duty cycle, switching cycles, and localization precision as previously described.[6] Briefly, total photons represents the number of photons emitted by each molecule throughout the whole image series and was calculated as the average photons per switching cycle multiplied by the average number of switching cycles. Duty cycle represents the fraction of time each fluorophore emits photons, with “on” frames divided by total frames. Switching cycles is the number of times a molecule changes from the “off” state to the “on” state, where it’s emitting photons above Localization precision is lateral localization precision, based on the standard deviation in the x and y direction of each identified molecule.[83]

5.5.4 SMLM Imaging of Microtubules

Fluorophore-labeled antibodies were prepared by conjugating BODIPY FL and AF647 to donkey anti-mouse secondary antibody (Jackson ImmunoResearch, West Grove, PA) using standard manufacturer protocols (Thermo Fisher Scientific). Conjugation reactions were purified with fast protein liquid chromatography (NGC Quest 10 Plus Chromatography System, Bio-Rad, Hercules, CA) by size exclusion (P6 gel filtration column, 40 x 12.6 mm, Bio-Rad). Final fluorophore to antibody conjugation ratios were ~1-2 fluorophore molecules per antibody, with concentrations determined using absorbance spectroscopy and fluorophore extinction coefficients (BODIPY FL = 80,000$M^{-1}cm^{-1}$ and AF647 = 239,000 $M^{-1}cm^{-1}$ [1]). The U2OS osteosarcoma human cell line was cultured in Dulbecco's Modified Eagle Medium without phenol red (Thermo Fisher Scientific) in 96-well glass bottom plates (Cellvis). The cells were permeabilized and fixed with Triton-X 100 and glutaraldehyde as previously described.[6] Cells were incubated with 10 $\mu g ml^{-1}$ anti-tubulin primary antibody (EMD Millipore, Billerica, MA) for 30 min and washed with 1x PBS 3 times for 5 min per wash. After washing, the fluorophore conjugated anti-mouse secondary antibodies were incubated with the cells at 10 µg/ml antibody for 30 min. Cells were washed 3 times for 5 min per wash with 1x PBS, fixed for 10 min with 4% paraformaldehyde, and stored in 1x PBS with 3 mM sodium azide prior to imaging. SMLM imaging was conducting using five imaging buffer conditions for 5,000 frames, including, three buffers, **(4)** 10 mM MEA, **(5)** 100 mM MEA, and **(6)** 143 mM βME, with **(v)** no additive, **(5)** 100 mM MEA with **(iii)** 5 mM 3CP, and **(5)** 100 mM MEA with **(i)** 2 mM COT Images were processed with custom Matlab scripts previously described.[6]

CHAPTER 6: Superresolution Microscopy with Novel BODIPY-Based Fluorophores[§]

[§]Bittel, A.M., Saldivar, I.S., Dolman, N.J., Nan, X., & Gibbs, S.L. *Superresolution Microscopy with Novel BODIPY-Based Fluorophores.* Will submit for publication July 2017.

6.1 ABSTRACT

Multicolor single-molecule localization microscopy (SMLM) expands our understanding of subcellular details and enables the study of biomolecular interactions through precise visualization multiple molecules in a single sample with resolution of ~10-20 nm. Probe selection is vital to multicolor SMLM image quality, as the fluorophores must not only exhibit minimal spectral crosstalk, but also must be compatible with the same photo-chemical conditions that promote fluorophore photoswitching. While there are numerous commercial photoswitchable fluorophores that are optimally excited at 561 nm, they are restricted to short Stokes shifts (<30 nm), resulting in a lack of fluorophores that are excited at 561 nm and emit above ~615 nm. Herein, we demonstrate BODIPY-based fluorophores with varied length Stoke shifts that exhibit photoswitching ability, providing additional color options for 561 nm excitation for SMLM. Specifically, **BAA-30a**, which has an emission maximum at 643 nm, provides an option to create a two-color image with 561 nm excitation when used with a shorter Stokes shift fluorophore.

6.2 INTRODUCTION

Superresolution microscopy (SRM) enables fluorescence imaging below the diffraction limit of light (~250 nm), greatly enhancing visualization of subcellular detail.[5,23,38] While multiple types of SRM exist, single-molecule localization microscopy (SMLM) has achieved the best spatial resolution of ~10 nm in fixed cells through the detection and

localization of single molecules.[93] SMLM methods include photoactivated localization microscopy (PALM)[23,31] and stochastic optical reconstruction microscopy (STORM),[5,38,54] which require photoswitchable fluorophores that stochastically switch between the fluorescent “on” state and nonfluorescent “off” state.[28] Fluorophore photoswitching properties directly impact the detection and localization accuracy of each fluorophore in SMLM, making probe selection critical to image quality.[6,29]

Multicolor SMLM expands our understanding of subcellular detail and enables the study of biomolecular interactions through precise visualization of multiple biomolecule in a single sample. However, probe selection becomes even more critical as the photoswitchable fluorophores must not only exhibit minimal spectral crosstalk, but also must be compatible with the same photo-chemical conditions that promote fluorophore photoswitching. While fluorophores have been found that photoswitch with similar imaging buffers,[2,35] there remain limited conventional fluorophores with optimal spectral properties for multicolor SMLM imaging. Commercially available photoswitchable fluorophores that have created quality SMLM images using 561-nm excitation all have relatively short Stokes shifts <30 nm, with an average of 20 nm. This results in a lack of fluorophores that emit above ~615 nm that can be excited at 561 nm, leaving a gap in spectral emission space of ~35 nm (Table 6-1, Figure 6-1). Identifying photoswitchable fluorophores compatible with standard imaging buffer that emit in this region would facilitate multicolor SMLM by enabling multiple fluorophores to be spectrally separated using 561-nm excitation and emission space between 565-650 nm.

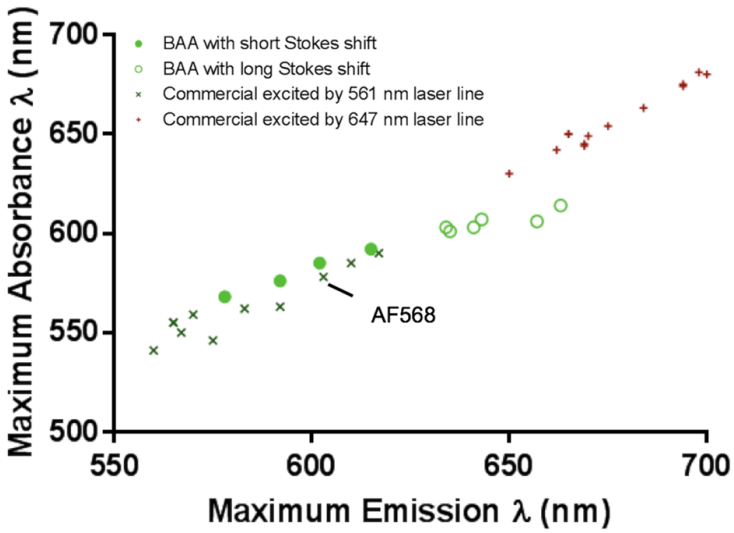

Figure 6-1 Maximum absorbance wavelength vs. maximum emission wavelength for BAA fluorophores with short Stokes shifts (●) and long Stokes shifts (○), and commercially available fluorophores excited by the 561 nm laser (x) and 647 nm laser (+). Details in Table 6-1.

Table 6-1 Summary of BAA and commercial fluorophores that fill the spectral space corresponding to the 561 nm and 647 nm laser excitation. Photophysical properties summarized include maximum excitation and emission wavelengths, and Stokes shift.

Fluorophore		λ_{Abs} (nm)	λ_{Ex} (nm)	Stokes shift (nm)	Laser (nm)
BAA fluorophores with short Stokes shift	BAA-37a	568	578	10	561
	BAA-55a	576	592	16	561
	BAA-22a	585	602	17	561
	BAA-5a	592	615	23	561
BAA fluorophores with long Stokes shift	BAA-77a	603	634	31	561
	BAA-2a	601	635	34	561
	BAA-48a	603	641	38	561
	BAA-30a	607	643	36	561
	BAA-39a	606	657	51	561
	BAA-75a	614	663	49	561
Commercial fluorophores excited by 561 nm laser line	CF543	541	560	19	561
	AF555	555	565	10	561
	CF555	555	565	10	561
	Dy547	550	567	17	561
	Cy3B	559	570	11	561
	TAMRA	546	575	29	561
	CF568	562	583	21	561
	ATTO565	563	592	29	561
	AF568	578	603	25	561
	Cy3.5	585	610	25	561
	AF594	590	617	27	561
Commercial fluorophores excited by 647 nm laser line	CF633	630	650	20	647
	CF640R	642	662	20	647
	AF647	650	665	15	647
	CF647	650	665	15	647
	ATTO647	645	669	24	647
	ATTO647N	644	669	25	647
	Cy5	649	670	21	647
	Dy654	654	675	21	647
	ATTO655	663	684	21	647
	Dy678	674	694	20	647
	Cy5.5	675	694	19	647
	CF680	681	698	17	647
	ATTO680	680	700	20	647
	CF680R	680	701	21	647
	AF680	679	702	23	647
	ATTO700	700	719	19	647
	Dy704	706	721	15	647
	AF700	702	723	21	647

Recently a BODIPY-based fluorophore library (BAA) has been synthesized with varied length Stokes shift fluorophores that are optimally excited using a 561-nm laser,[39] providing an opportunity to fill the spectral void and expand the number of fluorophore probe options available for multicolor SMLM. Herein, we selected six BODIPY-based fluorophores (BAA) with long Stokes shifts (>30 nm) that have emission between 634-663 nm, and were optimally excited with the 561-nm laser including **BAA-77a**, **BAA-2a**, **BAA-48a**, **BAA-30a**, and **BAA-39a**. Additionally, we selected four BAA fluorophores that had conventional short Stokes shifts (<30 nm) for further evaluation of BODIPY-based fluorophores for SMLM imaging including **BAA-37a**, **BAA-55a**, **BAA-22a**, and **BAA-5a**. All fluorophores were compared to AF568, since it is one of the most widely used photoswitchable fluorophores with the 561-nm excitation.

6.3 RESULTS AND DISCUSSION

6.3.1 Fluorophore Photoswitching Properties in Polyvinyl Alcohol (PVA)

BAA fluorophores were diluted and fixed in PVA to facilitate accurate measurement and analysis of photoswitching properties of individual molecules. Four properties were evaluated that have been shown to correlate with SMLM image quality including total photons (the number of photons emitted per switching event multiplied by the number of switching events), duty cycle (fraction of time the molecules emitted photons throughout image acquisition), switching cycles (the number of times the molecule switched between the “on” and “off” state), and localization precision.[6]

Measurements revealed that all ten BAA fluorophores photoswitched and had higher total photon output than AF568 (Figure 6-2). The long Stokes shift BAA fluorophores had lower overall photon output, ranging from 3,700 to 6,000 total photons compared to the short Stokes shifts BAA fluorophores, which ranged from 5,500 to 11,700 photons. BAA-5a had the highest total photon output, with 11,700 photons, which was nearly twice the total photon output as the next highest measured fluorophore. Conversely, all the BAA fluorophores had lower duty cycle than AF568. While the duty cycle of AF568 was 0.028,

the duty cycles of the BAA fluorophores ranged from 0.004 to 0.012. The number of switching cycles was relatively similar between the long Stokes shift BAA fluorophores, which ranged from 3.5 to 4.6, and AF568 (switching cycles = 3.9). All the short Stokes shift BAA fluorophores demonstrated fewer switching cycles than AF568, ranging from 3.2 to 3.4. A similar trend between groups was seen in the localization precision, where the long Stokes shift BAA fluorophore ranged from 22.2 nm to 29.0 nm, and were comparable to AF568 (localization precision = 23.3 nm), while the short Stokes shift BAA fluorophores all had greater localization precision ranging from 27.3 nm to 33.4 nm.

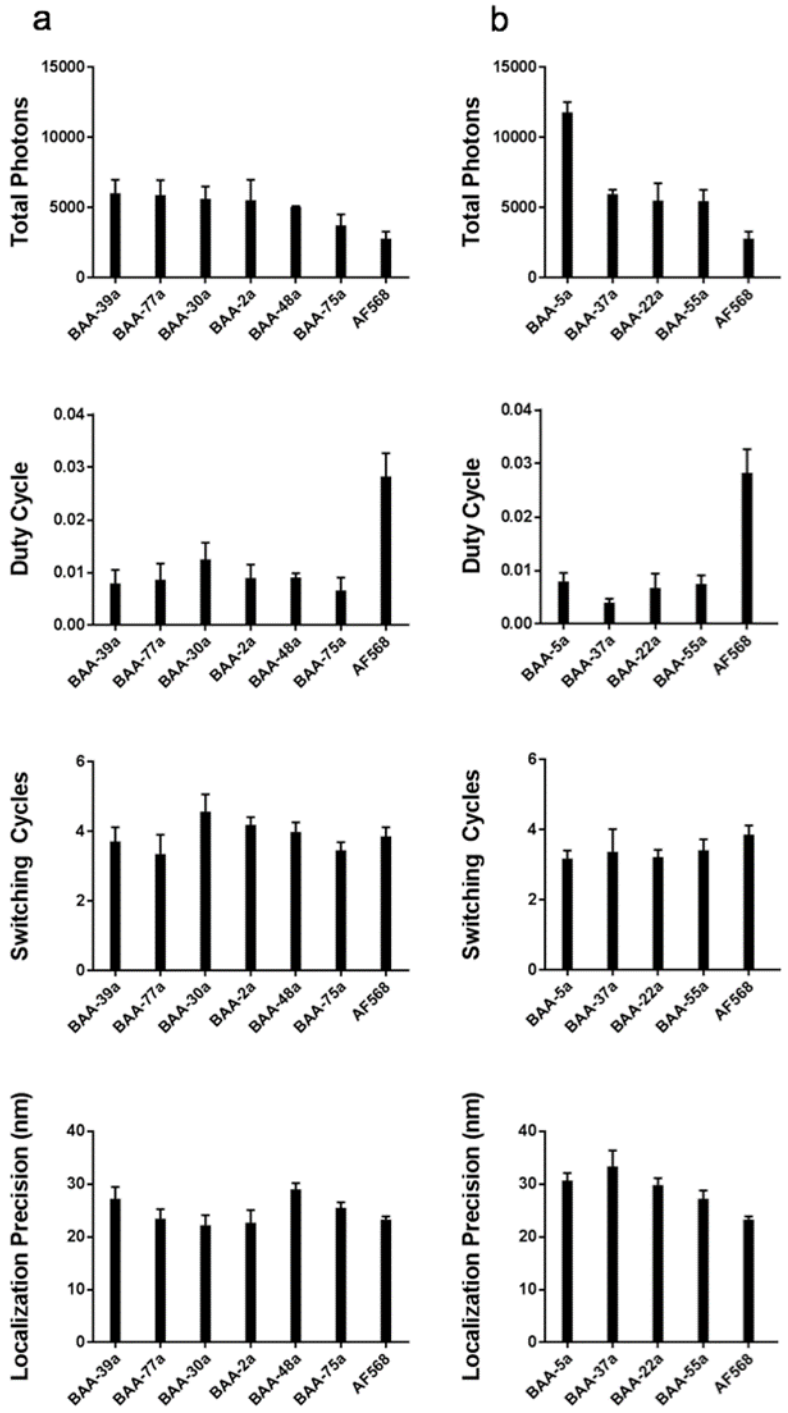

Figure 6-2 Photoswitching properties including total photons, duty cycle, number of switching cycles, and localization precision for BAA fluorophores and AF568, with data organized by decreasing total photons with standard deviation of triplicate measurements. (a) BAA fluorophores with long Stokes shifts vs. AF568. (b) BAA fluorophores with short Stokes shifts vs. AF568.

Overall, the photoswitching properties demonstrated the potential for the BAA fluorophores for use as SMLM labeling reagents using 561 nm excitation. Higher total photon output has been shown to be significantly correlated with high quality SMLM images,[6] suggesting that the BAA fluorophores could provide improved SMLM images compared to AF568. Additionally, since greater number of switching cycles and lower localization precision correlated with image quality,[6] the relatively greater number of switching cycles and lower localization precision of the long Stokes shift BAA fluorophores may result in higher quality SMLM images than the short Stokes shift BAA fluorophores. However, both the long Stokes shift and short Stokes shift BAA fluorophores had lower duty cycle than AF568, leaving it not quite clear if the BAA fluorophores would produce better images since higher duty cycle was also shown to be significantly correlated with improved SMLM image quality.[6]

6.3.2 SMLM Imaging with BAA Fluorophores

A BAA fluorophore from both the long and short Stokes shift groups were selected for SMLM imaging of microtubules based on their quantified photoswitching properties. **BAA-30a** was selected as the long Stokes shift BAA fluorophore because, its duty cycle and number of switching cycles were greater than the other long Stokes shift BAA probes and its localization precision was lower, predicting high overall SMLM image quality. Additionally, **BAA-30a** could be spectrally separated using an ET640/20m bandpass filter from fluorophores typically imaged with the 561-nm laser using conventional bandpass filters such as ET605/52m (Figure 6-3). **BAA-5a** was selected as a representative short Stokes shift BAA fluorophore since it had the highest total photon output by nearly twice and had a longer duty cycle than the other short Stokes shift BAA fluorophores, predicting high SMLM image quality.

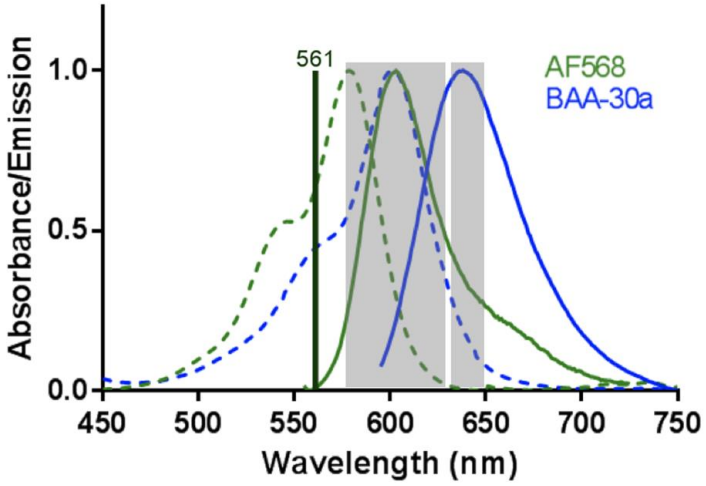

Figure 6-3 Absorbance (dotted) and emission (solid) spectra of AF568 and long Stokes shift BAA fluorophore **BAA-30a**. The 561 nm laser (green line) is displayed with two bandpass filters, ET605/52m (left) and ET640/20m (right) (gray shaded regions).

As expected, both **BAA-30a** and **BAA-5a** labeled microtubules generated SMLM images with defined microtubule structures (Figure 6-4). While the microtubules labeled with **BAA-30a** and **BAA-5a** were not as continuous as with AF568, they had a narrower width that was more closely matched with the expected microtubule width of 55 nm when labeled by immunofluorescence.[2,56,74,75] Images with **BAA-30a** and **BAA-5a** could be potentially improved by incubating the cells with more fluorophore labeled secondary antibody or using a longer acquisition time for SMLM imaging. **BAA-5a** appeared to generate higher quality SMLM images than **BAA-30a**, which could be explained by the fact that **BAA-5a** had much higher photon output than **BAA-30a**.

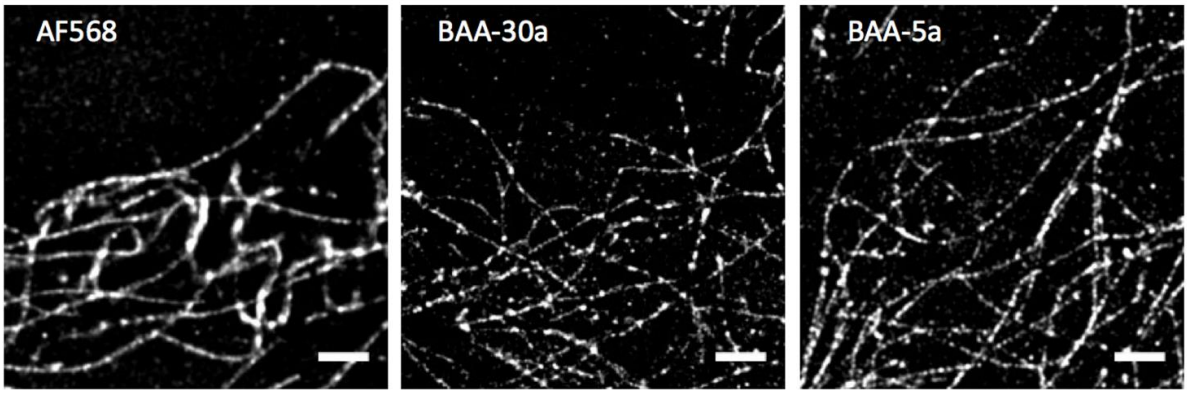

Figure 6-4 SMLM imaging of microtubules *in vitro* via indirect immunofluorescence in fixed cells labeled with AF568, **BAA-30a** and **BAA-5a**. (scale bar = 2 μm).

6.4 CONCLUSION

In summary, we evaluated BODIPY-based (BAA) fluorophores that could be optimally excited by the 561-nm laser for their photoswitching ability. We found that the BAA fluorophores all photoswitched, where some BAA fluorophores had higher total photon output and lower localization precision than AF568, predicting improved SMLM image quality. We further evaluated a long Stokes shift BAA fluorophore, **BAA-30a** (emission maximum = 643 nm), and a short stokes shift BAA fluorophore, **BAA-5a** (emission maximum = 615 nm), for SMLM image quality using labeling of microtubules *in vitro*. Both BAA fluorophores demonstrated successful labeling of microtubules, confirming their utility as photoswitchable fluorophores while providing additional spectral options for multicolor SMLM. **BAA-30a** provides an option to create a two-color image using a single color excitation, 561 nm, when used with shorter Stokes shift fluorophores such as the conventional AF568 or the novel **BAA-5a**.

6.5 METHODS

6.5.1 Single-Molecule Localization Microscope Configuration

All single-molecule and microtubule imaging was completed on a Nikon ECLIPSE Ti-U (Nikon Inc., Melville, NY) inverted microscope configured for total internal reflection fluorescence of the light path and equipped with a 60x oil immersion objective (NA = 1.49) (Nikon). Fluorophores were excited with a 561-nm laser (Opto Engine LLC, Midvale, UT) at fluence rate 0.49 $kWcm^{-2}$. Filters included Di01-R405/488/461/635-25x36 dichroic, NF01-568/647 notch, NF03-405E-25 notch and FF01-605/64-25 emission (Semrock Inc., Rochester, NY). Images were recorded using an EMCCD camera (Andor Technology, Concord, MA) in a 256 x 256 pixel area at 167 nm/pixel, with a 30 ms exposure time and gain setting of 300 via Micro-Manager.[89,95]

6.5.2 Single-Molecule Photoswitching Analysis

AlexaFluor 568 (AF568), obtained commercially in its N-hydroxysuccinimidyl ester (NHS) form (Thermo Fisher Scientific, Grand Carlsbad, CA), and BAA fluorophores (**BAA-77a**, **BAA-2a**, **BAA-48a**, **BAA-30a**, **BAA-39a**, **BAA-37a**, **BAA-55a**, **BAA-22a**, and **BAA-5a**)[39] were prepared at 10 mM stock solutions in dimethyl sulfoxide. Fluorophores were further diluted to $5x10^{-9}$ M in 1% polyvinyl alcohol (72,000 MW, MP Biomedicals, Newport Beach, CA) and dried in prewashed 96-well glass bottom plates as previously described.[6] Photoswitching measurements were completed in mercaptoethylamine (MEA)-based imaging buffer consisting of tris-buffered saline with 0.5 $mgml^{-1}$ glucose oxidase, 40 $ugml^{-1}$ catalase, 10% w/v glucose, and 10 mM β-mercaptoethylamine.[2,8] 5,000 frame imaging videos of each PVA prepared fluorophore sample were collected in triplicate.

Photoswitching data analysis was completed using custom MatLab scripts (Mathworks, Natick, MA) to quantitate four photoswitching properties including total photons, duty cycle, number of switching cycles, and localization precision[6,90]. Total photons were calculated as the photons per switching cycle multiplied by the number of switching cycles. Duty cycle was calculated as the number of frames a molecule was "on," or emitting photons above the set threshold, divided by the total number of frames. The number of switching cycles was calculated as the number of times a molecule emitted photons above the set threshold. Localization precision (σ_{xy}) was calculated using the standard deviation of the x (σ_x) and y (σ_y) coordinates recorded for each molecule throughout the 5,000-frame imaging video as $\sigma_{xy} = (\sigma_x^2 + \sigma_y^2)^{1/2}$.

6.5.3 Generation of Fluorophore-Labeled Antibodies

The BAA fluorophores selected for SMLM imaging, **BAA-5a** and **BAA-30a**, were converted to the NHS ester functional form using the following reactions. The carboxylic acid functionalized BAA fluorophore was diluted into dimethylformamide, mixed with 1-[Bis(dimethylamino)methylene]-1H-1,2,3-triazolo[4,5-b]pyridinium 3-oxid hexafluoro-phosphate (2.2 equiv.) and diisopropylethylamine (5.8 equiv.), and mixed for 30 min. N-

hydroxysulfosuccinimide (4 equiv.) was then added followed with an additional 60 min of mixing. The reaction was washed with deionized water and the product was extracted with ethyl acetate before drying by lyophilization. The NHS ester functionalized versions of AF568, **BAA-5a**, and **BAA-30a** were conjugated to donkey anti-rat secondary antibody (Jackson ImmunoResearch, West Grove, PA) by mixing 200 µg of antibody with fluorophores at approximately 3:1 fluorophore to antibody ratio in 1x PBS (pH 8) for 3 hr. Conjugation reactions were purified by fast protein liquid chromatography (NGC Quest 10 Plus Chromatography System, Bio-Rad, Hercules, CA) using size exclusion (P6 gel filtration column, 40 x 12.6 mm, Bio-Rad). Final fluorophore to antibody conjugation ratios were 1-2 fluorophore molecules per antibody, with concentrations determined using absorbance spectroscopy and fluorophore extinction coefficients (AF568 = 88,000 $M^{-1}cm^{-1}$ [2], **BAA-5a** = 24,700 $M^{-1}cm^{-1}$ [39], and **BAA-30a** = 17,600 $M^{-1}cm^{-1}$).

6.5.4 Cell culture and immunofluorescence staining

The U2OS osteosarcoma human cell line was cultured in Dulbecco's Modified Eagle Medium without phenol red (Thermo Fisher Scientific) in 96-well glass bottom plates. Cells were grown to 80% confluence after which they were permeabilized and fixed with Triton-X 100 and glutaraldehyde as previously described.[6] Cells were incubated with 10 $\mu g ml^{-1}$ anti-tubulin primary antibody (Jackson ImmunoResearch) for 30 min and washed with 1x PBS 3 times for 5 min per wash. The cells were then incubated with fluorophore conjugated anti-rat secondary antibodies at 20 µg/ml antibody for 30 min. The cells were again washed 3 times for 5 min per wash with 1x PBS, fixed for 10 min with 4% paraformaldehyde, and stored in 1x PBS with 3 mM sodium azide prior to imaging.

6.5.5 SMLM Imaging of Microtubules

Imaging of labeled microtubules in vitro was conducted in MEA imaging buffer on the SMLM. Images were collected for 10,000 frames and were processed with custom MatLab scripts described previously.[6]

CHAPTER 7: Conclusions and Future Directions

7.1 Dissertation Conclusions

Herein, a library of 95 BODIPY-based (BAA) fluorophores were designed, synthesized, and characterized for conventional and superresolution microscopy imaging. We demonstrated the applicability of our library with a subset of BAA fluorophores with varied length Stokes shifts to create a five-color image using a single excitation laser (561-nm) for the first time with confocal laser scanning microscopy. Furthermore, we found that specific BAA fluorophores have potential as organelle specific fluorophores for labeling fixed cells, but overall staining at immunofluorescence concentrations resulted in low SBR ideal for targeted imaging. Before selecting BAA fluorophores for imaging with SMLM, we developed methodology to efficiently evaluate fluorophores for their photoswitching capabilities. PVA was validated as a medium to isolate single fluorophore molecules for quantification of their total photon output and duty cycle, which significantly correlated to SMLM image quality. The PVA methodology enabled the screening of image buffer conditions to identify an optimal image buffer formulation for BODIPY-based fluorophores, with both 10 mM MEA and 100 mM MEA reducing agents with oxygen scavenger resulting in high quality SMLM images. Finally, short and long Stokes shift BAA fluorophores that could be optimally excited with the 561-nm laser were found to successfully photoswitch when evaluated in PVA with 10 mM MEA. Furthermore, a long Stokes shift BAA fluorophore, **BAA-30a** (emission maximum = 643 nm), and a short stokes shift BAA fluorophore, **BAA-5a** (emission maximum = 615 nm), demonstrated successful labeling of microtubules, confirming their utility as photoswitchable fluorophores while providing additional spectral options for multicolor SMLM.

7.2 Future Directions

Several topics presented in this dissertation deserve additional investigation explained as follows. I propose the following future directions should be addressed. 1) Organelle localization studies of BAA fluorophores categorized as vesicular and cytosolic. 2)

Quantitative structure-activity relationship (QSAR) modeling of BAA fluorophore organelle specificity and molecule properties. 3) Investigation of the BODIPY scaffold photoswitching mechanism. 4) BAA photoswitching property screening and QSAR modeling.

7.2.1 Organelle localization studies of BAA fluorophores categorized as vesicle and cytosol.

BAA fluorophores were found to localize to vesicular and cytosolic regions of fixed cells, however their precise organelle specificity was not determined (Chapter 3). Vesicular regions include adiposomes, lysosomes and peroxisomes, while the cytosol contains structures such as the endoplasmic reticulum, Golgi complex or mitochondria. Organelle specificity could be determined through dual labeling fixed cells with known targeted probes. Identifying organelle specific BAA fluorophores would provide additional tools for multicolor microscopy and enable quantitative structure-activity relationship analysis, explained as follows.

7.2.2 Quantitative structure-activity relationship (QSAR) modeling of BODIPY-based fluorophore organelle specificity and molecule properties.

BAA fluorophore localization to different organelles was attributed to the diverse styryl modifications of the core BODIPY FL structure providing an opportunity for QSAR modeling (Chapter 3). Molecular properties of BAA fluorophores were characterized including partition coefficient (LogD), number of rotatable bonds, number of hydrogen bond donors and acceptors, and the polar surface area. QSAR between the molecule properties and organelle specificity would provide an understanding for correlation between structure and subcellular localization, and potentially facilitate rational synthesis of future BODIPY-based organelle probes with desired spectral properties.

7.2.3 Investigation of the BODIPY scaffold photoswitching mechanism.

BAA fluorophores exhibited diverse photoswitching characteristics (Chapter 6). While photoswitching is influenced by reducing and oxidizing reactions,[28,40,58] the complete photoswitching mechanism of BODIPY is not known. Cyanine scaffolds have been shown to photoswitch due to the formation of cyanine-thiol adducts, where the thiol attaches to the polymethine bridge of the cyanine,[59] while oxazine has been shown to photoswitch due to reducing agent interactions with the nitrogen atom along the oxazine backbone.[96] However, neither of these mechanisms translate directly to BODIPY as its structure differs substantially from both cyanine and oxazine. Elucidating the BODIPY photoswitching mechanism could be completed by using a combination of mass spectroscopy and Fourier transform infrared spectroscopy to study BODIPY in its reduced state.

7.2.4 BAA photoswitching property screening and QSAR modeling.

Differences in photoswitching among the ten screened BAA fluorophores can be attributed to the diverse styryl modifications of the core BODIPY FL structure (Chapter 6). Screening the photoswitching properties of the remaining fluorophores of the 95-member BAA library would provide a substantial data set for QSAR modeling to further understand how styryl modifications influence BODIPY photoswitching.

References

1 Haugland, R. P., Spence, M. T. Z., Johnson, I. D. & Basey, A. *The Handbook: A Guide to Fluorescent Probes and Labeling Technologies* 10th edn, (Molecular Probes, 2005).

2 Dempsey, G. T., Vaughan, J. C., Chen, K. H., Bates, M. & Zhuang, X. Evaluation of fluorophores for optimal performance in localization-based super-resolution imaging. *Nature methods* **8**, 1027-1036, doi:10.1038/nmeth.1768 (2011).

3 Lampe, A., Haucke, V., Sigrist, S. J., Heilemann, M. & Schmoranzer, J. Multi-colour direct STORM with red emitting carbocyanines. *Biology of the cell* **104**, 229-237, doi:10.1111/boc.201100011 (2012).

4 Kanazawa, T., Era, A. & Ueda, T. Spectral Imaging: a Powerful Tool for Confocal Multicolor Imaging in Living Plant Cells. 6 (2015).

5 Rust, M. J., Bates, M. & Zhuang, X. Sub-diffraction-limit imaging by stochastic optical reconstruction microscopy (STORM). *Nature methods* **3**, 793-795, doi:10.1038/nmeth929 (2006).

6 Bittel, A. M. *et al.* Methodology for Quantitative Characterization of Fluorophore Photoswitching to Predict Superresolution Microscopy Image Quality. *Sci Rep* **6**, 29687, doi:10.1038/srep29687 (2016).

7 Olivier, N., Keller, D., Gonczy, P. & Manley, S. Resolution doubling in 3D-STORM imaging through improved buffers. *PloS one* **8**, e69004, doi:10.1371/journal.pone.0069004 (2013).

8 van de Linde, S. & Sauer, M. How to switch a fluorophore: from undesired blinking to controlled photoswitching. *Chemical Society reviews* **43**, 1076-1087, doi:10.1039/c3cs60195a (2014).

9 Lavis, L. D. & Raines, R. T. Bright ideas for chemical biology. *ACS chemical biology* **3**, 142-155, doi:10.1021/cb700248m (2008).

10 Karolin, J., Johansson, B. A. L., Strandberg, J. L. & NyZ, T. Fluorescence and Absorption Spectroscopic Properties of Diprrometheneboron Difluoride (BODIPY) Derivatives in Liquids, Lipid Membranes, and Proteins. *Journal of the American Chemical Society* **116**, 7801-7806, doi:10.1021/ja00096a042 (1994).

11 Ulrich, G., Ziessel, R. & Harriman, A. The chemistry of fluorescent bodipy dyes: versatility unsurpassed. *Angew Chem Int Ed Engl* **47**, 1184-1201, doi:10.1002/anie.200702070 (2008).

12 Loudet, A. & Burgess, K. BODIPY dyes and their derivatives: syntheses and spectroscopic properties. *Chemical reviews* **107**, 4891-4932, doi:10.1021/cr078381n (2007).

13 Vendrell, M. *et al.* Solid-phase synthesis of BODIPY dyes and development of an immunoglobulin fluorescent sensor. *Chem Commun (Camb)* **47**, 8424-8426, doi:10.1039/c1cc11774b (2011).

14 Lee, J. S. *et al.* Synthesis of a BODIPY library and its application to the development of live cell glucagon imaging probe. *Journal of the American Chemical Society* **131**, 10077-10082, doi:10.1021/ja9011657 (2009).

15 Umezawa, K., Matsui, A., Nakamura, Y., Citterio, D. & Suzuki, K. Bright, color-tunable fluorescent dyes in the Vis/NIR region: establishment of new "tailor-made" multicolor fluorophores based on borondipyrromethene. *Chemistry* **15**, 1096-1106, doi:10.1002/chem.200801906 (2009).

16 Er, J. C. *et al.* MegaStokes BODIPY-triazoles as environmentally sensitive turn-on fluorescent dyes. *Chemical Science* **4**, 2168-2176, doi:10.1039/c3sc22166k (2013).

17 Martin, A., Long, C., Forster, R. J. & Keyes, T. E. Near IR emitting BODIPY fluorophores with mega-stokes shifts. *Chemical Communications* **48**, 5617-5619, doi:10.1039/c2cc31150j (2012).

18 Zhu, H., Fan, J., Du, J. & Peng, X. Fluorescent Probes for Sensing and Imaging within Specific Cellular Organelles. *Accounts of chemical research* **49**, 2115-2126, doi:10.1021/acs.accounts.6b00292 (2016).

19 Rosania, G. R., Lee, J. W., Ding, L., Yoon, H. S. & Chang, Y. T. Combinatorial approach to organelle-targeted fluorescent library based on the styryl scaffold. *Journal of the American Chemical Society* **125**, 1130-1131, doi:10.1021/ja027587x (2003).

20 Zimmermann, T., Marrison, J., Hogg, K. & O'Toole, P. Clearing up the signal: spectral imaging and linear unmixing in fluorescence microscopy. *Methods Mol Biol* **1075**, 129-148, doi:10.1007/978-1-60761-847-8_5 (2014).

21 Garini, Y., Young, I. T. & McNamara, G. Spectral imaging: principles and applications. *Cytometry. Part A : the journal of the International Society for Analytical Cytology* **69**, 735-747, doi:10.1002/cyto.a.20311 (2006).

22 Valm, A. M., Oldenbourg, R. & Borisy, G. G. Multiplexed Spectral Imaging of 120 Different Fluorescent Labels. *PloS one* **11**, e0158495, doi:10.1371/journal.pone.0158495 (2016).

23 Betzig, E. *et al.* Imaging intracellular fluorescent proteins at nanometer resolution. *Science* **313**, 1642-1645, doi:10.1126/science.1127344 (2006).

24 Hell, S. W. Microscopy and its focal switch. *Nature methods* **6**, 24-32, doi:10.1038/nmeth.1291 (2009).

25 Hell, S. W. & Wichmann, J. Breaking the diffraction resolution limit by stimulated emission: stimulated-emission-depletion fluorescence microscopy. *Optics letters* **19**, 780-782 (1994).

26 Klar, T. A., Jakobs, S., Dyba, M., Egner, A. & Hell, S. W. Fluorescence microscopy with diffraction resolution barrier broken by stimulated emission. *Proceedings of the National Academy of Sciences of the United States of America* **97**, 8206-8210 (2000).

27 Gustafsson, M. G. Surpassing the lateral resolution limit by a factor of two using structured illumination microscopy. *Journal of microscopy* **198**, 82-87 (2000).

28 Ha, T. & Tinnefeld, P. Photophysics of fluorescent probes for single-molecule biophysics and super-resolution imaging. *Annual review of physical chemistry* **63**, 595-617, doi:10.1146/annurev-physchem-032210-103340 (2012).

29 van de Linde, S., Wolter, S., Heilemann, M. & Sauer, M. The effect of photoswitching kinetics and labeling densities on super-resolution fluorescence imaging. *Journal of biotechnology* **149**, 260-266, doi:10.1016/j.jbiotec.2010.02.010 (2010).

30 Nienhaus, K. & Nienhaus, G. U. Fluorescent proteins for live-cell imaging with super-resolution. *Chemical Society reviews* **43**, 1088-1106, doi:10.1039/c3cs60171d (2014).

31 Hess, S. T., Girirajan, T. P. & Mason, M. D. Ultra-high resolution imaging by fluorescence photoactivation localization microscopy. *Biophysical journal* **91**, 4258-4272, doi:10.1529/biophysj.106.091116 (2006).

32 van de Linde, S. *et al.* Direct stochastic optical reconstruction microscopy with standard fluorescent probes. *Nature protocols* **6**, 991-1009, doi:10.1038/nprot.2011.336 (2011).

33 Hedde, P. N. & Nienhaus, G. U. Super-resolution localization microscopy with photoactivatable fluorescent marker proteins. *Protoplasma* **251**, 349-362, doi:10.1007/s00709-013-0566-z (2014).

34 Heilemann, M., van de Linde, S., Mukherjee, A. & Sauer, M. Super-resolution imaging with small organic fluorophores. *Angew Chem Int Ed Engl* **48**, 6903-6908, doi:10.1002/anie.200902073 (2009).

35 Lehmann, M., Lichtner, G., Klenz, H. & Schmoranzer, J. Novel organic dyes for multicolor localization-based super-resolution microscopy. *Journal of biophotonics*, doi:10.1002/jbio.201500119 (2015).

36 Stein, I. H. *et al.* Linking single-molecule blinking to chromophore structure and redox potentials. *Chemphyschem : a European journal of chemical physics and physical chemistry* **13**, 931-937, doi:10.1002/cphc.201100820 (2012).

37 Vaughan, J. C., Dempsey, G. T., Sun, E. & Zhuang, X. Phosphine quenching of cyanine dyes as a versatile tool for fluorescence microscopy. *Journal of the American Chemical Society* **135**, 1197-1200, doi:10.1021/ja3105279 (2013).

38 Vaughan, J. C., Jia, S. & Zhuang, X. Ultrabright photoactivatable fluorophores created by reductive caging. *Nature methods* **9**, 1181-1184, doi:10.1038/nmeth.2214 (2012).

39 Bittel, A. M. *et al. Varied Length Stokes Shift BODIPY-based Fluorophores for Multicolor Microscopy* (2017).

40 Haugland, R. P., Spence, M. T. Z., Johnson, I. D. & Basey, A. *The Handbook: A Guide to Fluorescent Probes and Labeling Technologies*. 10th edn, (Molecular Probes, 2005).

41 Garcia-Martin, F., Bayo-Puxan, N., Cruz, L. J., Bohling, J. C. & Albericio, F. Chlorotrityl Chloride (CTC) Resin as a Reusable Carboxyl Protecting Group. *QSAR & Combinatorial Science* **26**, 1027-1035, doi:10.1002/qsar.200720015 (2007).

42 Baruah, M. *et al.* Solvent and pH dependent fluorescent properties of a dimethylaminostyryl borondipyrromethene dye in solution. *The journal of physical chemistry. A* **110**, 5998-6009, doi:10.1021/jp054878u (2006).

43 Atilgan, S., Ozdemir, T. & Akkaya, E. U. A sensitive and selective ratiometric near IR fluorescent probe for zinc ions based on the distyryl-bodipy fluorophore. *Organic letters* **10**, 4065-4067, doi:10.1021/ol801554t (2008).

44 Liu, X., Xu, Z. & Cole, J. C. Molecular Design of UV−vis Absorption and Emission Properties in Organic Fluorophores: Toward Larger Bathochromic Shifts, Enhanced Molar Extinction Coefficients, and Greater Stokes Shifts. *The Journal of Physical Chemistry C* **117**, 16584-16595, doi:10.1021/jp404170w (2013).

45 Nandy, R. & Sankararaman, S. Donor-acceptor substituted phenylethynyltriphenylenes - excited state intramolecular charge transfer, solvatochromic absorption and fluorescence emission. *Beilstein journal of organic chemistry* **6**, 992-1001, doi:10.3762/bjoc.6.112 (2010).

46 Marvin. *Marvin*, <http://www.chemaxon.com> (2016).

47 Williams, A. T. R., Winfield, S. A. & Miller, J. N. Relative fluorescence quantum yields using a Computer-controlled luminescence spectrometer. *Analyst*, 1067, doi:10.1039/an9830801067 (1983).

48 Demas, J. N., Crosby, G. A. The measurement of photoluminescence Quantum Yields. *The Journal of Physical Chemistry* **75**, 991-1023 (1971).

49 Douglas, M., Brannon, J. H. Absolute Luminescence Yield of Cresyl violet. A Standard for the Red. *The Journal of Physical Chemistry* **83**, 696-699 (1979).

50 Karstens, T., Kobs, K. Rhodamine b and rhodamine 101 as reference substances for Fluorescence Quantum Yield Measurements. *J. Phys. Chem* **84**, 1871-1872 (1980).

51 Schindelin, J. *et al.* Fiji: an open-source platform for biological-image analysis. *Nature methods* **9**, 676-682, doi:10.1038/nmeth.2019 (2012).

52 Klein, T., Proppert, S. & Sauer, M. Eight years of single-molecule localization microscopy. *Histochemistry and cell biology* **141**, 561-575, doi:10.1007/s00418-014-1184-3 (2014).

53 Huang, B. Super-resolution optical microscopy: multiple choices. *Current opinion in chemical biology* **14**, 10-14, doi:10.1016/j.cbpa.2009.10.013 (2010).

54 Heilemann, M. *et al.* Subdiffraction-resolution fluorescence imaging with conventional fluorescent probes. *Angew Chem Int Ed Engl* **47**, 6172-6176, doi:10.1002/anie.200802376 (2008).

55 van de Linde, S., Sauer, M. & Heilemann, M. Subdiffraction-resolution fluorescence imaging of proteins in the mitochondrial inner membrane with photoswitchable fluorophores. *Journal of structural biology* **164**, 250-254, doi:10.1016/j.jsb.2008.08.002 (2008).

56 Adam, V. *et al.* Rational design of photoconvertible and biphotochromic fluorescent proteins for advanced microscopy applications. *Chemistry & biology* **18**, 1241-1251, doi:10.1016/j.chembiol.2011.08.007 (2011).

57 van de Linde, S. *et al.* Investigating cellular structures at the nanoscale with organic fluorophores. *Chemistry & biology* **20**, 8-18, doi:10.1016/j.chembiol.2012.11.004 (2013).

58 van de Linde, S. *et al.* Photoinduced formation of reversible dye radicals and their impact on super-resolution imaging. *Photochemical & photobiological sciences : Official journal of the European Photochemistry Association and the European Society for Photobiology* **10**, 499-506, doi:10.1039/c0pp00317d (2011).

59 Dempsey, G. T. *et al.* Photoswitching mechanism of cyanine dyes. *Journal of the American Chemical Society* **131**, 18192-18193, doi:10.1021/ja904588g (2009).

60 Endesfelder, U. *et al.* Chemically induced photoswitching of fluorescent probes-a general concept for super-resolution microscopy. *Molecules* **16**, 3106-3118, doi:10.3390/molecules16043106 (2011).

61 Whelan, D. R. & Bell, T. D. Image artifacts in single molecule localization microscopy: why optimization of sample preparation protocols matters. *Scientific reports* **5**, 7924, doi:10.1038/srep07924 (2015).

62 Funatsu, T., Harada, Y., Tokunaga, M., Saito, K. & Yanagida, T. Imaging of single fluorescent molecules and individual ATP turnovers by single myosin molecules in aqueous solution. *Nature* **374**, 555-559, doi:10.1038/374555a0 (1995).

63 Dulin, D. *et al.* Reduced photobleaching of BODIPY-FL. *Physics Procedia* **3**, 1563-1567, doi:10.1016/j.phpro.2010.01.222 (2010).

64 Altman, R. B. *et al.* Cyanine fluorophore derivatives with enhanced photostability. *Nature methods* **9**, 68-71, doi:10.1038/nmeth.1774 (2012).

65 Gust, A. *et al.* A starting point for fluorescence-based single-molecule measurements in biomolecular research. *Molecules* **19**, 15824-15865, doi:10.3390/molecules191015824 (2014).

66 Dickson, R. M., Norris, D. J., Tzeng, Y. L. & Moerner, W. E. Three-dimensional imaging of single molecules solvated in pores of poly(acrylamide) gels. *Science* **274**, 966-969 (1996).

67 Dickson, R. M., Cubitt, A. B., Tsien, R. Y. & Moerner, W. E. On/off blinking and switching behaviour of single molecules of green fluorescent protein. *Nature* **388**, 355-358, doi:10.1038/41048 (1997).

68 Betzig, E. & Chichester, R. J. Single molecules observed by near-field scanning optical microscopy. *Science* **262**, 1422-1425, doi:10.1126/science.262.5138.1422 (1993).

69 Belov, V. N., Bossi, M. L., Folling, J., Boyarskiy, V. P. & Hell, S. W. Rhodamine spiroamides for multicolor single-molecule switching fluorescent nanoscopy. *Chemistry* **15**, 10762-10776, doi:10.1002/chem.200901333 (2009).

70 Bock, H. *et al.* Two-color far-field fluorescence nanoscopy based on photoswitchable emitters. *Applied Physics B* **88**, 161-165, doi:10.1007/s00340-007-2729-0 (2007).

71 Zondervan, R., Kulzer, F., Kol'chenko, M. A. & Orrit, M. Photobleaching of Rhodamine 6G in Polyvinyl alcohol at the Ensemble and Single-Molecule Levels. *J Phys Chem A* **108**, 1657-1665, doi:10.1021/jp037222e (2004).

72 Folling, J. *et al.* Fluorescence nanoscopy by ground-state depletion and single-molecule return. *Nature methods* **5**, 943-945, doi:10.1038/nmeth.1257 (2008).

73 Le Gall, A. *et al.* Improved photon yield from a green dye with a reducing and oxidizing system. *Chemphyschem : a European journal of chemical physics and physical chemistry* **12**, 1657-1660, doi:10.1002/cphc.201100085 (2011).

74 Nogales, E., Whittaker, M., Milligan, R. A. & Downing, K. H. High-resolution model of the microtubule. *Cell* **96**, 79-88 (1999).

75 Olivier, N., Keller, D., Go, P. & Manley, S. Resolution Doubling in 3D-STORM Imaging through Improved Buffers. *PloS one* **8**, doi:10.1371/journal.pone.0069004 (2013).

76 Chozinski, T. J., Gagnon, L. A. & Vaughan, J. C. Twinkle, twinkle little star: photoswitchable fluorophores for super-resolution imaging. *FEBS letters* **588**, 3603-3612, doi:10.1016/j.febslet.2014.06.043 (2014).

77 Flors, C., Ravarani, C. N. & Dryden, D. T. Super-resolution imaging of DNA labelled with intercalating dyes. *Chemphyschem : a European journal of chemical physics and physical chemistry* **10**, 2201-2204, doi:10.1002/cphc.200900384 (2009).

78 Lukinavicius, G. *et al.* A near-infrared fluorophore for live-cell super-resolution microscopy of cellular proteins. *Nature chemistry* **5**, 132-139, doi:10.1038/nchem.1546 (2013).

79 Shim, S. H. *et al.* Super-resolution fluorescence imaging of organelles in live cells with photoswitchable membrane probes. *Proceedings of the National Academy of Sciences of the United States of America* **109**, 13978-13983, doi:10.1073/pnas.1201882109 (2012).

80 Vogelsang, J., Cordes, T., Forthmann, C., Steinhauer, C. & Tinnefeld, P. Controlling the fluorescence of ordinary oxazine dyes for single-molecule switching and superresolution microscopy. *Proceedings of the National Academy of Sciences of the United States of America* **106**, 8107-8112, doi:10.1073/pnas.0811875106 (2009).

81 Thompson, R. E., Larson, D. R. & Webb, W. W. Precise nanometer localization analysis for individual fluorescent probes. *Biophysical journal* **82**, 2775-2783, doi:10.1016/S0006-3495(02)75618-X (2002).

82 Yildiz, A. *et al.* Myosin V walks hand-over-hand: single fluorophore imaging with 1.5-nm localization. *Science* **300**, 2061-2065, doi:10.1126/science.1084398 (2003).

83 Deschout, H. *et al.* Precisely and accurately localizing single emitters in fluorescence microscopy. *Nature methods* **11**, 253-266, doi:10.1038/nmeth.2843 (2014).

84 Glantz, S. A. *Primer of Biostatistics*. 7 edn, 169-173 (McGraw-Hill, 2012).

85 Zondervan, R., Kulzer, F., Koh'chenko, M. A. & Orrit, M. Photobleaching of Rhodamine 6G in Polyvinyl alcohol at the Ensemble and Single-Molecule Levels. *J Phys Chem A* **108**, 1657-1665 (2004).

86 Shroff, H., Galbraith, C. G., Galbraith, J. A. & Betzig, E. Live-cell photoactivated localization microscopy of nanoscale adhesion dynamics. *Nature methods* **5**, 417-423, doi:10.1038/nmeth.1202 (2008).

87 Burgert, A., Letschert, S., Doose, S. & Sauer, M. Artifacts in single-molecule localization microscopy. *Histochemistry and cell biology* **144**, 123-131, doi:10.1007/s00418-015-1340-4 (2015).

88 Edelstein, A. D. *et al.* Advanced methods of microscope control using muManager software. *Journal of biological methods* **1**, doi:10.14440/jbm.2014.36 (2014).

89 Edelstein, A., Amodaj, N., Hoover, K., Vale, R. & Stuurman, N. Computer control of microscopes using microManager. *Current protocols in molecular biology* **Chapter 14**, Unit14 20, doi:10.1002/0471142727.mb1420s92 (2010).

90 Nan, X. *et al.* Single-molecule superresolution imaging allows quantitative analysis of RAF multimer formation and signaling. *Proceedings of the National Academy of Sciences of the United States of America* **110**, 18519-18524, doi:10.1073/pnas.1318188110 (2013).

91 Martin Ovesny´, M., Pavel Krˇı´zˇek, P., Borkovec, J., Sˇ vindrych, Z. & Hagen, G. M. ThunderSTORM: a comprehensive ImageJ plug-in for PALM and STORM data analysis and super-resolution imaging. *Bioimage informatics* **30**, 2389-2390, doi:10.1093/bioinformatics/btu202 (2014).

92 Glantz, S. A. S., B. K. *Primer of Applied Regression and Analysis of Variance*. (McGraw-Hill., 1990).

93 Xu, K., Babcock, H. P. & Zhuang, X. Dual-objective STORM reveals three-dimensional filament organization in the actin cytoskeleton. *Nature methods* **9**, 185-188, doi:10.1038/nmeth.1841 (2012).

94 Carlini, L., Benke, A., Reymond, L., Lukinavicius, G. & Manley, S. Reduced dyes enhance single-molecule localization density for live superresolution imaging. *Chemphyschem : a European journal of chemical physics and physical chemistry* **15**, 750-755, doi:10.1002/cphc.201301004 (2014).

95 Edelstein, A. D. *et al.* Advanced methods of microscope control using μManager software. *Journal of biological methods* **1**, doi:10.14440/jbm.2014.36 (2014).

96 Kottke, T., Van de Linde, S., Sauer, M., Kakorin, S. & Heilemann, M. Identification of the Product of Photoswitching of an Oxazine Fluorophore Using Fourier Transform Infrared Difference Spectroscopy. *The Journal of Physical Chemistry Letters*, 3156-3159, doi:10.1021/jz101300t (2010).